

The molecular motor kinesin: From single-molecule mechanisms to joint action

Dissertation

der Fakultät für Biologie der
Ludwig-Maximilian-Universität

München



vorgelegt von

Bettina Ebbing

aus Wolfratshausen

08.01.2008

Erstgutachter:	PD Dr. Günther Woehlke
Zweitgutachter:	Prof. Manfred Schliwa
eingereicht:	08.01.2008
Tag der mündlichen Prüfung:	04.04.2008

Ehrenwörtliche Erklärung:

Hiermit erkläre ich, dass die vorliegende Dissertation von mir selbständig und ohne unerlaubte Hilfsmittel angefertigt wurde und ich keine anderen als die angegebenen Quellen und Hilfsmittel verwendet habe.

Bettina Ebbing

Table of Contents

1	Introduction	- 1 -
1.1	STRUCTURE OF THIS THESIS.....	- 1 -
1.2	INTRACELLULAR TRANSPORT	- 2 -
1.2.1	<i>Axonal transport</i>	- 2 -
1.2.2	<i>Molecular motors</i>	- 3 -
1.2.3	<i>Kinesin</i>	- 4 -
1.2.4	<i>The chemo-mechanical cycle</i>	- 6 -
1.3	OPTICAL TECHNIQUES	- 8 -
1.3.1	<i>TIRF microscopy</i>	- 9 -
1.3.2	<i>Confocal microscopy</i>	- 11 -
1.3.3	<i>FRET</i>	- 12 -
1.3.4	<i>Optical tweezers</i>	- 14 -
1.4	OUTLINE OF THE PRESENT THESIS.....	- 16 -
1.5	REFERENCES	- 17 -
2	Molecular determinants of processivity in kinesin.....	- 20 -
2.1	ABSTRACT.....	- 20 -
2.2	INTRODUCTION.....	- 21 -
2.3	RESULTS.....	- 22 -
2.3.1	<i>Design of chimaeras</i>	- 22 -
2.3.2	<i>Co-operative gliding behaviour</i>	- 22 -
2.3.3	<i>Single-molecule behaviour</i>	- 24 -
2.4	DISCUSSION.....	- 26 -
2.5	METHODS.....	- 27 -
2.5.1	<i>Cloning, protein expression and purification</i>	- 27 -
2.5.2	<i>Gliding assays</i>	- 28 -
2.5.3	<i>Single-molecule motility assays</i>	- 28 -
2.6	REFERENCES	- 29 -
3	Kinesin-1's neck-linker docking	- 31 -
3.1	ABSTRACT.....	- 31 -
3.2	INTRODUCTION.....	- 32 -
3.3	RESULTS.....	- 34 -
3.3.1	<i>Mutant design and proof of expected disulfide bonds</i>	- 34 -
3.3.2	<i>Motility behaviour</i>	- 35 -

3.3.3	<i>Microtubule affinities</i>	- 37 -
3.4	DISCUSSION.....	- 39 -
3.5	MATERIAL AND METHODS	- 40 -
3.5.1	<i>Protein expression and purification</i>	- 40 -
3.5.2	<i>NcKin protein backgrounds</i>	- 41 -
3.5.3	<i>Introduction of disulfide bridges</i>	- 41 -
3.5.4	<i>Gliding assay</i>	- 41 -
3.5.5	<i>Microtubule Co-sedimentation assay</i>	- 42 -
3.5.6	<i>Statistical analysis of experimental results</i>	- 42 -
3.6	REFERENCES	- 43 -
4	Time-resolved FRET between Kinesin-1 and its substrate ATP.....	- 45 -
4.1	ABSTRACT.....	- 45 -
4.2	INTRODUCTION.....	- 46 -
4.3	RESULTS.....	- 47 -
4.3.1	<i>Design of FRET constructs</i>	- 47 -
4.3.2	<i>Spectroscopic bulk assay</i>	- 48 -
4.3.3	<i>Single-molecule TIRF-assay</i>	- 50 -
4.3.4	<i>Confocal assay</i>	- 51 -
4.3.5	<i>Measuring single ATP events</i>	- 53 -
4.4	DISCUSSION AND FUTURE PROSPECTS	- 57 -
4.5	MATERIAL AND METHODS	- 58 -
4.5.1	<i>Cloning, protein expression and purification</i>	- 58 -
4.5.2	<i>Protein labelling and spectroscopic assay</i>	- 59 -
4.5.3	<i>TIRF assay</i>	- 59 -
4.5.4	<i>Confocal assay</i>	- 60 -
4.6	REFERENCES	- 61 -
5	Effect of spastic paraplegia mutations in KIF5A kinesin on transport activity- 63 -	
5.1	ABSTRACT.....	- 63 -
5.2	INTRODUCTION.....	- 64 -
5.3	RESULTS.....	- 66 -
5.3.1	<i>Motility and processivity</i>	- 66 -
5.3.2	<i>Enzymatic activity</i>	- 68 -
5.3.3	<i>Heterozygous patients</i>	- 69 -
5.3.4	<i>Cargo transport assays</i>	- 70 -
5.4	DISCUSSION.....	- 76 -
5.5	MATERIALS AND METHODS	- 79 -

5.5.1	<i>Cloning, protein expression and purification</i>	- 79 -
5.5.2	<i>ATPase assay</i>	- 79 -
5.5.3	<i>Gliding assays</i>	- 80 -
5.5.4	<i>Laser Trapping assay</i>	- 80 -
5.5.5	<i>Quantum dot assays</i>	- 81 -
5.5.6	<i>Data analysis</i>	- 81 -
5.6	REFERENCES	- 82 -
	Summary	- 85 -
	Publications	- 88 -
	Meeting Abstracts	- 89 -
	Curriculum Vitae	- 90 -
	Acknowledgements.....	- 92 -

1 Introduction

1.1 Structure of this thesis

The present thesis studies the mechanism of the microtubule motor protein kinesin using different biochemical and biophysical approaches. It is divided into five parts, each presenting one publication-style chapter focussing on one specific approach. The first chapter gives a general introduction into the kinesin-family of motor proteins, as well as on the techniques used in this thesis. Chapter 2 compares a processive and a non-processive kinesin, chapter 3 elucidates the primary mechanical event leading to motility in conventional kinesins (Kinesin-1 subfamily). Chapter 4 presents a biophysical study aimed at measuring the ATP turnover with microscopic methods, chapter 5 investigates the basis of defective kinesins found in spastic paraplegia patients. These studies thus address the mechanism of kinesin at a molecular level, using wildtype and mutant motor proteins, as well as *in vitro* assays for kinesin's gliding and enzymatic activity.

1.2 Intracellular transport

Cell motility is one of the major achievements in evolution. Primitive cells were probably immobile, floating in the primordial soup. The innovation of directed intracellular motion allowed cell motility. The possibility to alter the cell shape and subcellular structures like cilia enabled the cell to direct its movement. In multicellular organisms, migration of cells during development and in search of foreign organisms to defend the host against infection are required for the organisms' health. On the other hand, uncontrolled cell migration is a property of malignant cancer cells.

Not only migrating cells, but also stationary cells exhibit dramatic changes in their morphology. Striking examples are the contraction of muscle cells, the elongation of nerve axons or the constriction of a dividing cell during mitosis. But also more subtle movements within the cell are essential elements in growth and differentiation of cells – active separation of chromosomes, cytoplasmic streaming and transport of membrane vesicles. These internal movements are carefully controlled by the cell to take place at specific times and in particular locations.

Many types of motility are based on ATP-hydrolysing enzymes that convert chemical energy into mechanical work. This conversion is accomplished by a special class of enzymes, so-called motor proteins. Together with the cytoskeleton, a cytoplasmic system of fibres, they are essential for intracellular transport and thus for cell motility. Three types of cytosolic fibres build the cytoskeleton: actin filaments (7 to 9 nm in diameter), intermediate filaments (10 nm in diameter) and microtubules (24 nm in diameter). These cytoskeletal fibres are well-ordered polymers built from small protein subunits held together by noncovalent bonds. (Lodish *et al.*, 2000). The cytoskeleton plays a structural role by supporting the cell membrane and providing tracks along which organelles and other elements transported by molecular motors move. Due to their regulated, polar arrangements, cytoskeletal fibres can also produce movement by themselves without associated molecular motors.

1.2.1 Axonal transport

A highly sophisticated form of intracellular transport is axonal transport. In the human body axons can be up to one meter in length and numerous proteins, mRNA or even whole organelles, need to be brought from the neuronal cell body to the synapse

(Kandel *et al.*, 1995). Insufficient supply of the synapse leads to neurodegeneration representing the origin of severe neuronal diseases.

Transport in axons occurs in anterograde and in retrograde direction, and has two major components of distinct velocity, termed fast and slow components of axonal transport (Lasek, 1967). Anterograde transport going towards the cell periphery is driven by different kinesin motors (1.2.3), retrograde transport by dynein. Anterograde transport is responsible for supply of the synapse and maintenance of the structure, whereas retrograde transport collects metabolites and pieces of membranes for recycling in the cell body and delivers chemical messages. It is thought that vesicular cargoes are mainly delivered by fast axonal transport, slow axonal transport is associated with cytoskeletal and cytosolic proteins (Kandel *et al.*, 1995). Recent findings suggest that slow and fast components of axonal transport are driven by the same molecular motors and that the difference in velocity is due to more frequent stops (Brown *et al.*, 2005).

1.2.2 Molecular motors

Not only axonal transport, but also muscle contraction, meiosis and mitosis, organelle transport and almost every biological movement is driven by protein machines called molecular motors. These specialized proteins convert chemical energy or ion potentials into mechanical work. Despite this common feature they vary in their function and structure. Figure 1.1 illustrates the structure of three different representatives of cytoskeletal motors.

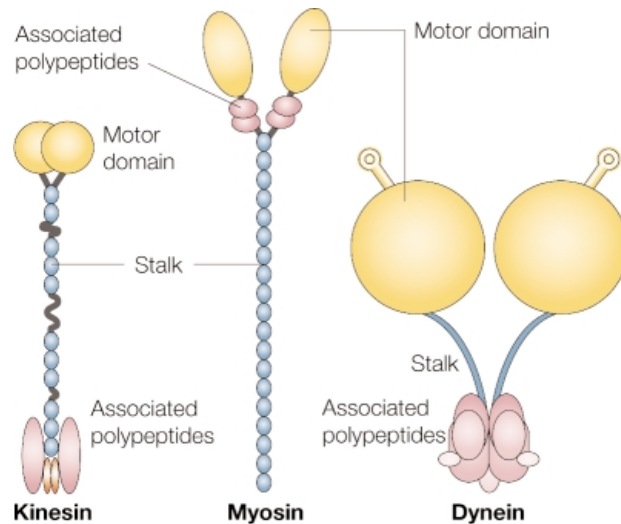


Figure 1.1 Representatives of cytoskeletal motors.

Kinesin-1 and cytoplasmic dynein are shown here as representatives of microtubule binding motors. Myosin II represents an actin-based motor. All three motors have dimerised heavy chains. In the case of myosin and kinesin they are joined by an extended coiled-coil – the stalk, shown in blue. The motor domains contain the catalytic sites and are shown in yellow. The associated light chains are shown in purple. (from Woehlke and Schliwa, 2000)

The three classes of motor proteins, namely myosins, kinesins and dyneins, use two types of cytoskeletal filaments as tracks. Myosins interact with actin filaments, whereas kinesins and dyneins interact with microtubules. Typically, these motors have a globular motor domain, also referred to as “head” domain. This catalytic head domain contains two crucial properties of a molecular motor: a site for ATP hydrolysis and a nucleotide-dependent binding site to the track. In many cases, the globular head is followed by an extended stalk, which dimerises via a coiled-coil structure to yield a double-headed molecular motor (Figure 1.1). The associated polypeptides (intermediate and light chains) differ largely for all three motor classes indicating a broad variety of functions (Woehlke and Schliwa, 2000).

1.2.3 Kinesin

After myosin and dynein, a third force-generating ATPase, which is involved in intracellular transport, was identified (Brady, 1985; Vale *et al.*, 1985). Named after the Greek word *kinein* (to move), kinesin was found to transport axoplasmic organelles on microtubules. These first identified kinesins from brain tissues and from squid giant axons belong to the Kinesin-1 family (also conventional kinesin). In some higher vertebrates, one member of this family was found exclusively in neurons and is therefore named neuronal kinesin heavy chain (nKHC or KIF5A) (Niclas *et al.*, 1994).

All conventional and unconventional kinesins share a high degree of sequence similarity in their motor domains, whereas all other parts are diverse (Vale and Fletterick, 1997). The motor domain is defined as the force-generating element of the protein and can be C- or N-terminal. In several kinesin families, two globular motor domains form dimers via a coiled-coil, usually termed neck. In addition to these two domains, many kinesin proteins contain a long coiled-coil domain termed stalk. Finally, there is often a globular domain at the C-terminus, termed tail domain. It usually has a regulatory function and binds to cargos or light chains.

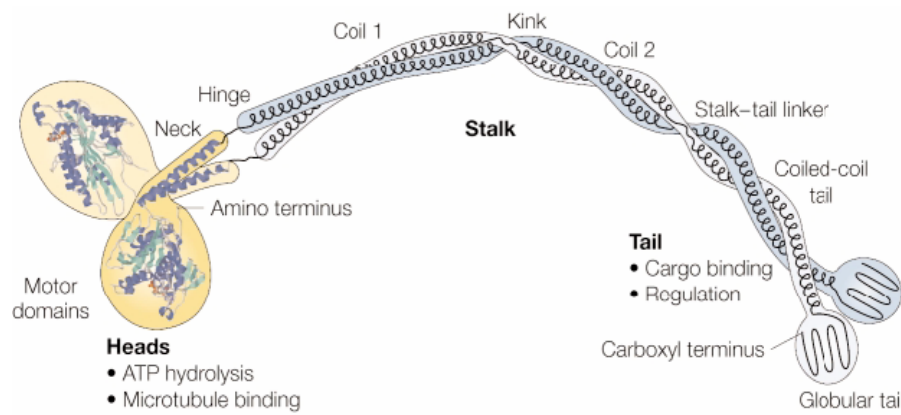


Figure 1.2 Domain organisation of conventional kinesin.

The motor domain and the neck (yellow) are overlaid by the crystal structure. The stalk consists of coiled-coil structures and flexible regions, whereas the tail region is globular and binds to the cargo or light chains. (from Woehlke and Schliwa, 2000)

The two heavy chains of conventional kinesin are twice as heavy as the two associated light chains (110-140 kD versus 60-80 kD) (Bloom *et al.*, 1988; Kuznetsov *et al.*, 1988). Only the heavy chains are required for kinesin's motility, whereas the light chains have regulatory and cargo-binding function (Stenoien and Brady, 1997; Verhey *et al.*, 1998). The domain organisation of heavy chains is shown schematically in Figure 1.2. At the N-terminus, ~320 amino acids form the motor domain. It contains the microtubule and nucleotide binding sites and its three-dimensional structure has been solved (Kull *et al.*, 1996; Woehlke *et al.*, 1997). The neck-linker joins the N-terminal motor domain with the C-terminal coiled-coil neck. Depending on the bound nucleotide, the neck-linker adopts different positions relative to the catalytic core (Rice *et al.*, 1999). The neck-domain and the approximately 50 nm long coiled-coil stalk domain are joined by a flexible hinge domain. The stalk is interrupted by a second flexible region, called the kink. The kink allows the molecule to bend in a way

that the C-terminally globular tail domain comes close to the motor domain and inhibits its ATPase activity. If the tail binds a cargo directly or via light chains the inhibition is repealed (Adio *et al.*, 2006; Seiler *et al.*, 2000).

1.2.4 The chemo-mechanical cycle

The first identified kinesin (conventional kinesin, KIF5B, Kinesin-1 or uKHC) is the best studied member of the kinesin superfamily and is considered prototypic for the entire superfamily. Today, the chemo-mechanical cycle of kinesin is resolved in great detail and some key questions are still to be solved. Figure 1.3 shows a consensus kinetic model of the chemo-mechanical cycle (Cross, 2004; Valentine and Gilbert, 2007).

Conventional kinesin can walk distances up to 1 μm along microtubules without detaching (Howard *et al.*, 1989). This phenomenon is called processivity and as a consequence, at least one head of the dimeric motor always remains attached to the microtubule. Each step is coupled to the hydrolysis of one ATP molecule (Hua *et al.*, 1997; Schnitzer and Block, 1997). With each step the center of the molecule is displaced 8 nm along the microtubule, representing the distance between adjacent tubulin dimers (Svoboda *et al.*, 1993). A prerequisite for processive movement is the precise coordination of the chemo-mechanical cycles of both heads. A commonly accepted model is the “hand-over-hand” model (Asbury *et al.*, 2003; Kaseda *et al.*, 2003; Schief *et al.*, 2004; Yildiz *et al.*, 2004) (Figure 1.3). Here, one head passes the other and binds to the next microtubule binding site. Therefore, one head takes a 16 nm step, but the centre of mass is displaced 8 nm per step. During one cycle the heads switch between strong and weak microtubule binding states in a nucleotide-dependent manner (Gilbert *et al.*, 1998; Hackney, 1994; Ma and Taylor, 1997).

In solution, a kinesin dimer contains one ADP per head. Upon microtubule binding, only one head locks onto the microtubule and loses its ADP. If ATP is bound to this head, the neck-linker docks (Rice *et al.*, 1999) and brings the second head into a favourable position to bind the next microtubule binding site. Microtubule binding takes place after the ADP release (Sablin and Fletterick, 2001). In this intermediate state, both heads are bound to adjacent tubulin binding sites. The rear head hydrolyses the nucleotide and after the release of inorganic phosphate it detaches from the microtubule while the other head holds on. At this point, the heads have exchanged their roles and a new chemo-mechanical cycle starts.

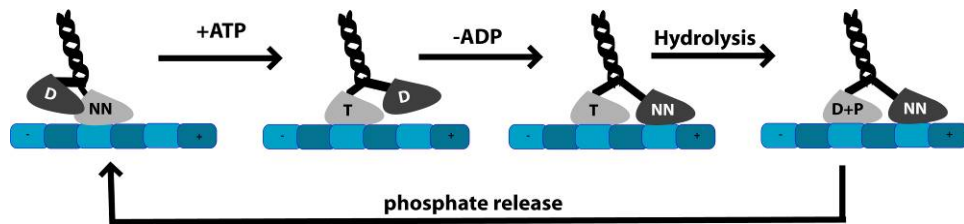


Figure 1.3 Chemo-mechanical cycle of Kinesin-1

This sequence of events summarises the chemo-mechanical cycle of one kinesin head (see text for details). Kinesin is shown in black/grey; microtubules in blue; abbreviations for nucleotides bound to kinesin heads: ATP (T); ADP (D); phosphate (P); no nucleotide (NN)

This is a somewhat oversimplified model, however, as many aspects like force, strain or conformational changes are not taken into account. Most of the data is obtained from pre-steady state kinetics and bulk experiments, where the values are averaged over many molecules without evaluating the quality of single ones (e.g. dead motors). Recently developed techniques allow to measure speeds, forces and kinetics of single molecules. A variety of these techniques was employed in this thesis and will be described in the next section.

1.3 Optical techniques

To overcome the boundaries of temporal and spatial resolution is the major driving force for the development of highly sophisticated optical techniques. The limit of spatial resolution of a light microscope is set by the wavelength of visible light. The best resolution one can get with a conventional light microscope is to distinguish objects, which are 0.2 μm apart. Due to this fact it is hard to image subcellular structures and various approaches like electron microscopy have been developed to overcome this restriction.

Until today, we are not at the limit of all four dimensions (time and space), although it is possible to image single molecules with a sub-millisecond time resolution (Verbrugge *et al.*, 2007). A big step towards higher spatial resolution was the invention of fluorescent dyes (Coons and Kaplan, 1950). Here, it is possible to illuminate only the subject of interest by labelling it with a fluorescent dye, which is then purposely excited and detected with a microscope. Depending on the requirements different fluorescent microscopes can be used (Figure 1.4). The basic epifluorescence microscope illuminates the whole sample and reduces the background only by using an emission filter.

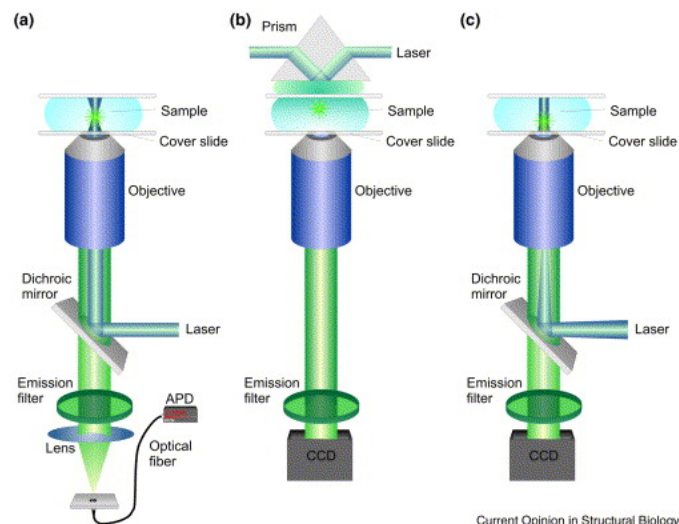


Figure 1.4 Different types of fluorescent microscopes.

Based on an epifluorescent microscope (c), the resolution can be improved by minimising the excitation volume. The most popular one is the confocal microscope (a), where the excitation volume is reduced to a single spot, which allows scanning the sample in three dimensions and rebuilding the pictures digitally. Another approach is called "Total Internal Reflection Fluorescence" or TIRF microscopy (b), where the excitation volume is only a thin layer. The reduction of the excitation volume leads to less unspecific background fluorescence and therefore to a better resolution of the specific fluorescent signal. (from Hausteiner and Schwiile, 2004)

1.3.1 TIRF microscopy

TIRF microscopy uses the emerging evanescent wave due to the reflection of a laser beam at the glass-water boundary.

The incident laser beam is directed in a supercritical angle to the glass surface, where it is reflected (Figure 1.5). For the reflection it is necessary that the immersion oil has a similar refractive index as the glass and that the medium of the sample has a lower refractive index than the glass. With these two prerequisites the only possible area of reflection is the glass-water boundary. Due to the reflection an evanescent wave emerges and penetrates the sample, but its intensity decays exponentially with the distance to the glass-water boundary. Therefore the evanescent wave can only excite fluorophores at close proximity to the glass surface. Depending on the angle, the refractive indices and the wavelength of the laser beam, the excited layer is between 70 and 300 nm deep and usually 150-200 nm (Schneckenburger, 2005).

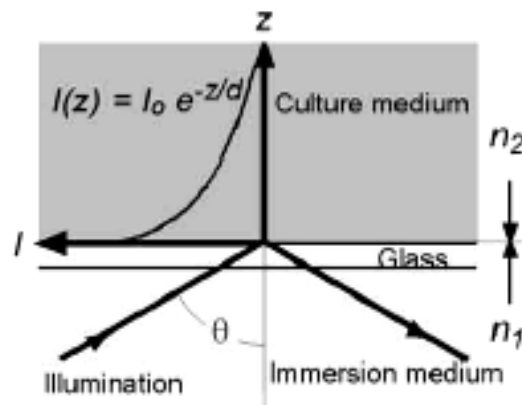


Figure 1.5 Principle of TIRF microscopy.

The incident laser is directed in a supercritical angle to the glass-water boundary, where it is reflected. The intensity of the emerging evanescent wave decays exponentially with the depth. The refractive index of the culture medium n_2 has to be smaller than the refractive index of the glass and immersion oil n_1 . (from Sako and Uyemura, 2002)

This exciting layer is fixed to the surface and can not be moved in the third dimension, but allows 2D imaging at high time resolution and low background. These properties are used to image specifically adhesion structures of cells or anything else occurring only at the glass surface.

TIRF microscopes are usually available as a prism-type TIRF or an objective-type TIRF. They differ in the way how the incident laser beam is brought to the supercritical angle. The prism-type TIRF directs the laser through a prism, where it is broken in the right angle to reflect at the glass surface. In this microscope the excitation and emission path is separated and there is no access to the sample during imaging.

The objective-type TIRF directs the incident laser through an objective with a numerical aperture higher than 1.38 N.A. (Sako and Uyemura, 2002). This is important, because the laser passes the objective off-axis and is refracted by the lens of the objective. The higher the numerical aperture, the stronger the refraction and only a strong refraction can bring the laser beam into a supercritical angle (Figure 1.6).

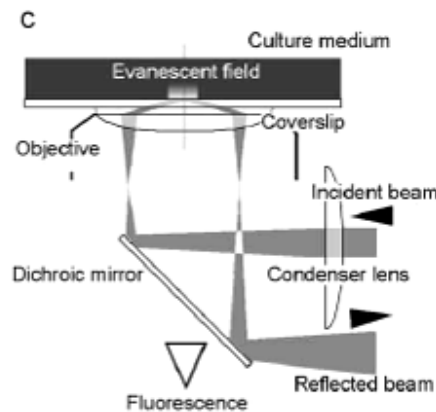


Figure 1.6 Objective-type TIRF microscope.

The incident laser beam is directed through the objective off-axis. Therefore it is refracted by the high numerical aperture lens and brought into a supercritical angle to the glass-water boundary. The reflected laser beams back through the objective to the dichroic mirror, which blocks the detection part from excitation light. The evanescent wave emerges from the glass water-boundary and excites a thin layer of the sample. (from Sako and Uyemura, 2002)

The advantage of this type of TIRF microscope is that the excitation and emission path is on the same side of the microscope and the sample is accessible during imaging, e.g. for changing the medium or adding reagents.

In this thesis an objective-type TIRF was used to reduce the background in microscopic assays and allowed to image single kinesins, site specific labelled with a fluorophore.

1.3.2 Confocal microscopy

Another approach to enhance resolution involves a confocal microscope (Egger and Petran, 1967). Here, the excitation volume is reduced to a small spot, which originates from a focussed laser beam. In a conventional confocal microscope a scanning device can position this spot in three dimensions. A photomultiplier detects the intensity of fluorescence in the spot and after scanning a special region in the sample the image can be assembled digitally. In front of the photomultiplier a pinhole cuts off emission light from regions out of focus. The special confocal microscope used in this thesis was build by Sander Verbrugge from the Vrije Universiteit in Amsterdam ((Verbrugge *et al.*, 2007);Figure 1.7). Here, the scanning device does not move the confocal spot, but the sample with a scanning table. Therefore, the spot is very stable and well defined. This setup was built to measure the change of fluorescence intensity in one spot over time rather than to scan whole images.

The emission light is detected by a highly sensitive single-photon-counting avalanche photodiode. Such a detector counts the time between photon arrivals with nanosecond accuracy. The number of photons arrived within a defined time (binning time) is summed up and displayed on the screen. Thus, change of intensity in the spot is detected while the measurement ongoing.

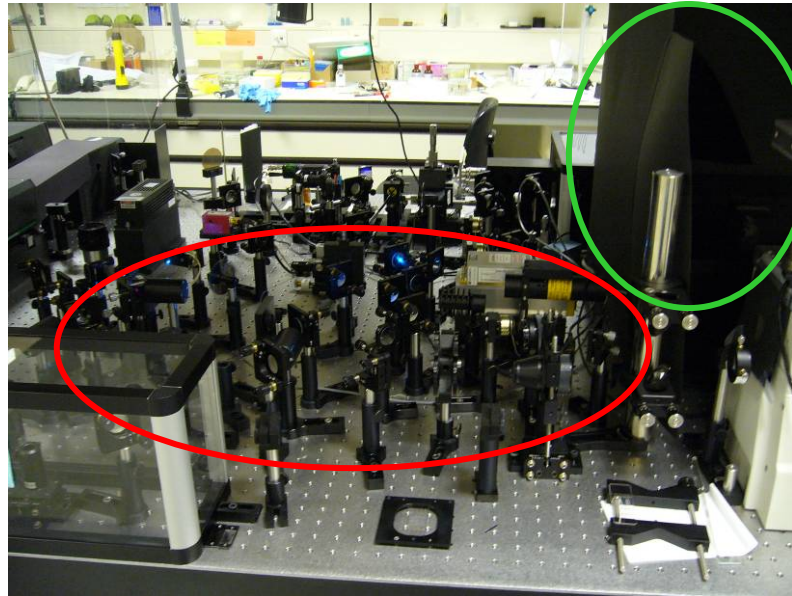


Figure 1.7 Confocal setup at the VU Amsterdam.

This confocal setup was built by Sander Verbrugge (Verbrugge *et al.*, 2007) at the Vrije Universiteit Amsterdam. The excitation part (red circle) is open and can be fine-tuned during measurements. The emission part (green circle) is shielded from light. The sample holder and scanner are constructed into a Nikon microscope corpus.

In the present thesis this techniques was used to measure intensity fluctuations of a fluorophore-labelled kinesin stepping through the spot. The intensity fluctuations were due to “Förster-Resonance-Energy-Transfer” or FRET, which is explained in more detail in the next subsection.

1.3.3 FRET

FRET is a technique used in fluorescent microscopy or spectroscopy to elucidate the interaction of two molecules. The prerequisites for FRET are a donor fluorophore with an emission spectrum that overlaps with the absorption spectrum of an acceptor fluorophore, and a close proximity of donor and acceptor dye ((Lakowicz, 1999); Figure 1.8).

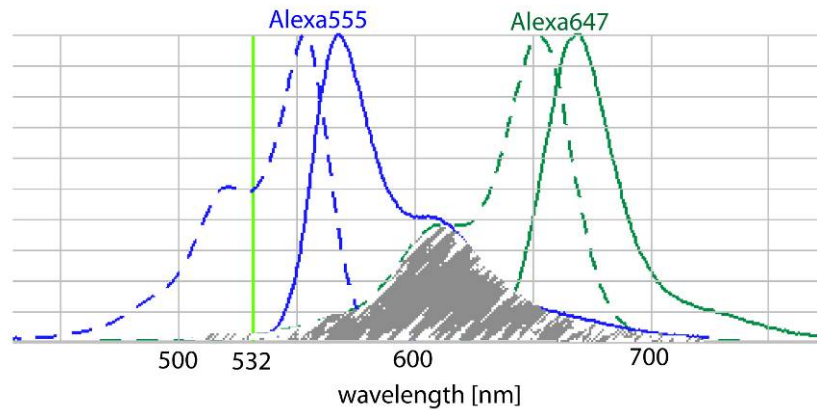


Figure 1.8 Overlapping spectra of donor and acceptor fluorophores.

The excitation (dashed lines) and emission (solid lines) spectra of Alexa555 and Alexa647 fluorophores as an example of a FRET pair. The overlap of the emission spectra of the donor (Alexa555, blue) and the excitation spectra of the acceptor (Alexa647, green) is hatched in grey. The integral of this overlap is deciding for the Förster radius R_0 . (Spectra from Invitrogen SpectraViewer)

The efficiency of the energy transfer from one donor to the acceptor is described by the Förster equations, which is dependent on the Förster radius (R_0) (Förster, 1948) equation(1)).

$$(1) \quad E = \frac{1}{1 + (r/R_0)^6}$$

The Förster radius is the distance at which the efficiency is 50% and is usually 1 to 10 nm. Depending on the overlapping integral of the two spectras the Förster radius is specific for every FRET pair. Common FRET pairs are Cy2 and Cy3, YFP and GFP or GFP and rhodamine.

The protein of interest can be tagged N- or C-terminally, and co-expressed with the fluorescent proteins (YFP, GFP etc.). This makes labelling procedures unnecessary and ensures a one to one labelling stoichiometry. The disadvantages are the poor spectroscopic properties of these fluorescent proteins, in particular low quantum yield and blinking. Therefore it is recommended to use organic dyes that are more stable and have high quantum yields. This is especially important for single molecule applications.

For the detection of FRET always the donor is excited and the emission of the donor, the acceptor or both can be measured. In case of donor emission, the fluorescent intensity decays if FRET occurs. On the other hand, if the acceptor emission is measured it is enhanced as soon as the energy is transferred from the donor (Figure 1.9).



Figure 1.9 Principle of FRET

The protein is labelled with the donor fluorophore (green) and the nucleotide is labelled with the acceptor fluorophore (red). The donor is excited directly with a laser beam. If the nucleotide binds to the protein, the two fluorophores come in close proximity to each other and the acceptor is excited via FRET.

In this thesis FRET was used to measure the binding time of fluorescent ATP to the site specific labelled kinesin. The energy transfer was measured in bulk in a fluorimeter and on single molecules in a confocal setup.

1.3.4 Optical tweezers

Optical tweezers, also known as optical traps, are instruments that are usually implemented in a conventional light microscope. This instrument allows manipulating small colloidal particles with a strongly focussed laser beam. Since its invention by Arthur Ashkin (1986), optical traps are broadly used in medicine and science. They allow the direct manipulation of viruses and cells as well as cell compartments in living cells (Ashkin and Dziedzic, 1987; Sheetz and Kuo, 1993) without destroying the examined biological system. With optical tweezers it was possible to measure the force producing properties of single molecular motors for the first time by adsorbing them at low densities to dielectric microspheres, which were then manipulated by the tweezer (Block *et al.*, 1990), Figure 1.10).

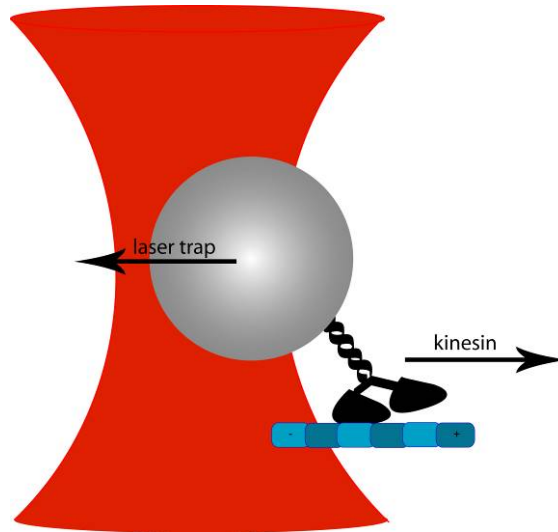


Figure 1.10 Kinesin in an optical trap.

The polystyrene bead (grey) with attached kinesin molecule (black) is trapped in the focussed laser beam (red). Brought in contact with the microtubule (blue) the kinesin starts to walk along its track and pulls the bead out of the trap. The back pulling force is directly proportional to the displacement of the bead.

The possibility to measure forces between one and several hundred piconewton and to detect movements on sub-nanometer scales makes optical tweezers a perfect instrument for investigating force generating proteins, like kinesin. The optical tweezers used in this thesis were built by Dr. Anabel Clemen and later on supervised by Dr. Johann Jaud from the Physik Department, Lehrstuhl E22 für Biophysik, Technische Universität München. The motor protein is adsorbed to a polystyrol bead, which can be trapped and manipulated with optical tweezers. After trapping, the bead is brought to surface-attached microtubules, where kinesins can bind and start to walk (Figure 1.10.) The microtubules are labelled with fluorophores and can be detected with a coupled fluorescent microscope.

1.4 Outline of the present thesis

This thesis consists of a collection of published and submitted research articles. They all have one common theme: the biochemical and biophysical properties of kinesin motors. The methods used in this present work vary from kinetic ensemble to single-molecule measurements and focus on fundamental properties of human and fungal, processive and non-processive kinesins.

Chapter 2 deals with questions about **processivity**. What makes a motor processive? What are the structural determinants? And is it possible to transfer them to an unprocessive motor? To investigate these questions the dimeric but unprocessive motor NKin3 from the filamentous fungus *Neurospora crassa* was compared with its processive counterpart NcKin. The processivity of chimaeras with swapped motor domains were examined in various *in vitro* assays. A meaningful assay to determine the processivity is the filament-gliding assay. But the average runlength can only be determined in single-molecule assays, which were performed in a TIRF microscope.

Chapter 3 addresses the consequences of **neck-linker docking** in the chemo-mechanical cycle. The neck-linker docking is essential for the functionality of kinesin (Rice et al, 1999). But how does the neck-linker promote the stepping of the motor? This question was investigated with NcKin mutants possessing an artificial disulfide bridge between the neck-linker and the motor core. This disulfide bridge can be switched on or off reversibly by oxidation and reduction. These mutants have different properties depending on the particular position where the disulfide bridge formed. Apart from their filament-gliding activity, their affinity to microtubules is altered. This was investigated with a microtubule co-sedimentation assay.

Chapter 4 describes the most challenging project of this thesis. The aim was to measure the **binding times of single ATP molecules** to a single kinesin while it is walking along a microtubule. The method of choice was FRET. Specially designed human kinesin constructs were labelled with a donor fluorophore next to the ATP binding site. ATP was labelled with an acceptor fluorophore. The occurrence of FRET was shown in a spectroscopic bulk experiment, measurements on a single molecule level were performed with a special confocal microscope in collaboration with the Vrije Universiteit Amsterdam. This setup is highly sensitive and measures with sub-millisecond accuracy.

Chapter 5 characterises the defects of human neuronal kinesin (KIF5A) mutants linked to the neurodegenerative disease **hereditary spastic paraplegia (HSP)**. Which properties are altered in these mutants in comparison to the wildtype protein? Why do patients develop the disease, although they still have one wildtype allele of the gene? To answer this question a novel cargo transportation assay was developed, where mixtures of heterodimeric and homodimeric kinesins work in concert. This mimics the axonal transport in heterozygous patients and gives an insight why this disease emerges.

1.5 References

- Adio S, Reth J, Bathe F, Woehlke G. 2006. Review: regulation mechanisms of Kinesin-1. *J Muscle Res Cell Motil*:1-8.
- Asbury CL, Fehr AN, Block SM. 2003. Kinesin moves by an asymmetric hand-over-hand mechanism. *Science* 302(5653):2130-2134.
- Ashkin A, Dziedzic JM. 1987. Optical trapping and manipulation of viruses and bacteria. *Science* 235(4795):1517-1520.
- Ashkin A, Dziedzic JM, Bjorkholm JE, Chu S. 1986. Observation of a single-beam gradient force optical trap for dielectric particles. *Optics Letters* 11:288-290.
- Block SM, Goldstein LS, Schnapp BJ. 1990. Bead movement by single kinesin molecules studied with optical tweezers [see comments]. *Nature* 348(6299):348-352.
- Bloom GS, Wagner MC, Pfister KK, Brady ST. 1988. Native structure and physical properties of bovine brain kinesin and identification of the ATP-binding subunit polypeptide. *Biochemistry* 27(9):3409-3416.
- Brady ST. 1985. A novel brain ATPase with properties expected for the fast axonal transport motor. *Nature* 317(6032):73-75.
- Brown A, Wang L, Jung P. 2005. Stochastic Simulation of Neurofilament Transport in Axons: The "Stop-and-Go" Hypothesis. *Mol Biol Cell* 16(9):4243-4255.
- Coons AH, Kaplan MH. 1950. Localization of antigen in tissue cells; improvements in a method for the detection of antigen by means of fluorescent antibody. *J Exp Med* 91(1):1-13.
- Cross RA. 2004. The kinetic mechanism of kinesin. *Trends Biochem Sci* 29(6):301-309.
- Egger MD, Petran M. 1967. New reflected-light microscope for viewing unstained brain and ganglion cells. *Science* 157(786):305-307.
- Förster T. 1948. Zwischenmolekulare Energiewanderung und Fluoreszenz. *Annalen der Physik* 437(1):55-75.

- Gilbert SP, Moyer ML, Johnson KA. 1998. Alternating site mechanism of the kinesin ATPase. *Biochemistry* 37(3):792-799.
- Hackney DD. 1994. The rate-limiting step in microtubule-stimulated ATP hydrolysis by dimeric kinesin head domains occurs while bound to the microtubule. *J Biol Chem* 269(23):16508-16511.
- Haustein E, Schwille P. 2004. Single-molecule spectroscopic methods. *Curr Opin Struct Biol* 14(5):531-540.
- Howard J, Hudspeth AJ, Vale R. 1989. Movement of microtubules by single kinesin molecules. *Nature* 342(Nov. 9):154-158.
- Hua W, Young EC, Fleming ML, Gelles J. 1997. Coupling of kinesin steps to ATP hydrolysis. *Nature* 388(6640):390-393.
- Kandel ER, Schwartz JH, Jessell TM. 1995. *Neurowissenschaften*.
- Kaseda K, Higuchi H, Hirose K. 2003. Alternate fast and slow stepping of a heterodimeric kinesin molecule. *Nat Cell Biol* 5(12):1079-1082.
- Kull FJ, Sablin EP, Lau R, Fletterick RJ, Vale RD. 1996. Crystal structure of the kinesin motor domain reveals a structural similarity to myosin [see comments]. *Nature* 380(6574):550-555.
- Kuznetsov SA, Vaisberg EA, Shanina NA, Magretova NN, Chernyak VY, Gelfand VI. 1988. The quaternary structure of bovine brain kinesin. *Embo J* 7(2):353-356.
- Lakowicz J. 1999. *Principles of Fluorescence Spectroscopy*.
- Lasek RJ. 1967. Bidirectional transport of radioactively labelled axoplasmic components. *Nature* 216(5121):1212-1214.
- Lodish H, Berk A, Zipursky SL, Matsudaira P, Baltimore D, Darnell JE. 2000. *Molecular Cell Biology*. 4th ed.
- Ma YZ, Taylor EW. 1997. Interacting head mechanism of microtubule-kinesin ATPase. *J Biol Chem* 272(2):724-730.
- Niclas J, Navone F, Hom-Booher N, Vale RD. 1994. Cloning and localization of a conventional kinesin motor expressed exclusively in neurons. *Neuron* 12(5):1059-1072.
- Rice S, Lin AW, Safer D, Hart CL, Naber N, Carragher BO, Cain SM, Pechatnikova E, Wilson-Kubalek EM, Whittaker M, Pate E, Cooke R, Taylor EW, Milligan RA, Vale RD. 1999. A structural change in the kinesin motor protein that drives motility. *Nature* 402(6763):778-784.
- Sablin EP, Fletterick RJ. 2001. Nucleotide switches in molecular motors: structural analysis of kinesins and myosins. *Curr Opin Struct Biol* 11(6):716-724.
- Sako Y, Uyemura T. 2002. Total internal reflection fluorescence microscopy for single-molecule imaging in living cells. *Cell Struct Funct* 27(5):357-365.

- Schief WR, Clark RH, Crevenna AH, Howard J. 2004. Inhibition of kinesin motility by ADP and phosphate supports a hand-over-hand mechanism. *Proc Natl Acad Sci U S A*.
- Schneckenburger H. 2005. Total internal reflection fluorescence microscopy: technical innovations and novel applications. *Curr Opin Biotechnol* 16(1):13-18.
- Schnitzer MJ, Block SM. 1997. Kinesin hydrolyses one ATP per 8-nm step. *Nature* 388(6640):386-390.
- Seiler S, Kirchner J, Horn C, Kallipolitou A, Woehlke G, Schliwa M. 2000. Cargo binding and regulatory sites in the tail of fungal conventional kinesin. *Nat Cell Biol* 2(6):333-338.
- Sheetz MP, Kuo SC. 1993. Tracking nanometer movements of single motor molecules. *Methods Cell Biol* 39:129-136.
- Stenoien DL, Brady ST. 1997. Immunochemical analysis of kinesin light chain function. *Mol Biol Cell* 8(4):675-689.
- Svoboda K, Schmidt CF, Schnapp BJ, Block SM. 1993. Direct observation of kinesin stepping by optical trapping interferometry [see comments]. *Nature* 365(6448):721-727.
- Vale RD, Fletterick RJ. 1997. The design plan of kinesin motors. *Ann Rev Cell Dev Biol* 13:745-777.
- Vale RD, Reese TS, Sheetz MP. 1985. Identification of a novel force-generating protein, kinesin, involved in microtubule-based motility. *Cell* 42(1):39-50.
- Valentine MT, Gilbert SP. 2007. To step or not to step? How biochemistry and mechanics influence processivity in Kinesin and Eg5. *Curr Opin Cell Biol* 19(1):75-81.
- Verbrugge S, Kapitein LC, Peterman EJ. 2007. Kinesin moving through the spotlight: single-motor fluorescence microscopy with submillisecond time resolution. *Biophys J* 92(7):2536-2545.
- Verhey KJ, Lizotte DL, Abramson T, Barenboim L, Schnapp BJ, Rapoport TA. 1998. Light chain-dependent regulation of Kinesin's interaction with microtubules. *J-Cell-Biol* 143(4):1053-1066 issn: 0021-9525.
- Woehlke G, Ruby AK, Hart CL, Ly B, Hom-Booher N, Vale RD. 1997. Microtubule interaction site of the kinesin motor. *Cell* 90(2):207-216.
- Woehlke G, Schliwa M. 2000. Walking on two heads: the many talents of kinesin. *Nat Rev Mol Cell Biol* 1(1):50-58.
- Yildiz A, Tomishige M, Vale RD, Selvin PR. 2004. Kinesin walks hand-over-hand. *Science* 303(5658):676-678.

2 Molecular determinants of processivity in kinesin

2.1 Abstract

The protein family of kinesins can be divided in processive and non-processive motors. Processive motors have the ability to move along microtubules in a stepwise fashion without detaching. Non-processive motors detach after every cycle of ATP hydrolysis. To find out which parts of kinesin are required for coupling of kinesin's two motor heads, chimaeras with swapped domains of the processive *Neurospora crassa* kinesin (NcKin) and its non-processive counterpart NcKin3 were tested for their motile properties. The chimaera with the NcKin motor domain and the NcKin3 neck/stalk portion moved processively along microtubules although with a significantly decreased average runlength, suggesting a perturbing effect of the non-processive neck. The reverse chimaera containing motor domains of the non-processive kinesin NcKin3 was unable to perform processive movement, despite the presence of the Kinesin-1 neck coiled-coil. These observations suggest that determinants of processivity are in the motor core and that this processive movement is enhanced by the neck. The present thesis contributed the characterisation of multiple and single-molecule motility assays to the study.

2.2 Introduction

Conventional kinesin is the founding member of the kinesin superfamily and belongs to the class of Kinesin-1 motors (Lawrence *et al.*, 2004; Vale *et al.*, 1985). Its stepwise movement over long distances without detachment from the filament is one of its astonishing properties. This processive behaviour can be explained by the hand-over-hand model, which is now in principle commonly accepted (Hackney, 1995; Ma and Taylor, 1997; Yildiz *et al.*, 2004). Here, the movement is based on the alternated binding of the two motor heads to the following microtubule binding site. The rear head does not detach from the microtubule before the front head has bound tightly. This mechanism requires precisely coordinated microtubule affinities of the two motor domains. Otherwise, the motor would dissociate from the microtubule in between steps, or stick to the filaments when both motor domains are in a strong microtubule binding state (Crevel *et al.*, 2004; Cross, 2004; Hackney, 1994; Howard *et al.*, 1989).

This remarkably fine-tuned coordination is supported by several structural and kinetic properties. Some models predict that intramolecular strain between leading and trailing head builds up and controls coordination (Guydosh and Block, 2006; Hancock and Howard, 1999; Rosenfeld *et al.*, 2003). However, the size of this force is unclear and hard to measure, and thus the precise mechanism how strain is linked to motor kinetics is unknown.

To locate structural determinants involved in processive head-head coordination, we made use of chimaeric kinesins of a processive, conventional Kinesin-1 motor, and a recently discovered dimeric Kinesin-3 motor that is not processive but also moves to the microtubule plus-end (Adio *et al.*, 2006). This is in contrast to previous studies which investigated chimaeras with the non-processive, minus-end directed kinesin Ncd. These studies found, that the directionality is not determined by the motor domain, but it influences the processivity of the motor (Case *et al.*, 1997; Henningsen and Schliwa, 1997; Hirose *et al.*, 2000). The present question is, whether the processivity is also influenced if the motor domains have the same directionality and whether it is possible to transfer processivity to a non-processive motor.

2.3 Results

2.3.1 Design of chimaeras

Chimaeras with swapped motor domains of the fungal kinesins NcKin and NcKin3 served as experimental models for the present study (Figure 2.1). NcKin is a 'conventional' processive Kinesin-1, whereas NcKin3 is a non-processive Kinesin-3 (Adio et al., 2006; Jaud et al., 2006; Lakamper et al., 2003). One construct contained NcKin's motor head attached to the neck of NcKin3 (Head1/Neck3). The reverse chimaera contained the motor head of NcKin3 joined with the neck of NcKin (Head3/Neck1). The fusion points were chosen between the neck-linker and the neck coiled-coil. We then asked which part of the motor was necessary and sufficient for processive movement.

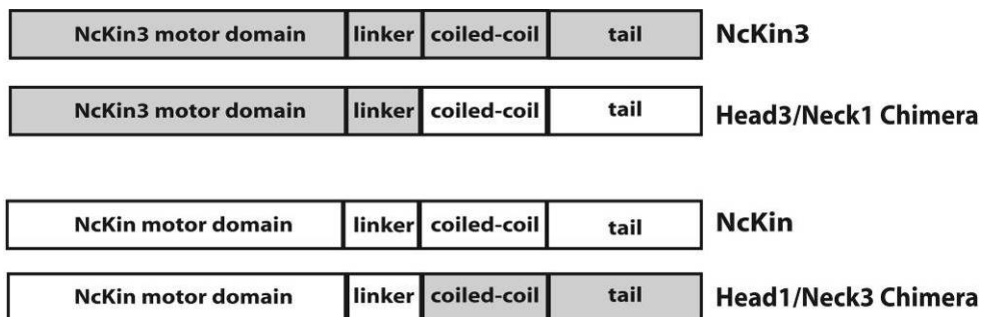


Figure 2.1 Design of chimeric kinesins.

The motor domain and neck-linker of the processive Kinesin-1 motor (amino acids 1-342) was connected to the coiled-coil and tail domain of the non-processive Kinesin-3 motor (amino acids 428 to 558). This construct was named Head1/Neck3 chimaera. Vice versa, the Head3/Neck1 chimaera was generated by fusing the Kinesin-3 motor domain and linker region (amino acids 1-429) to the coiled coil of the NcKin protein (amino acids 340-433).

2.3.2 Co-operative gliding behaviour

In multi-motor gliding assays, motors were attached to the coverslip, and fluorescently labelled microtubules were transported over the surface. The velocity of microtubule transport is an indirect measurement for the velocity of the motors. In general, the coating density of motors on a coverslip influences the microtubule gliding velocity, and only in the special case of processive motors the velocity is independent of the motor density (Howard et al., 1989). While non-processive kinesins work in a cooperative manner, a single processive kinesin displaces microtubules at the same

speed as multiple kinesins. Thus, the dependence on the coating density is the first hint if a motor is processive or not. The Head1/Neck3 chimaera showed similar gliding velocities at high and low coating density to wildtype NcKin ($1.48 \pm 0.01 \mu\text{m/s}$ at $1.6 \mu\text{M}$ and $1.61 \pm 0.03 \mu\text{m/s}$ at $0.3 \mu\text{M}$). In contrast, gliding velocity of the NcKin3 reference construct was accelerated at higher motor densities (Adio *et al.*, 2006). The reverse chimaera Head3/Neck1 was not accelerated by higher motor coating densities. In fact, gliding velocity decreased from $0.58 \pm 0.04 \mu\text{m/s}$ at low densities to $0.45 \pm 0.01 \mu\text{m/s}$ at high densities, indicating mutual hindrance of the motors.

To further investigate the processivity of the kinesin mutants, we observed microtubule transport by a single motor. Therefore, the motor density was decreased to the point, where a microtubule can only be bound by one kinesin. Under these conditions the microtubule can pivot around its anchoring point during displacement and is never displaced further than its own length (Figure 2.2 A). The observation of this special behaviour provides strong evidence for processivity.

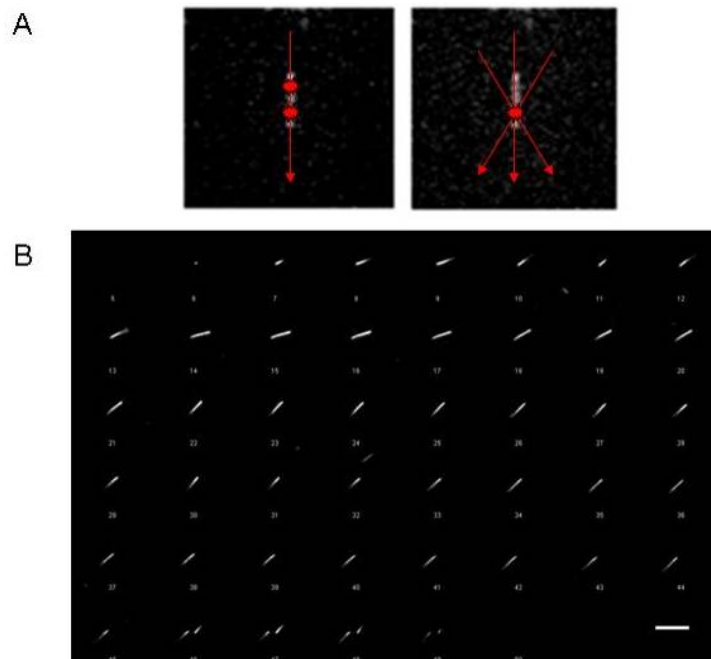


Figure 2.2 Pivoting in the conventional gliding assay.

(A) Attachment points of kinesins are indicated in red, moving direction of the microtubules with red arrows. If only one kinesin binds the microtubule, the direction of movement pivots around this point. (B) Gliding assay with Head1/Neck3 chimaera shows pivoting around one point. The microtubule is only displaced its own length. Scale bar $5 \mu\text{m}$.

Both NcKin and the Head1/Neck3 chimaera showed characteristic pivoting behaviour (Figure 2.2 B), suggesting that they are processive enzymes. Pivoting at low motor densities was never observed for NcKin3 and the Head3/Neck1 chimaera.

Additionally, microtubules moved further than their own length, indicating, that more than one kinesin is necessary to displace a microtubule. It is therefore most likely that NcKin3 and the Head3/Neck1 chimaera are non-processive motors.

2.3.3 Single-molecule behaviour

To directly prove processivity of the Head1/Neck3 chimaera, we tested the mutants along with wildtype references in single-molecule motility assays. Fluorescently labelled kinesin motors were observed over time in a TIRF-microscope to detect processive runs. Similar to the NcKin wildtype reference, the Head1/Neck3 mutant moved continuously along microtubules (Figure 2.3) at a velocity of $1.40 \pm 0.03 \mu\text{m/s}$ (mean \pm S.E.) and over distances of up to $3 \mu\text{m}$ (Table I, Figure 2.3).

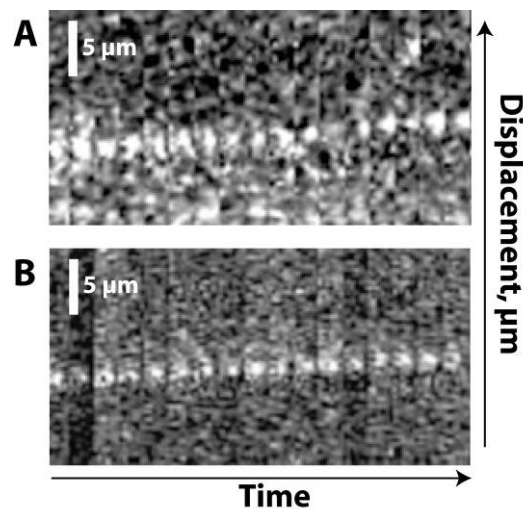


Figure 2.3 Single-molecule properties of the Head1/Neck3 chimaera.

(A) Kymographs show displacements of a single fluorophore-labelled Head1/Neck3 motors along the microtubule. (B) Wildtype NcKin was used as a control. Isolated chimeric motors performed processive runs on a microtubule with a velocity essentially identical to the average velocity under multiple motor conditions. Motors were observed for 5 sec with an integration time of 200 ms at an ATP concentration of $20 \mu\text{M}$.

To quantify the extend of processivity, the runlength of the chimeric kinesins was measured. For that purpose the histogram containing the runlength of 74 individual motors was analysed by single exponential curve fitting. The runlength of the

Head1/Neck3 chimaera was $0.67 \pm 0.13 \mu\text{m}$ which is 2-3-fold shorter than for wildtype NcKin ($\sim 1.8 \mu\text{m}$, (Lakamper *et al.*, 2003)) (Table I, Figure 2.4).

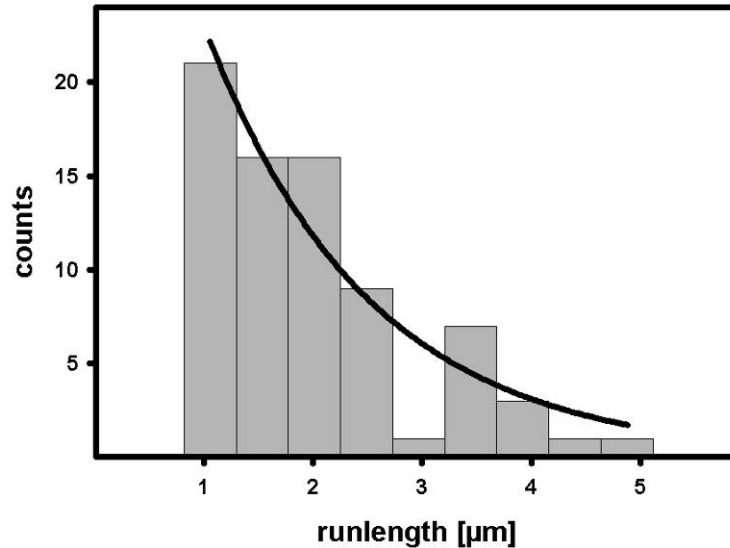


Figure 2.4 Runlength of the Head1/Neck3 chimaera.

The runlengths of the Head1/Neck3 chimaera was plotted in a histogram and fitted with an exponential decay ($0.67 \pm 0.13 \mu\text{m}$). Short runlengths are probably underestimated due to limited time resolution (200 ms integration time).

The reverse Head3/Neck1 chimaera never showed any processive runs under single molecule conditions. Together with the observations from multi-motor gliding assays we can state that this motor is non-processive. Our data show that the motor domain of processive NcKin is able to induce processive behaviour in otherwise non-processive NcKin3. Conversely, the results show that the neck of NcKin3 is capable to join two kinesin motor domains in a way that promotes processive motility, albeit to reduced extent compared to the NcKin wildtype control.

Table I: Gliding velocities and runlengths of chimeric and wild type motors

Construct	Velocity [$\mu\text{m/s}$] (multi-motor)	Velocity [$\mu\text{m/s}$] (single-molecule)	Runlength [μm] (single-molecule)
NcKin3 (Adio et al., 2006)	0.52 ± 0.04	n/a	n/a
Head3/Neck1	0.58 ± 0.04 n=90	n/a	n/a
NcKin	2.29 ± 0.01 n=60	2.38 ± 0.01 n=16	1.75 ± 0.09 (Lakamper and Meyhofer, 2005)
Head1/Neck3	1.60 ± 0.02 n=120	$1.40 \pm 0.03 \mu\text{m/s}$ n=80	$0.67 \pm 0.13 \mu\text{m}$ n=74

n/a: not applicable

2.4 Discussion

The chimaeras showed that on one hand, the motor domain determines the processivity and on the other hand, that the stalk/neck domain can influence the grade of processivity. The Head1/Neck3 had some structural elements which were sufficient to transfer the ability to step continuously into a non-processive background. These structural elements are obviously absent in the reverse construct, Head3/Neck1, which is unable to move processively, despite its Kinesin-1 neck domain. These findings are in good agreement with data obtained from chimaeras with the non-processive Ncd (Case *et al.*, 1997). Transferring the motor domain of Ncd to a processive motor also yielded in a non-processive motor. Taken together, it does not matter which directionality or processivity the motor domain had as a wildtype protein, the structural elements for processivity lie within the motor domain.

In addition to the information on motor domain, our study also reveals important features of kinesin's neck. In agreement with previous studies, the Head1/Neck3 construct (lacking the conventional neck-domain) shows severely altered processivity. Mutational analysis of the conventional kinesin neck suggested that passive mechanical features (stiffness, in particular) affect the runlengths of processive kinesins, and is optimised in wildtype (Jaud *et al.*, 2006). The Head1/Neck3 chimaera showed a slower velocity and diminished runlength, indicating that the likelihood of

forward stepping is generally affected. Apparently, the wildtype neck of processive kinesins minimizes the time required for diffusive search for the next microtubule-binding site while the coiled coil of NcKin3 impairs positioning of the diffusing head.

Which are the physical counterparts of the structural elements in the motor domain which mediate processivity? From previous studies it is known, that the neck-linker is crucial for motility (Rice *et al.*, 1999). The neck-linker is a short stretch of about 15 aa, which links the head with the neck. During the chemo-mechanical cycle the neck-linker undergoes conformational changes and docks to the motor core upon ATP binding. This neck-linker docking is thought to induce forward stepping of the other head. Furthermore, current models explain the coordination between motor heads with intramolecular strain which is built on the neck-linker (Guydosh and Block, 2006; Hyeon and Onuchic, 2007; Rosenfeld *et al.*, 2003). Mounting experimental evidence suggests that the leading motor head of conventional kinesin is inhibited in its ATP binding as long as the lagging head remains filament-bound. That way, the motor prevents premature detachment and achieves directed stepping to the microtubule plus-end. As all constructs of this study contained motor core and neck-linker of its parent motor, the motor core / neck-linker interaction is a likely structural element for determining processivity.

2.5 Methods

2.5.1 Cloning, protein expression and purification

Wildtype reference constructs were prepared as described (Bathe *et al.*, 2005). For the generation of the Head1/Neck3 chimaera the N-terminal 342 amino acids of the NcKin436 proteins were amplified from the pT7-NKin436 expression vector by PCR. The reverse primer introduced a *Bs*WII restrictions site at the C-terminus of the NcKin head domain that allowed replacement of the codons for the N-terminal 427 amino acids in pT7-NcKin3_558cys and pT7-NcKin3_558hTail plasmids.

For generation of the Head3/Neck1 chimaera the N-terminal 429 amino acids of NcKin3 were amplified by PCR on basis of the pT7-NcKin3_558cys plasmid. Here, the reverse primer introduced a *Ngo*MIV restriction site at the C-terminus of the head domain that allowed replacement of the NcKin head domain in the pT7-NKin436 and pT7-NcKin436_hTail plasmids.

All constructs that do not contain the human kinesin Tail (hTail) sequence have a short peptide sequence added to the C-terminus that confers a reactive cysteine to the protein (PSIVHRKCF, (Itakura *et al.*, 1993)). This allows labelling with maleimide compounds.

Expression and purification of the proteins was performed as described in (Adio *et al.*, 2006). Microtubules were prepared from pig brain tubulin (Mandelkow *et al.*, 1985), the Atto488 and Biotin labelling of tubulin, and the polymerisation of microtubules were performed as described in (Hyman *et al.*, 1991). For kinetic experiments microtubules were treated with apyrase 0.01 U/ml prior to centrifugation.

2.5.2 Gliding assays

A flow cell was incubated for 5 min with hTail-tagged motors in motility buffer (10 mM MgCl₂, 10 mM ATP, 100 mM KCl, 20 µM paclitaxel, 1 mg/ml BSA, 0.8 mg/ml casein in BRB80+ (80 mM PIPES·KOH, pH 6.8, 5 mM MgCl₂, 1 mM EGTA)). After washing with blocking buffer (1 mg/ml BSA, 0.8 mg/ml casein in BRB80+), the flow chamber was filled with Atto488-labelled microtubules in motility buffer. Both kinesin and microtubule solutions were supplied with an oxygen scavenging system (0.1 mg/ml glucose oxidase, 0.02 mg/ml catalase, 2.25 mg/ml glucose). Gliding of the microtubules was observed with a total internal reflection (TIRF) microscope and gliding velocity of individual microtubules was measured using the manufacturers' software (Olympus Biosystems GmbH, Planegg, Germany). For statistical analysis SigmaPlot 2000 Software (Systat, Point Richmond, CA, USA) was used.

2.5.3 Single-molecule motility assays

Motors were labelled with the maleimide conjugate of the Atto488-fluorophore (ATTOtec GmbH, Siegen, Germany). Biotin-labelled microtubules were fixed on the surface of a flow chamber which was incubated with 2 mg/ml BSA-biotin (Sigma-Aldrich Co., St. Louis, MO, USA) and subsequently with 1 mg/ml Streptavidin in BRB80+ buffer and 20 µM taxol. After washing with 1 mg/ml BSA in BRB80+ motility mix (0.1-0.5 nM Atto488-labeled kinesin, 20 µM - 2 mM ATP, oxygen scavenger (see above), 0.2 mg/ml casein, 100 mM KCl in BRB80+) was flushed in. The gliding activity was observed in an Olympus IX71 TIRF microscope with an excitation wavelength of 488 nm and a Hamamatsu C-9100 front-illuminated CCD-camera. The optical resolution was 160 nm per 2x2-binned pixel with an integration time of 200 ms.

2.6 References

- Adio, S., Bloemink, M., Hartel, M., Leier, S., Geeves, M.A. and Woehlke, G. (2006) Kinetic and mechanistic basis of the non-processive Kinesin-3 motor NcKin3. *J Biol Chem*.
- Adio, S., Bloemink, M., Hartel, M., Leier, S., Geeves, M.A. and Woehlke, G. (2006) Kinetic and Mechanistic Basis of the Nonprocessive Kinesin-3 Motor NcKin3. *J. Biol. Chem.*, 281, 37782-37793.
- Bathe, F., Hahlen, K., Dombi, R., Driller, L., Schliwa, M. and Woehlke, G. (2005) The complex interplay between the neck and hinge domains in kinesin-1 dimerization and motor activity. *Mol Biol Cell*, 16, 3529-3537.
- Case, R.B., Pierce, D.W., Hom Booher, N., Hart, C.L. and Vale, R.D. (1997) The directional preference of kinesin motors is specified by an element outside of the motor catalytic domain. *Cell*, 90, 959-966 issn: 0092-8674.
- Crevel, I.M., Nyitrai, M., Alonso, M.C., Weiss, S., Geeves, M.A. and Cross, R.A. (2004) What kinesin does at roadblocks: the coordination mechanism for molecular walking. *Embo J*, 23, 23-32.
- Cross, R.A. (2004) The kinetic mechanism of kinesin. *Trends Biochem Sci*, 29, 301-309.
- Guydosh, N.R. and Block, S.M. (2006) Backsteps induced by nucleotide analogs suggest the front head of kinesin is gated by strain. *Proc Natl Acad Sci U S A*, 103, 8054-8059.
- Hackney, D.D. (1994) Evidence for alternating head catalysis by kinesin during microtubule-stimulated ATP hydrolysis. *Proc Natl Acad Sci U S A*, 91, 6865-6869.
- Hackney, D.D. (1995) Highly processive microtubule-stimulated ATP hydrolysis by dimeric kinesin head domains. *Nature*, 377, 448-450.
- Hancock, W.O. and Howard, J. (1999) Kinesin's processivity results from mechanical and chemical coordination between the ATP hydrolysis cycles of the two motor domains. *Proc Natl Acad Sci U S A*, 96, 13147-13152.
- Henningsen, U. and Schliwa, M. (1997) Reversal in the direction of movement of a molecular motor [see comments]. *Nature*, 389, 93-96 issn: 0028-0836.
- Hirose, K., Henningsen, U., Schliwa, M., Toyoshima, C., Shimizu, T., Alonso, M., Cross, R.A. and Amos, L.A. (2000) Structural comparison of dimeric Eg5, *Neurospora* kinesin (Nkin) and Ncd head-Nkin neck chimera with conventional kinesin. *Embo J*, 19, 5308-5314.
- Howard, J., Hudspeth, A.J. and Vale, R. (1989) Movement of microtubules by single kinesin molecules. *Nature*, 342, 154-158.
- Howard, J., Hudspeth, A.J. and Vale, R.D. (1989) Movement of microtubules by single kinesin molecules. *Nature*, 342, 154-158.

- Hyeon, C. and Onuchic, J.N. (2007) Mechanical control of the directional stepping dynamics of the kinesin motor. *Proc Natl Acad Sci U S A*.
- Hyman, A., Drechsel, D., Kellogg, D., Salser, S., Sawin, K., Steffen, P., Wordeman, L. and Mitchison, T. (1991) Preparation of modified tubulins. *Methods Enzymol*, 196, 478-485.
- Itakura, S., Yamakawa, H., Toyoshima, Y.Y., Ishijima, A., Kojima, T., Harada, Y., Yanagida, T., Wakabayashi, T. and Sutoh, K. (1993) Force-generating domain of myosin motor. *Biochem Biophys Res Commun*, 196, 1504-1510.
- Jaud, J., Bathe, F., Schliwa, M., Rief, M. and Woehlke, G. (2006) Flexibility of the neck domain enhances Kinesin-1 motility under load. *Biophys J*.
- Lakamper, S., Kallipolitou, A., Woehlke, G., Schliwa, M. and Meyhofer, E. (2003) Single fungal kinesin motor molecules move processively along microtubules. *Biophys J*, 84, 1833-1843.
- Lakamper, S. and Meyhofer, E. (2005) The E-hook of tubulin interacts with kinesin's head to increase processivity and speed. *Biophys J*, 89, 3223-3234.
- Lawrence, C.J., Dawe, R.K., Christie, K.R., Cleveland, D.W., Dawson, S.C., Endow, S.A., Goldstein, L.S., Goodson, H.V., Hirokawa, N., Howard, J., Malmberg, R.L., McIntosh, J.R., Miki, H., Mitchison, T.J., Okada, Y., Reddy, A.S., Saxton, W.M., Schliwa, M., Scholey, J.M., Vale, R.D., Walczak, C.E. and Wordeman, L. (2004) A standardized kinesin nomenclature. *J Cell Biol*, 167, 19-22.
- Ma, Y.Z. and Taylor, E.W. (1997) Interacting head mechanism of microtubule-kinesin ATPase. *J Biol Chem*, 272, 724-730.
- Mandelkow, E.M., Herrmann, M. and Ruhl, U. (1985) Tubulin domains probed by limited proteolysis and subunit-specific antibodies. *J Mol Biol*, 185, 311-327.
- Rice, S., Lin, A.W., Safer, D., Hart, C.L., Naber, N., Carragher, B.O., Cain, S.M., Pechatnikova, E., Wilson-Kubalek, E.M., Whittaker, M., Pate, E., Cooke, R., Taylor, E.W., Milligan, R.A. and Vale, R.D. (1999) A structural change in the kinesin motor protein that drives motility. *Nature*, 402, 778-784.
- Rosenfeld, S.S., Fordyce, P.M., Jefferson, G.M., King, P.H. and Block, S.M. (2003) Stepping and stretching. How kinesin uses internal strain to walk processively. *J Biol Chem*, 278, 18550-18556.
- Vale, R.D., Reese, T.S. and Sheetz, M.P. (1985) Identification of a novel force-generating protein, kinesin, involved in microtubule-based motility. *Cell*, 42, 39-50.
- Yildiz, A., Tomishige, M., Vale, R.D. and Selvin, P.R. (2004) Kinesin walks hand-over-hand. *Science*, 303, 676-678.

3 Kinesin-1's neck-linker docking

3.1 Abstract

Kinesin-1 motor proteins step along microtubules by a mechanism in which the heads alternate between microtubule-bound and unbound states in a highly coordinated fashion. This coordination is supported by the action of the neck-linker that docks onto the core motor domain upon ATP binding. The introduction of crosslinkable cysteins gave us the possibility to simulate a continuously docked neck-linker. Here, we investigate the motility properties and the microtubule affinities of docked and undocked neck-linker mutants. The motility of Kinesin-1 motors is severely affected for docked neck-linker. This could be due to a lower microtubule affinity in this conformation. Based on our experiments we suggest that the neck-linker docking alters the microtubule affinity of the individual heads during the chemo-mechanical cycle. The study was initiated by Katrin Hahlen; the contribution of the present thesis was the direct measurement of binding affinities and the confirmation of motility data.

3.2 Introduction

Most dimeric kinesins generate motility by the alternating action of two identical motor domains (Hackney, 1995; Hancock and Howard, 1998; Ma and Taylor, 1997; Yildiz *et al.*, 2004). For this hand-over-hand mechanism, one head has to remain bound to the microtubule until the second head binds simultaneously. Consequently, the intermediate state, where one nucleotide-free head is strongly attached to the filament, while the other one remains in a weakly microtubule-binding ADP state is crucial (Figure 3.1). Upon ATP-binding, a very rapid structural change of the neck-linker of the microtubule-bound motor head occurs that allows the partner head to lose its ADP and to bind tightly to the microtubule (Rosenfeld *et al.*, 2002).

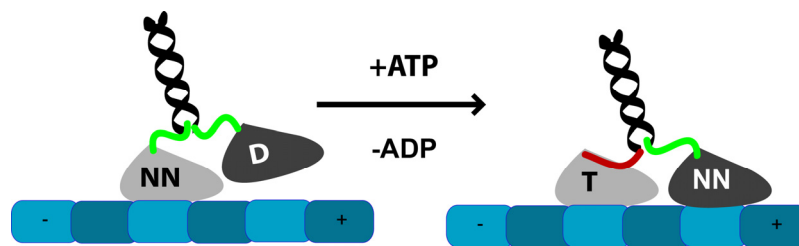


Figure 3.1 Neck-linker docking upon ATP binding.

In the ATP waiting state, one head (light grey) binds tightly to the microtubule (blue), while the other one (dark grey) is free to diffuse. Both neck-linkers are undocked (green) until ATP binds to the microtubule bound head. Then the neck-linker docks (red) and the second head binds to the adjacent microtubule binding domain. After ATP hydrolysis the neck-linker undocks and the head detaches (not shown). (NN: no nucleotide is bound to the nucleotide binding pocket; T: ATP is bound; D: ADP is bound)

The neck-linker, a short stretch of ~15 amino acid residues that follows C-terminally from the catalytic core motor domain, is thought to exist in at least two different conformations, one that is docked or 'zippered' to the motor core, and a flexible undocked structure (Rice *et al.*, 2003; Rice *et al.*, 1999).

The docked neck-linker is visible in some crystal structures (Sack *et al.*, 1997; Sindelar *et al.*, 2002), and its path along microtubule-bound kinesin has been deduced from cryo-EM (Rice *et al.*, 1999; Skiniotis *et al.*, 2003). According to these data, the neck-linker docks along a groove in the core motor domain where it is held by a meshwork of hydrogen bonds. The nature of the undocked conformation is not

clear, and might differ in truncated, monomeric constructs (that have been used for many of the structural investigations) and dimeric ones.

To explain the mechanism of Kinesin-1 motility the conformational change of the neck-linker has been used. It is thought that neck-linker docking allows or causes the second head to bind to the adjacent microtubule-binding site. It has been shown that the neck-linker is important to provide energy and to determine directionality (Rice et al., 2003). Furthermore, it provides the spatial freedom to bridge the 8 nm gap between adjacent microtubule binding-sites. Motility assays with arrested neck-linker in the docked state by disulfide bonds failed to step, supporting the structural importance of the neck-linker region (Tomishige and Vale, 2000). However, the reality is more complex because from the crystal structure and the known geometry of the kinesin-microtubule complex a strain is predicted to arise between the two heads when they are in the intermediate state where both heads bind simultaneously. This strain is thought to change the kinetic properties of the motor domains and facilitates dissociation of the rear head, and/or slows down the ATP binding of the leading head (Carter and Cross, 2005; Crevel *et al.*, 2004; Hackney, 2002; Rosenfeld *et al.*, 2003). The models assume that the leading, nucleotide-free head possesses a flexible neck-linker that exerts a strain on its rear partner (Figure 3.1). This strain has been proposed to accelerate dissociation of the rear head from the microtubule (Carter and Cross, 2005; Crevel *et al.*, 2004; Hackney, 2002; Rosenfeld *et al.*, 2003). In addition, the rearward strain on the leading head seems to inhibit ATP binding, which keeps the head in a strong microtubule binding state and prevents premature release (Rosenfeld *et al.*, 2003). According to these models, the neck-linker thus plays a central role in the generation of motility by altering the kinetic properties of the motor heads during the chemo-mechanical cycle.

The present study tests whether there are other effects that prevent motility of kinesins with immobilised neck-linker besides restricting the diffusional freedom of the leading head. Our results on crosslinked neck-linker mutants show that indeed there is another effect, namely an altered microtubule affinity.

3.3 Results

3.3.1 Mutant design and proof of expected disulfide bonds

Kinesin-1's neck-linker plays an important mechanical role in the generation of movement, and a permanently docked neck-linker prevents microtubule motility (Tomishige and Vale, 2000). In the Tomishige/Vale study, the neck-linker was kept in a docked state by inducing disulfide bonds between neck-linker and motor core. It was suggested that the crosslinked neck-linker of the microtubule-bound head restricts the mobility of the second, unbound kinesin head in a way that does not allow stepping. But how is the unbound head prevented from stepping and are there other effects caused by neck-linker immobilisation? We therefore looked for possible effects of neck-linker docking, and cloned NcKin kinesin constructs in which we introduced pairs of crosslinkable cysteine residues at the interface between neck-linker and motor core (Figure 3.2). The initial NcKin kinesin had two residual cysteines, which are not surface exposed and therefore not able to form disulfide-bridges (cysteine-light construct). The choice of the fungal Kinesin-1 NcKin, which is much faster than conventional kinesins from animals, was made to amplify the effects of the crosslinked neck-linker.

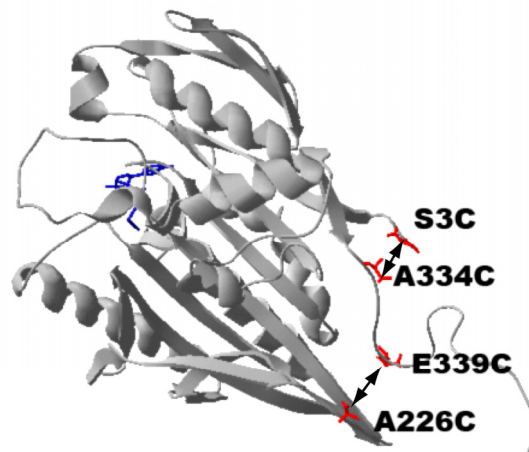


Figure 3.2 Positions of crosslinked residues in crystal structure model.

The figure shows a crystallographic model of the motor domain of *Neurospora crassa* Kinesin-1 (1GOJ). Residues mutated into cysteines to form disulfide bonds are shown in red. Crosslinks are indicated by arrows. The model was generated in SwissPDB Viewer.

To immobilize the neck-linker, two different positions were chosen (S3C-A334C, brief: SA-crosslink and A226C-E339C, AE-crosslink). Judged from the distances in crystal structures (Protein Data Bank Numbers: 1GOJ, 2KIN, 1MJK), these pairs of residues are supposed to form disulfide bonds without major structural distortions. The AE-crosslink fixes the neck-linker over its entire length, whereas the SA-crosslink is located rather in the middle. Beside monomeric constructs (NK343), dimeric constructs with a human kinesin tail (NK436hKT) were cloned to attach them to glass surfaces in motility assays.

The formation and the positions of the disulfide bonds were confirmed by ESI-Q-TOF mass spectrometry (done by Jörg Reinders and Albert Sickmann from the Rudolf-Virchow-Centre for Experimental Biomedicine, University Würzburg). The untreated NK343-AE protein had the predicted total mass of 37219.8 Da and was detected at the expected size. Under oxidizing conditions (DTNB treatment), it could be carbamidomethylated at two positions, leading to an increase in mass of 114.0 Da. Under reducing conditions (DTT treatment), 4 residues were modified (two from the crosslink and two residual endogenous cysteines). MALDI-LIFT-MS/MS showed that the endogenous residues are also modified under oxidizing conditions only, implying that the introduced residues form the expected disulfide bond.

3.3.2 Motility behaviour

As a start, the effect of disulfide bonds on the motor activity of NcKin436hKT mutants was measured. By contrast to the wildtype control (2.41 $\mu\text{m}/\text{sec}$), all crosslinked kinesin mutants slowed down to velocities in multiple motor gliding assays: 0.07 $\mu\text{m}/\text{sec}$ for the SA-crosslink and 0.26 $\mu\text{m}/\text{sec}$ for the AE-crosslink (Table I). The calculated residual velocity of 12% of the AE-crosslink mutant is an upper limit because huge variations in the behaviour of individual microtubules were observed. The more drastic effect was observed in the SA mutant that only showed 3% residual gliding velocity. In general, moving microtubules were extremely rare, and those that were displaced usually stalled after a very brief period of time (< 1-2 s). As described further below, this behaviour is most likely due to the presence of a mixed population of crosslinked, inactive motors, with a small contamination of uncrosslinked, and therefore wildtype-like proteins.

Table I Effect of oxidation on the gliding velocities of NcKin cysteine mutants.

The table summarises the gliding velocities of reduced (DTT) and oxidised (DTNB) NcKin mutants, and oxidized proteins after rescue with excess DTT. The values give average microtubule gliding velocities \pm SEM in $\mu\text{m/s}$ (usually averages of 20–25 microtubules; for some weakly microtubule-binding preparations 7-15), and the number of independent preparations tested (n).

Constructs	Gliding velocities [$\mu\text{m/s}$]			
	DTT	DTNB	Residual gliding ability	Rescue
NcKin	2.53 \pm 0.10; n=3	2.41 \pm 0.06; n=2	-	2.66 \pm 0.22; n=2
NcKin-A226C/E339C	2.13 \pm 0.21; n=3	\leq 0.26 \pm 0.09; n=3	12 %	2.41 \pm 0.18; n=2
NcKin-S3C/A334C	2.32 \pm 0.18; n=2	0.07 \pm 0.01; n=2	3 %	2.20 \pm 0.01; n=2

One possible explanation why the gliding velocities are disturbed is that the second, unbound kinesin head is unable to bind to a new microtubule site. Curiously, in these assays, the gliding activity of crosslinked mutants was not completely abolished. This could be due to the fact that the crosslinked motors still show residual activity, or that oxidation produces a mixed population of crosslinked, fully inactive motors, and uncrosslinked motors with wildtype properties. To learn how a mixture of native and inactive motor behaved, we performed mixed gliding assays. In these assays, the crosslinkable AE and SA-crosslink mutants were mixed with wildtype motor (without reactive cysteine residues) and measured in multiple motor gliding assays. The results showed that adding inactive, crosslinked mutants to active wildtype motors lead to a gradual decrease in gliding velocity. However, both crosslink mutants were very different in their efficiency to slow down the wildtype motor population. Whereas a portion of \sim 50% of the crosslinked SA-mutant led to 50% slower gliding, as few as 1% wildtype kinesin mixed with oxidized AE-mutant still drove half-maximal gliding velocity. These observations prove that very few uncrosslinked motors may have been responsible for the observed residual velocity in assays of the oxidized AE-mutant. Moreover, they suggest that the AE-mutant may have a severely reduced microtubule affinity.

3.3.3 Microtubule affinities

To check whether the AE-crosslink was arrested in a weak microtubule-binding state, the affinities were determined in microtubule co-sedimentation assays (Figure 3.3, Table II). Monomeric and dimeric constructs of both, the AE- and the SA-crosslink, were tested for their ability to bind to microtubules in the presence of ADP and AMP-PNP.

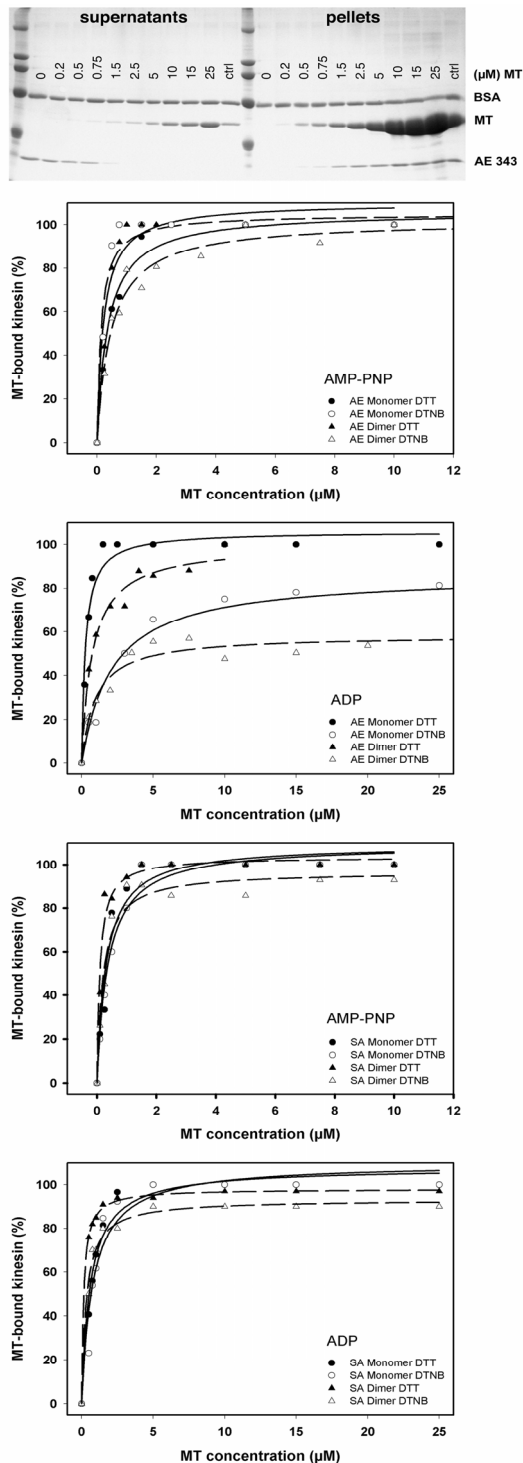


Figure 3.3 Microtubule affinity of mutant kinesins.

To determine the microtubule affinity, a constant amount of kinesin was mixed with increasing amounts of microtubules in the presence of ADP or AMP-PNP. The microtubule-bound kinesin fraction was separated from the unbound fraction by centrifugation. The figure shows an example SDS-gel of an experiment with NcKin-343 AE (top). The protein content per lane was quantified in ImageJ, and plotted against the microtubule concentration (4 graphs below the gel). The top graph plots the binding affinities of AE-crosslink mutants under AMP-PNP conditions, either as monomer (circles) or dimer (triangles), and oxidised (open symbols) or reduced (filled symbols). Experiments in the presence of ADP and experiments with AE-mutants in the presence of AMP-PNP and ADP are shown below. For the affinities listed in table II multiple independent preparations were analysed, and their half-maximal binding concentrations were used to calculate the averaged dissociation constant. The affinities of the monomeric and dimeric AE-crosslink mutants in the presence of ADP were significantly lower in oxidised than in reduced samples.

The analysis showed that the oxidised, crosslinked AE mutant is compromised in its ability to bind microtubules when bound to ADP. The microtubule affinity of the oxidised monomeric mutant decreased roughly 4-fold in the presence of ADP, the affinity of the dimer almost 2-fold (Table II). These differences were significant in the ANOVA ($P < 0.05$), in contrast to the differences of the SA mutant. Noteworthy, the differences in the presence of AMP-PNP were not significant. These assays further substantiated that the crosslinked AE-mutant (but not the SA-mutant) had a weaker affinity to microtubules than wildtype.

Table II Microtubule affinities of crosslinked kinesin mutants.

Dissociation constants of kinesin-microtubule complexes in different nucleotide states were determined by centrifugation. The averages give K_d values \pm SEM and are based on assays on two or three independent preparations.

Construct	ADP		AMP-PNP	
	DTT	DTNB	DTT	DTNB
NcKin-343 A226C/E339C	$0.52 \pm 0.16 \mu\text{M}$	$2.00 \pm 0.14 \mu\text{M}$	$0.25 \pm 0.11 \mu\text{M}$	$0.18 \pm 0.04 \mu\text{M}$
NcKin-436hKT A226C/E339C	$0.58 \pm 0.19 \mu\text{M}$	$1.04 \pm 0.09 \mu\text{M}$	$0.22 \pm 0.10 \mu\text{M}$	$0.41 \pm 0.06 \mu\text{M}$
NcKin-343 S3C/A334C	$1.05 \pm 0.44 \mu\text{M}$	$0.79 \pm 0.01 \mu\text{M}$	$0.25 \pm 0.06 \mu\text{M}$	$0.53 \pm 0.16 \mu\text{M}$
NcKin-436hKT S3C/A334C	$0.22 \pm 0.07 \mu\text{M}$	$0.32 \pm 0.01 \mu\text{M}$	$0.19 \pm 0.08 \mu\text{M}$	$0.44 \pm 0.23 \mu\text{M}$

3.4 Discussion

The neck-linker is known to exist in at least two conformations: one that is captured in some crystal structures, comprises two short β -strands and is associated with the motor core and another one that is less well described structurally, but is known to be flexible based on EPR studies (Kozielski *et al.*, 1997; Rice *et al.*, 2003; Rice *et al.*, 1999; Sindelar *et al.*, 2002; Song *et al.*, 2001). Kinesin is thought to switch between these two states during its chemo-mechanical cycle. According to previous studies, microtubule-bound, nucleotide-free kinesin has an undocked neck-linker, and transits into the docked neck-linker state very rapidly upon binding of ATP (Rosenfeld *et al.*, 2002). Neck-linker docking is thought to be 'kinesin's first step' that induces stepping of the other, unbound head.

The importance to switch between docked and undocked positions was demonstrated in a study where disulfide bonds were introduced to immobilise kinesin's neck-linker (Tomishige and Vale, 2000). This manipulation led to the disruption of motility on the single-molecule level, suggesting that the 'second' kinesin head was unable to step forwards, and the dimer was arrested in a microtubule-bound state. The present study uses the same technique to further characterise the intermediate that is trapped by the permanently docked neck-linker. Is this intermediate trapped only because of the restricted diffusional freedom of the leading head or also by altering the kinetic properties of the motor heads?

Our data confirm that the arrested neck-linker prevents motility regardless of the position of the crosslink. In contrast to the previous study (Tomishige and Vale, 2000) we find that neck-linker immobilisation can also lead to an almost complete inhibition of activity. However, the neck-linker needs a conformational flexibility to achieve normal enzymatic activity. But how does the docked neck-linker state inhibit the motor activity? The primary effect of neck-linker docking seems to be a reduction of microtubule affinity that was observed in competitive gliding assays with crosslinked and wildtype NcKin. For the AE-crosslink 1% wildtype protein was enough to show residual gliding, which is an order of magnitude higher microtubule affinity for the wildtype. In the case of the SA-crosslink this effect was observed not before 50% wildtype protein, indicating a less pronounced microtubule affinity effect.

This microtubule affinity defect was confirmed in microtubule co-sedimentation assays for the AE-crosslink (Figure 3.3). Binding kinesins to microtubules with ADP

simulates the ATP waiting state (Figure 3.1, first intermediate), where both neck-linker are usually undocked. At least, Rice *et al.* (1999) found the microtubule-bound ADP form of kinesin in a non-docked neck-linker conformation. An artificially docked neck-linker yields in a higher dissociation rate and is therefore probably the primary effect of disrupted motility. The difference in microtubule affinity was not significant with the non-hydrolysable ATP analogue AMP-PNP. Kinesin bound with AMP-PNP to microtubules is supposed to simulate the ATP state (Figure 3.1, second intermediate). Here, the neck-linker is docked and the motor molecule has in the natural state a high microtubule affinity. The lower microtubule affinity in the ADP bound state could not be confirmed significantly for the SA-crosslink. This is probably due to the location of the crosslink. While the AE-crosslink is positioned at the very end of the neck-linker, the SA-crosslink is located in the middle. Therefore the effect could well be less pronounced, as already indicated in competitive gliding assays.

Remarkably, according to available Kinesin-1 crystal structures the neck-linker docks in the vicinity of the primary microtubule-binding domain (Alonso *et al.*, 1998; Woehlke *et al.*, 1997). Taken together, it is most likely that neck-linker docking alters the microtubule affinity of individual kinesin heads during the chemo-mechanical cycle.

3.5 Material and Methods

3.5.1 Protein expression and purification

Kinesin was expressed and purified as described (Crevel *et al.*, 1999; Kallipolitou *et al.*, 2001). Briefly, *Neurospora crassa* kinesin (NcKin) was bacterially expressed using a T7 promoter system, isolated from *E. coli* cells and purified on a HiTrap SP sepharose column (Amersham Biosciences, Uppsala, Sweden) in 20 mM Na-phosphate buffer, pH 7.4 and 5 mM MgCl₂. The protein was eluted with increasing NaCl concentrations. Human kinesin mutants were purified according to published procedures (Tomishige and Vale, 2000). DTT was present during the cell rupture but omitted during the ion exchange chromatography. Tubulin was prepared and polymerised as described (Huang and Hackney, 1994; Mandelkow *et al.*, 1985).

3.5.2 NcKin protein backgrounds

As protein background a 'cysteine-light' NcKin construct was used that did not contain maleimide-reactive cysteine residues, as confirmed by dye labelling experiments. Only two native cysteine residues remained: C38 and C59. Furthermore, truncated NcKin backgrounds of different lengths were used. The C-terminal deletion construct NcKin-343 (NcKin residues 1-343; (Kallipolitou *et al.*, 2001)) was used to study the behaviour of monomeric constructs, NcKin-436hKT (NcKin residues 1-436 and human kinesin residues 432-546; (Bathe *et al.*, 2005)) that of dimeric kinesins. In this chimaera, part of the human kinesin stalk was appended to be able to bind NcKin mutants to glass coverslips. The addition of the human tail portion only affects the behaviour of the motor in few, very specific mutant contexts (Bathe *et al.*, 2005). As a control, the AE-mutant comprising residues 1-436 of NcKin was tested and did not show a significant kinetic difference in the microtubule-dependent ATPase assay between variants lacking or containing the partial human stalk. Therefore, all other mutants were only tested in the chimeric background containing the human stalk.

3.5.3 Introduction of disulfide bridges

To introduce crosslinks between kinesin's motor core and neck-linker, pairs of amino acid residues were selected, according to known crystal structures, in close proximity to each other to allow the formation of disulfide bonds (Figure 3.2; (Sack *et al.*, 1997; Song *et al.*, 2001)). The selected wildtype residues were changed to cysteines in Kinesin-1 of *N. crassa* (NcKin) using a PCR-based mutagenesis protocol (Stratagene QuickChange, La Jolla, USA) on a bacterial expression vector (Kallipolitou *et al.*, 2001). In the *N. crassa* kinesin sequence, the introduced cysteine residues were located at positions S3 and A334 (SA-mutant) or A226 and E339 (AE-mutant), respectively. In a sequence alignment, S3/A334 and A226/E339 correspond to the locations that have been investigated previously in human kinesin (Tomishige and Vale, 2000). The disulfide bridges formed upon oxidation with 0.2mM DTNB or in air saturated buffer and broke upon reduction with 1-5mM DTT.

3.5.4 Gliding assay

A flow cell was incubated for 5 min with hTail-tagged motors in motility buffer (10 mM MgCl₂, 10 mM ATP, 100 mM KCl, 20 µM paclitaxel, 1 mg/ml BSA, 0.8 mg/ml casein in BRB80+ (80 mM PIPES·KOH, pH 6.8, 5 mM MgCl₂, 1 mM EGTA)). After washing with blocking buffer (1 mg/ml BSA, 0.8 mg/ml casein in BRB80+), the flow chamber was

filled with atto488-labelled microtubules in motility buffer. Both kinesin and microtubule solutions were supplied with an oxygen scavenging system (0.1 mg/ml glucose oxidase, 0.02 mg/ml catalase, 2.25 mg/ml glucose). Gliding of the microtubules was observed with a total internal reflection microscope and gliding velocity of individual microtubules was measured using the manufacturers' software (Olympus Biosystems GmbH, Planegg, Germany). For statistical analysis SigmaPlot 2000 Software (Systat, Point Richmond, CA, USA) was used.

3.5.5 Microtubule Co-sedimentation assay

The microtubule affinity of kinesin was determined using a fixed amount of kinesin (300 – 500 nM), and increasing amounts of microtubules (0 – (10 to 50) μ M, depending on the mutant and condition used; (Woehlke *et al.*, 1997)). The tubulin dimer concentration was used to analyse the assays. Kinesin and microtubules were mixed in 12A25 buffer, and the microtubule-bound kinesin fraction was separated from free kinesin by 15 minutes centrifugation at 120,000 g in a Beckman Optima ultracentrifuge. After centrifugation the supernatant was removed, the pellet was re-suspended in the original volume, and both samples were analysed on a SDS-gel. The Coomassie-stained gel was photographed with a CCD camera (Stratagene EagleEye, La Jolla, USA) and analysed densitometrically in the computer program ImageJ (applying uncalibrated OD settings; <http://rsb.info.nih.gov/ij/>).

For unknown reasons, the supernatant contained variable amounts of tubulin, ranging from estimated 1 – 10%. If this was unpolymerized tubulin, the actual microtubule concentration would be over-estimated $\leq 10\%$; if it contained small microtubule fragments that kinesin can still bind to the bound fraction would be under-estimated $\leq 10\%$.

3.5.6 Statistical analysis of experimental results

To decide whether an observed effect was significant, tables of gliding velocity of each single protein assay and preparation were considered (analysis software: GraphPad Prism 4.0, GraphPad Software Inc., San Diego, CA). In cases where the number of independent protein preparations was 3 or more, a paired t-test could be used to test the null-hypothesis that (otherwise identical) DTT- and DTNB-treated protein samples behaved identically. Data obtained on DTT-treated proteins served as a reference to check whether any diverging mutant DTNB value was significantly different. The consistency of data obtained on different constructs under DTT

conditions was tested the same way, and each mutant was compared to all others in a one-way ANOVA.

3.6 References

- Alonso, M.C., van Damme, J., Vandekerckhove, J. and Cross, R.A. (1998) Proteolytic mapping of kinesin/ncd-microtubule interface: nucleotide-dependent conformational changes in the loops L8 and L12. *Embo J*, **17**, 945-951.
- Bathe, F., Hahlen, K., Dombi, R., Driller, L., Schliwa, M. and Woehlke, G. (2005) The complex interplay between the neck and hinge domains in kinesin-1 dimerization and motor activity. *Mol Biol Cell*, **16**, 3529-3537.
- Carter, N.J. and Cross, R.A. (2005) Mechanics of the kinesin step. *Nature*, **435**, 308-312.
- Crevel, I., Carter, N., Schliwa, M. and Cross, R. (1999) Coupled chemical and mechanical reaction steps in a processive *Neurospora* kinesin. *Embo J*, **18**, 5863-5872.
- Crevel, I.M., Nyitrai, M., Alonso, M.C., Weiss, S., Geeves, M.A. and Cross, R.A. (2004) What kinesin does at roadblocks: the coordination mechanism for molecular walking. *Embo J*, **23**, 23-32.
- Hackney, D.D. (1995) Highly processive microtubule-stimulated ATP hydrolysis by dimeric kinesin head domains. *Nature*, **377**, 448-450.
- Hackney, D.D. (2002) Pathway of ADP-stimulated ADP release and dissociation of tethered kinesin from microtubules. Implications for the extent of processivity. *Biochemistry*, **41**, 4437-4446.
- Hancock, W.O. and Howard, J. (1998) Processivity of the motor protein kinesin requires two heads. *J Cell Biol*, **140**, 1395-1405.
- Huang, T.G. and Hackney, D.D. (1994) *Drosophila* kinesin minimal motor domain expressed in *Escherichia coli*. Purification and kinetic characterization. *J Biol Chem*, **269**, 16493-16501.
- Kallipolitou, A., Deluca, D., Majdic, U., Lakamper, S., Cross, R., Meyhofer, E., Moroder, L., Schliwa, M. and Woehlke, G. (2001) Unusual properties of the fungal conventional kinesin neck domain from *Neurospora crassa*. *Embo J*, **20**, 6226-6235.
- Kozielski, F., Schonbrunn, E., Sack, S., Muller, J., Brady, S.T. and Mandelkow, E. (1997) Crystallization and preliminary X-ray analysis of the single-headed and double-headed motor protein kinesin. *J Struct Biol*, **119**, 28-34.
- Ma, Y.Z. and Taylor, E.W. (1997) Interacting head mechanism of microtubule-kinesin ATPase. *J Biol Chem*, **272**, 724-730.

- Mandelkow, E.-M., Herrmann, M. and Rühl, U. (1985) Tubulin Domains Probed by Limited Proteolysis and Subunit-specific Antibodies. *J. Mol. Biol.*, **185**, 311-327.
- Rice, S., Cui, Y., Sindelar, C., Naber, N., Matuska, M., Vale, R. and Cooke, R. (2003) Thermodynamic properties of the kinesin neck-region docking to the catalytic core. *Biophys J*, **84**, 1844-1854.
- Rice, S., Lin, A.W., Safer, D., Hart, C.L., Naber, N., Carragher, B.O., Cain, S.M., Pechatnikova, E., Wilson-Kubalek, E.M., Whittaker, M., Pate, E., Cooke, R., Taylor, E.W., Milligan, R.A. and Vale, R.D. (1999) A structural change in the kinesin motor protein that drives motility. *Nature*, **402**, 778-784.
- Rosenfeld, S.S., Fordyce, P.M., Jefferson, G.M., King, P.H. and Block, S.M. (2003) Stepping and stretching. How kinesin uses internal strain to walk processively. *J Biol Chem*, **278**, 18550-18556.
- Rosenfeld, S.S., Xing, J., Jefferson, G.M., Cheung, H.C. and King, P.H. (2002) Measuring kinesin's first step. *J Biol Chem*, **277**, 36731-36739.
- Sack, S., Muller, J., Marx, A., Thormahlen, M., Mandelkow, E.M., Brady, S.T. and Mandelkow, E. (1997) X-ray structure of motor and neck domains from rat brain kinesin. *Biochemistry*, **36**, 16155-16165 issn: 10006-12960.
- Sindelar, C.V., Budny, M.J., Rice, S., Naber, N., Fletterick, R. and Cooke, R. (2002) Two conformations in the human kinesin power stroke defined by X-ray crystallography and EPR spectroscopy. *Nat Struct Biol*, **9**, 844-848.
- Skiniotis, G., Surrey, T., Altmann, S., Gross, H., Song, Y.H., Mandelkow, E. and Hoenger, A. (2003) Nucleotide-induced conformations in the neck region of dimeric kinesin. *Embo J*, **22**, 1518-1528.
- Song, Y.H., Marx, A., Muller, J., Woehlke, G., Schliwa, M., Krebs, A., Hoenger, A. and Mandelkow, E. (2001) Structure of a fast kinesin: implications for ATPase mechanism and interactions with microtubules. *Embo J*, **20**, 6213-6225.
- Tomishige, M. and Vale, R.D. (2000) Controlling kinesin by reversible disulfide cross-linking. Identifying the motility-producing conformational change. *J Cell Biol*, **151**, 1081-1092.
- Woehlke, G., Ruby, A.K., Hart, C.L., Ly, B., Hom-Booher, N. and Vale, R.D. (1997) Microtubule interaction site of the kinesin motor. *Cell*, **90**, 207-216.
- Yildiz, A., Tomishige, M., Vale, R.D. and Selvin, P.R. (2004) Kinesin walks hand-over-hand. *Science*, **303**, 676-678.

4 Time-resolved FRET between Kinesin-1 and its substrate ATP

4.1 Abstract

Although it is now generally accepted that kinesin moves along microtubules in a stepwise hand-over-hand fashion, the coupling of stepping and ADP-release from the rear head is still controversial. To clarify this issue, we established a novel single-molecule method to observe FRET between fluorescently labelled human ubiquitous kinesin and ATP. This setup allowed observing single ATP binding events directly while human kinesin was stepping along the microtubule. In motility assays these labelled kinesins moved at wildtype velocity and reached normal run lengths, indicating normal kinetic behaviour. Single ATP turnovers were measured in a confocal microscope setup with a sub-millisecond time-resolution. Here, the confocal spot was focussed on a microtubule along which moving donor-labelled kinesins were visible as bell-shaped fluorescence time traces. FRET could be observed in acceptor and donor channel with low fluorescent ATP concentrations. To achieve a higher ATP concentration, we added non-fluorescent ATP and measured ATP binding times, and compared it with the duration of a single step. We found that one ATP is bound longer than the step of one head endures, indicating an overlap of the nucleotide binding times of the two heads.

4.2 Introduction

Single-molecule techniques provide powerful tools to understand the function of biomolecules. They became popular three decades ago, when electrophysiologists started to observe the behaviour of single ion-channels (Auerbach and Sachs, 1984; Neher and Sakmann, 1976). Apart from patch-clamping, further single-molecule technologies developed rapidly and are now available to investigate a broad range of biophysical and biochemical questions. These techniques became enormously popular because of their power in providing previously unattainable data on biological processes. Data of heterogeneous or not synchronised populations are now available and provide the unique opportunity to determine the detailed kinetics. Two important approaches to study single molecules are visualisation by fluorescence, and manipulation using optical or magnetic tweezers, or atomic force microscopy (AFM). Especially fluorescence localisation gave new insight in the field of molecular motors. The stepping behaviour of fluorescently labelled cytoskeletal motors can be followed with 1.5 nm accuracy (Yildiz *et al.*, 2003). The technique of FIONA (fluorescence imaging with one nanometer accuracy) resolved the hand-over-hand mechanism not only of myosin but also of kinesin (Yildiz *et al.*, 2003; Yildiz *et al.*, 2004).

After its first application in 1996 (Ha *et al.*, 1996), single-molecule FRET has been used to follow conformational changes in a wide variety of contexts. The results included new insights in the effects of calcium-binding on calmodulin domains (Brasselet *et al.*, 2000), the folding of telomers (Lee *et al.*, 2005), transcription initiation (Kapanidis *et al.*, 2006), kinesin's neck-linker conformation (Tomishige *et al.*, 2006) and kinesin's waiting conformation between the steps (Mori *et al.*, 2007). Latter results were obtained with TIRF-microscopy and needed integration times of 60 ms, which made it necessary to slow down the motor velocity using fairly low ATP concentrations (0.5 – 1 μM). A second experimental approach used in some of the studies is confocal microscopy. One advantage is that a time resolution up to nanoseconds can be achieved (Haustein and Schwille, 2004; Verbrugge *et al.*, 2007). Furthermore, the excitation volume is confined to the size of the focal spot and therefore much smaller and more defined as compared to TIRF. This makes it possible to increase the overall concentration of fluorophores in the sample. If donor and acceptor concentrations are not equimolar, but differ in order of magnitudes, the confocal setup is especially useful.

We used the advantages of confocal microscopy and FRET to measure the time of ATP turnovers by conventional kinesin. The challenge is to image high ATP concentrations combined with high time-resolution. The result will yield new insights into the chemo-mechanical cycle based on all qualitative advantages of single-molecule data.

4.3 Results

4.3.1 Design of FRET constructs

The purpose of this study is to measure the binding time of single ATP molecules to single kinesins while walking along a microtubule. Our measurements were performed with human conventional kinesin, which is the best-studied kinesin motor. We truncated a cysteine-light construct after the dimerisation domain (391 aa) to prevent unspecific binding to glass surfaces. For site specific labelling, we reintroduced cysteines located next to the ATP binding pocket. A set of three different positions in close proximity to the bound ATP was chosen with help of the crystal structure (Protein Database Numbering: 1BG2; Figure 4.1).

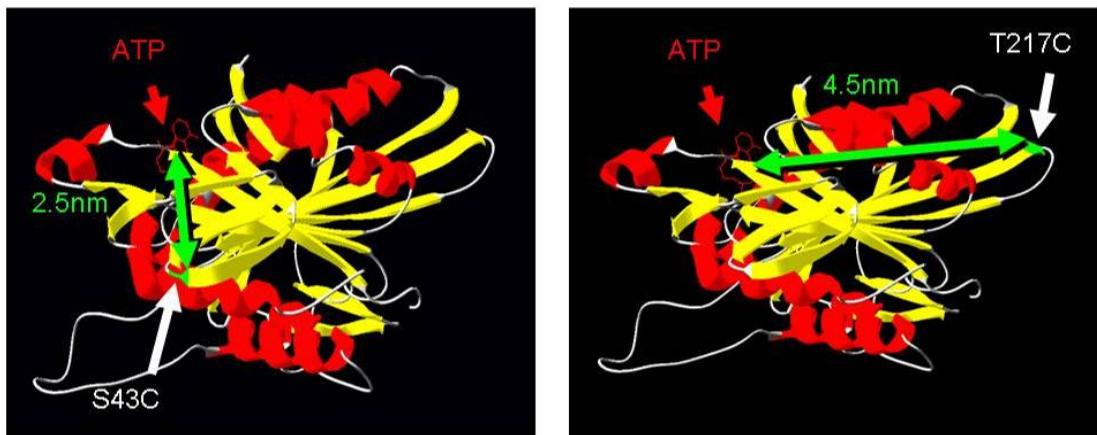


Figure 4.1 Positions of reactive cysteines and distances to ATP.

The figure shows crystallographic models of the motor domain of human Kinesin-1 (Protein Database Numbering: 1BG2), which was used to generate FRET constructs. Residues mutated into cysteines for site specific labelling are shown in green and indicated with white arrows. Distances to the ATP (red) are displayed by green arrows. In the case of HKin391-S43C the distance is 2.5 nm and in the case of HKin391-T217C 4.5 nm. The model was generated in SwissPDB Viewer.

Position S43 and T217 have 2.5 and 4.5 nm distances to the bound ATP, are surface-exposed and are not conserved among the Kinesin-1 superfamily, suggesting low

functional impact. A third point mutation (E309C) with the same characteristics failed the expression in *E.coli*.

As fluorophores have different properties in different protein environments, two combinations of donor and acceptor were tested. The dyes were chosen by the following criteria: (1) high photostability, (2) high extinction coefficient, (3) high quantum yield, (4) spectral overlap of donor emission and acceptor excitation, (5) large spectral separation to minimise donor emission leakage into the spectral range of acceptor emission and to reduce the amount of direct excitation of the acceptor by the laser (Ha, 2001). The latter is especially important because the acceptor dye concentration will be 100 - 10.000 fold higher than the donor dye concentration in our experiments. Atto488 and Cy3 were the first choice, because Atto488 was found to be very stable in TIRF assays (chapter 2) and Cy3 is known from previous single molecule FRET experiments (Kapanidis *et al.*, 2006; Tomishige *et al.*, 2006). An alternative fluorophore system was Alexa555 and Alexa647. The purified kinesins were labelled via maleimide with fluorophores and free dye and inactive motors were separated in a microtubule affinity step.

4.3.2 Spectroscopic bulk assay

To confirm FRET between the labelled kinesin and fluorescent ATP, spectroscopic bulk assays were performed. To this end, we released kinesin after labelling and microtubule affinity spin-down using fluorescent ATP. The excess of fluorescent dye was removed by centrifuging the solution in a membrane-containing filter tube. The remaining protein solution was diluted and an emission scan was performed in a fluorimeter (Figure 4.2, red line). The fluorescent ATP was released with an excess of non-fluorescent ATP (Figure 4.2, black line).

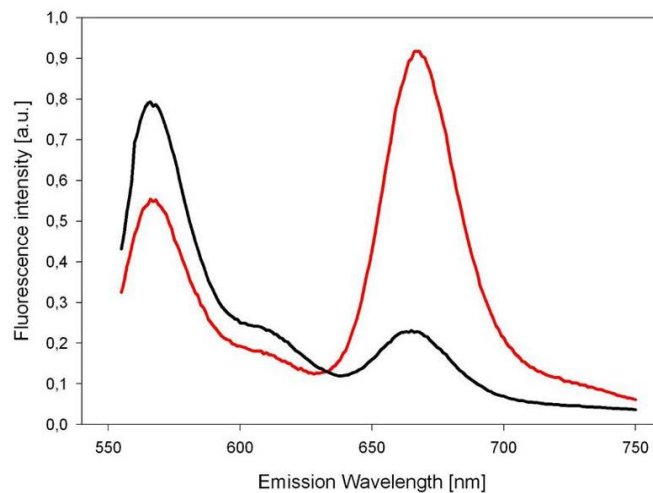


Figure 4.2 Spectroscopic FRET measurement.

These example traces of an emission scan (excitation wavelength of 535 nm) show FRET between HKin391-S43C labelled with Alexa555- and Alexa647-ATP. The red line shows the Alexa647-ATP bound state and the black line the non-fluorescent ATP bound state. The donor fluorescence intensity in the FRET curve (red curve at 570 nm emission) is clearly quenched, whereas the acceptor intensity is strongly enhanced (at 670 nm emission) in comparison with the non-FRET curve (black).

In Figure 4.2 the energy transfer between the donor and the acceptor fluorophore is clearly visible. If fluorescent ATP is bound to the labelled kinesin, the emission intensity of the donor is quenched and the emission intensity of the acceptor is strongly enhanced. In theory, the degree of quenching and of the enhancement should be same, which is not the case in the latter experiment. One reason for this could be the higher quantum yield of the acceptor (0.1 for Alexa555 and 0.33 for Alexa647, according to Molecular Probes' Homepage) and another reason unequal concentrations of donor and acceptor fluorophores. If e.g. only 80% of donor molecules bind an acceptor, all acceptor fluorophores would be excited via FRET but only 80% of the donor molecules would be quenched. Therefore all residual donor fluorophores (20%) emit with their full intensity and the average donor quench would appear less pronounced. This situation could arise as a consequence of filtering the protein solution after labelling. Fluorescent ATP could be in shortage (kinesin without fluorescent ATP) and the donor quench seems to be less pronounced. Due to these problems, it was not possible to calculate the exact FRET efficiencies of the two FRET constructs. However, in our experiments the FRET efficiency of HKin391-S43C was higher than the one of HKin391-T217C (data not shown). The results could be confirmed with two fluorophore pairs: Atto488 - Cy3 and Alexa555 - Alexa647. Taken together the results indicate that these constructs are good tools to resolve ATP-

binding times. Due to higher FRET efficiency of HKin391-S43C, the first set of experiments was performed with this construct.

4.3.3 Single-molecule TIRF-assay

Despite the spectroscopic properties of the FRET construct it is crucial to check if the point mutations alter the kinetic properties. The lack of the tail domain prevented measuring the velocity in conventional multi-motor gliding assays, but suitable for single-molecule motility assays. In these assays rhodamine-labelled microtubules were attached to the coverslip and kinesins labelled with Atto488 were added. Their movement was imaged with a TIRF microscope. The measured velocity of $0.77 \pm 0.1 \mu\text{m/s}$ is in excellent agreement the wildtype velocity ($0.78 \pm 0.09 \mu\text{m/s}$ for HKin560 (Lakamper *et al.*, 2003)). Another important property of a processive molecular motor is its average runlength. This can also be determined with single-molecule motility assays and proved to be similar to the wildtype value (HKin391-S43C: $0.86 \mu\text{m}$ (Figure 4.3); HKin 560: $0.83 \mu\text{m}$ (Lakamper *et al.*, 2003)). In terms of velocity and runlength, the FRET construct HKin391-S43C behaved like the wildtype, indicating that the kinetic cycle is not altered due to the point mutation.

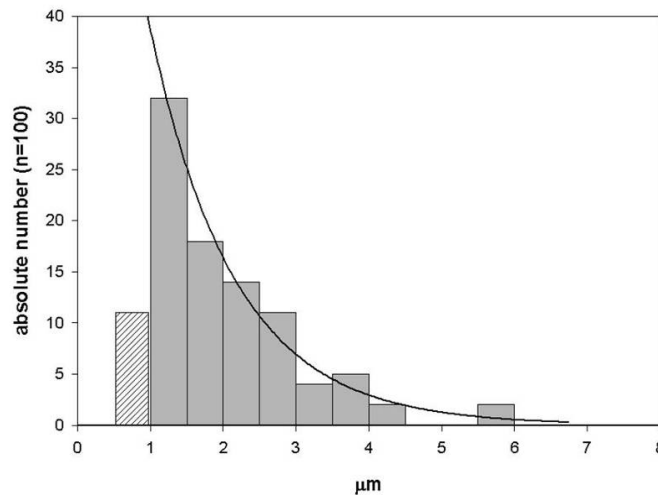


Figure 4.3 Runlength of HKin391-S43C.

The average runlength of labelled FRET constructs (here HKin391-S43C labelled with Atto488) was measured in the TIRF assay (single-molecule motility assay). The measured runlengths were plotted into a histogram, which was then fitted with an exponential decay ($\tau = 0.86 \mu\text{m}$). Runlengths below $1 \mu\text{m}$ are underestimated due to the limited time resolution of 200 ms/frame. Therefore they are not included in the fit (indicated by hatched bar).

4.3.4 Confocal assay

Due to the restricted time resolution for single molecule assays in the TIRF microscope (150 - 300 ms integration time of CCD camera), we chose another microscopic setup with shorter sampling rates. The method of choice was a confocal microscope, which was especially build for sensitive single-molecule measurements with molecular motors (Verbrugge *et al.*, 2007). With this setup it is possible to image with sub-millisecond time-resolution. In contrast to conventional confocal microscopes, this setup moves the sample with a piezo-table instead of scanning with the confocal spot through the sample.

The motility assay is in principle the same as with the TIRF setup (Figure 4.4). The major difference is that surface attached microtubules are labelled with a dye having similar spectral properties as the dye of molecular motor. The confocal spot is placed in the middle of a microtubule, which is then bleached in this spot to reduce background fluorescence.

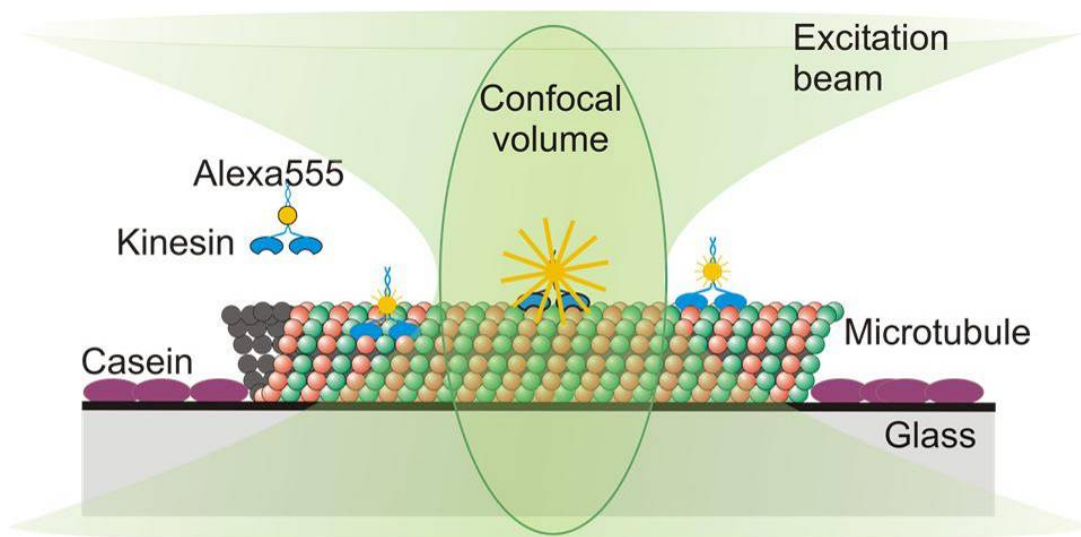


Figure 4.4 Principle of confocal measurements.

The microtubule is attached to the glass via a positively charged surface. Casein prevents nonspecific sticking of the kinesin to the glass. Labelled kinesins run on the microtubule through the confocal spot, where the fluorophore is excited. (from Verbrugge *et al.*, 2007)

Labelled kinesins walk through the confocal spot and show up as bell-shaped peaks in fluorescence time traces. This is because the excitation intensity of the confocal volume is Gauss-distributed and the emission of kinesin-bound fluorophore is proportional on the excitation intensity. The closer the kinesin is to the spot centre the

higher is its emission intensity. Therefore, the fluorescence of a labelled kinesin moving at constant velocity through the confocal spot will appear as a Gaussian peak in a fluorescence time trace (Figure 4.5). A "single-photon-counting" avalanche photodiode measures the time between photon arrivals with 12.5 ns time resolution. The arrival times are binned into time intervals, usually 10 ms, and displayed as time-intensity traces (Figure 4.5). The original arrival times are stored on the main board and are available for analysis.

These measurements showed that Atto488-labelled kinesins blinked at a 10-100ms range. This is exactly the time range of interest and makes the dye useless for our experiments. All following experiments were performed with Alexa555-labelled kinesins (Figure 4.5).

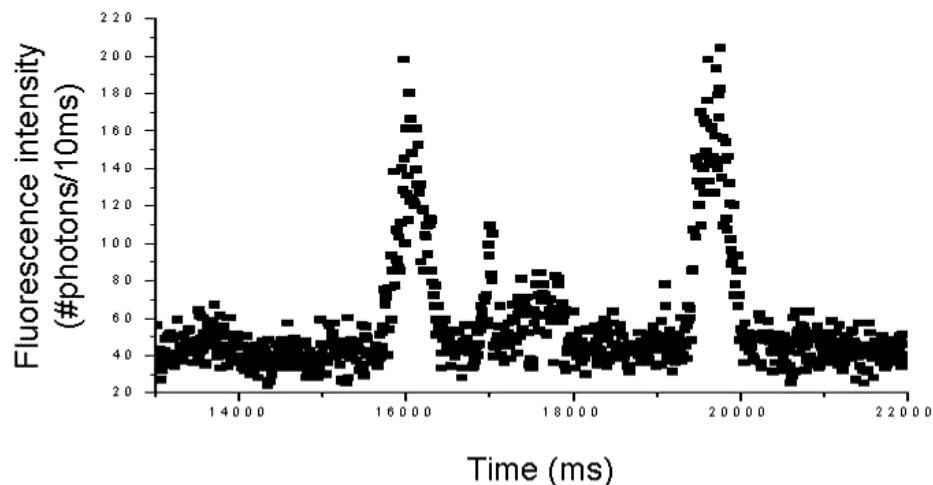


Figure 4.5 Example trace of HKin391-S43C with saturating ATP.

Fluorescence intensity traces obtained when the confocal spot was positioned on a locally bleached microtubule. The time trace of 9 s shows two events, with comparable amplitude. These events are due to a motors landing before the confocal spot, walking in and through it and consequently showing a complete Gaussian profile. This Gaussian profile can be used to determine the velocity of the motor, when the spot size is known.

The Gaussian shape of the events indicates that the kinesin's velocity is constant during the passage through the confocal spot. Since the detected emission intensity is proportional to the location in the confocal point, the motor's velocity can be calculated from the ratio of the spatial width (obtained from Gaussian fit to images of single fluorophores; $\sigma = 100 \pm 3 \mu\text{m}$) of the confocal spot and the temporal width of an event (also σ of Gaussian fit). The average of the temporal widths at saturating ATP is $151 \pm 5 \text{ ms}$. Therefore, an average velocity of $0.66 \pm 0.02 \mu\text{m/s}$ can be calculated.

The average value obtained in this assay is slightly lower than our value from TIRF assays (0.77 $\mu\text{m/s}$). This difference can be due to different buffer and temperature conditions (see Material and Methods).

To further characterise the behaviour of the FRET construct in the confocal assay, the velocity was measured at different ATP concentrations. These data were analysed with Michaelis-Menten kinetics and yielded in a V_{max} of 0.63 $\mu\text{m/sec}$ and a K_m value of 19.5 μM ATP (Figure 4.6). These values show that the construct behaves as wildtype and will furthermore help to interpret data obtained with fluorescent ATP.

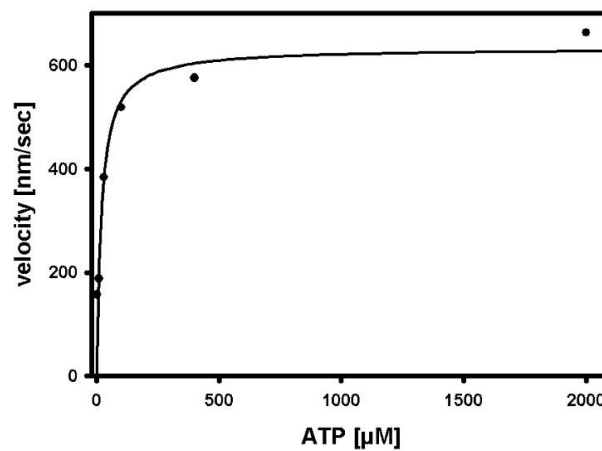


Figure 4.6 Michaelis-Menten kinetics measured with the confocal setup.

The graph shows the average velocities of the HKin391-S43C construct at different ATP concentrations. The data points were fitted with a hyperbola and revealed a V_{max} of 0.63 $\mu\text{m/s}$ and K_m of 19.5 μM ATP. (with courtesy of S. Verbrugge, VU Amsterdam)

4.3.5 Measuring single ATP events

One of Kinesin-1's astonishing properties is its stepwise movement over long distances without detachment from the microtubule. This processive behaviour can be explained by the hand-over-hand or alternating-site model, which is now commonly accepted (Hackney, 1995; Ma and Taylor, 1997; Yildiz *et al.*, 2004). These models suppose that conventional kinesin walks along the microtubule like an orangutan moves with its hands along a rope. One head is always attached to the microtubule and for a certain time both heads bind simultaneously. Afterwards the heads exchange roles and the leading head becomes the trailing one. The chemo-mechanical cycles of the heads are dependent on each other and well coordinated. The nucleotide of the detached head is not released until an ATP binds to the microtubule-bound head (Figure 4.7). As a consequence, one ATP is bound longer than half of the total kinetic cycle (for two heads), which corresponds one 8 nm step

(red arrows, Figure 4.7). With the experimental setup described before, it is possible to measure the binding time of ATP during one kinetic cycle. The overlapping time, where two nucleotides are bound can be calculated from the velocity (time for one 8 nm step). In particular it would be interesting, how this overlapping time depends on the overall ATP concentration. Although it is thought, that the events following ATP binding are independent from the ATP concentration it has never been shown directly.

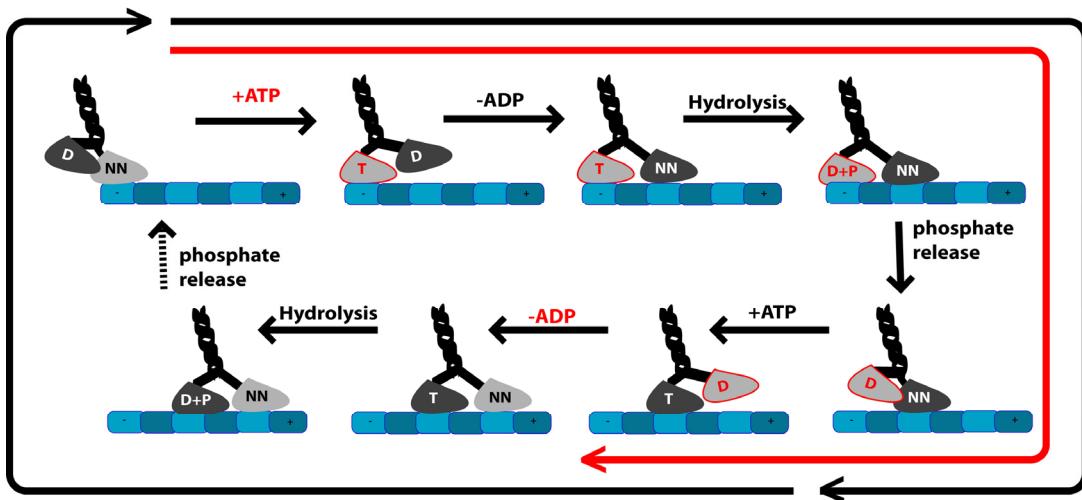


Figure 4.7 Kinetic model of the chemo-mechanical cycle with fluorescent ATP.

The figure shows one complete kinetic cycle, meaning one 8 nm step of every head. Microtubules are shown in blue and kinesin in black with one light- and one dark-grey head. Fluorescent nucleotides are displayed in red, non-fluorescent in white and black. The light-grey head is tightly bound to the microtubule in a no-nucleotide state, while the dark-grey ADP-bound head is weakly bound and free for diffusive search of the next microtubule binding site. Upon fluorescent ATP binding the dark-grey head releases its nucleotide and binds tightly to the microtubule. With binding of the fluorescent ATP the energy from the excited fluorophore at the motor domain of the light-grey head can be transferred to the acceptor fluorophore at the ATP. The cycle continues with hydrolysis, phosphate release and binding of a new ATP (this time non-fluorescent) to the dark-grey head. This continuation is triggered by the release of fluorescent ADP from the light grey head (end of FRET signal). The cycle can be divided in a FRET (red arrow) and No-FRET part. The time of FRET is supposed to be longer than for No-FRET, because of the overlapping time, where a nucleotide is bound to each head. The black arrows indicate one 8 nm step each. (T: ATP; D: ADP; NN: no nucleotide; P: phosphate)

The first experimental step was to see whether the FRET construct can walk with fluorescent ATP and if it is possible to resolve single ATP bindings in the confocal setup. Therefore we added 1 μM fluorescent ATP to the sample, which is far below the K_m value. At this concentration HKin391-S43C is supposed to walk about 0.03 $\mu\text{m/s}$, corresponding to 3-4 steps per second (estimated from Michaelis-Menten kinetics with non-fluorescent ATP (Figure 4.6)). At this velocity one Gaussian curve is

too shallow and too long to detect its shape. However, at such low fluorescent ATP concentrations it was possible to image both the donor and the acceptor channel. Due to a low labelling ratio only one kinesin head is labelled and every second step contains a FRET signal, which is represented by anti-correlated fluorescence intensity levels (Figure 4.8). Every intensity change illustrates one single step of a single kinesin. This is a strong indication that HKin391-S43C can walk with fluorescent ATP and that binding events of single ATPs can be detected.

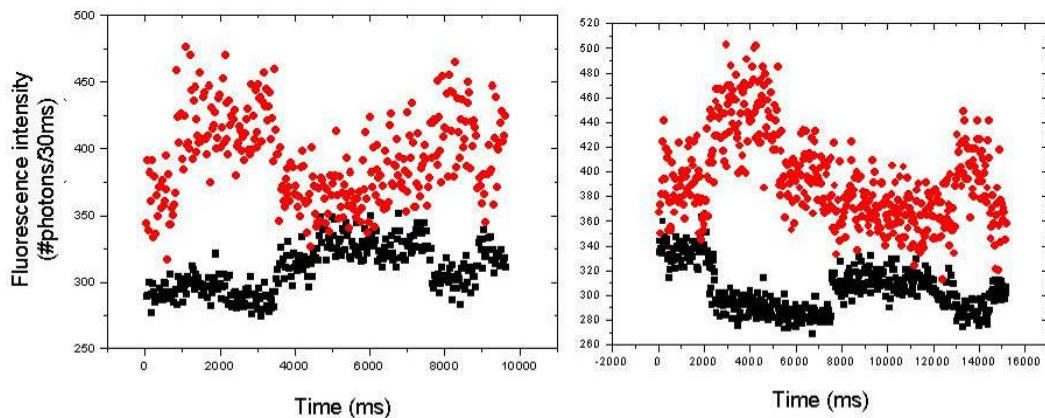


Figure 4.8 Consecutive traces with only fluorescent ATP.

These traces show a single-head labelled kinesin (S43C, Alexa555) walking through the confocal spot at $1\ \mu\text{M}$ Alexa647-ATP for over 20 s in two consecutive acquisition units (raw data is stored on main board after 10 s). The acceptor intensity level (red) alternates with the donor intensity level (black), showing the alternation of the labelled head (FRET) and the unlabelled head (no FRET).

Due to the high fluorescent background traces in the acceptor channel became too noisy at fluorescent ATP concentrations over $1\ \mu\text{M}$. Therefore, fluorescent ATP was mixed with non-fluorescent ATP to increase the overall ATP concentration. A convenient concentration was $5\ \mu\text{M}$ non-fluorescent ATP and $0.3\ \mu\text{M}$ fluorescent ATP. Under these conditions it was possible to detect Gaussians and to image in both channels with reasonable noise (Figure 4.9).

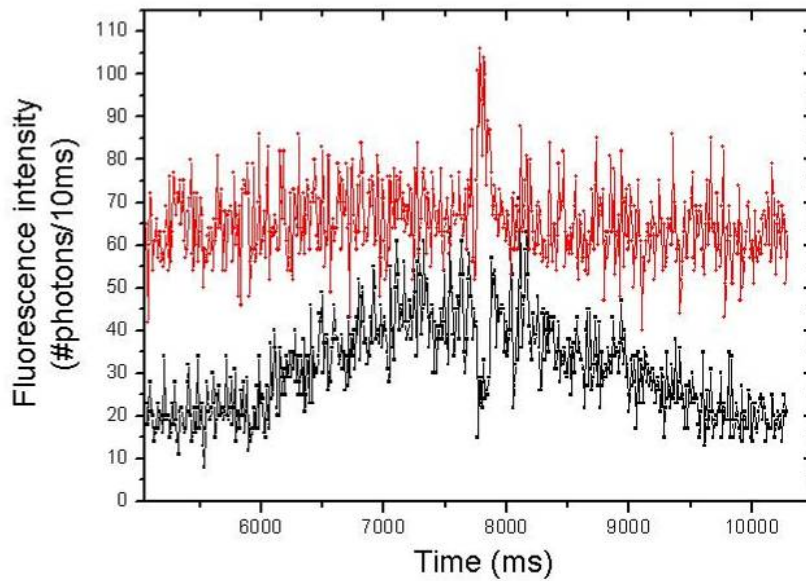


Figure 4.9 Example trace with small amounts of fluorescent ATP mixed with non-fluorescent ATP.

This trace shows a single-head labelled kinesin (S43C, Alexa555) walking through the spot at 5 μM non-fluorescent ATP mixed with 0.3 μM Alexa647-ATP. The donor channel (black) shows a complete bell-shaped intensity-time trace with one dip in the fluorescent intensity on the top. The acceptor intensity (red) is enhanced at the same time, which is due to a single fluorescent binding event. In this case it was bound for 110 ms.

Due to the unfavourable ratio of fluorescent ATP to non-fluorescent ATP (1:16.7) these binding events were rare. Nevertheless, it was possible to determine the ATP binding time of 22 individual traces, with a mean value of $113 \pm 12\text{ms}$ (Figure 4.10).

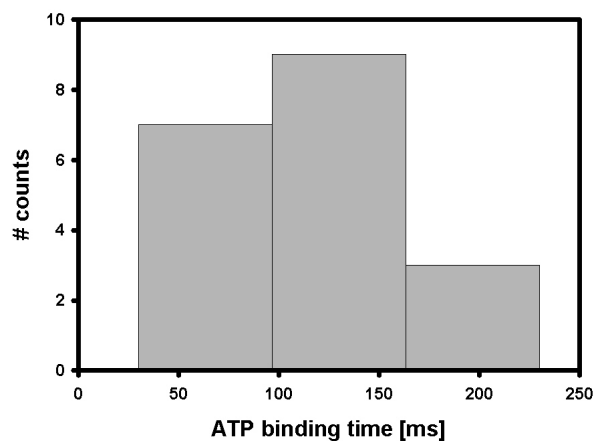


Figure 4.10 Distribution of fluorescent ATP binding times.

Measuring single ATP binding events at 5 μM non-fluorescent ATP mixed with 0.3 μM Alexa647-ATP ($n = 22$) yielded in a histogram with a mean value of $113 \pm 12\text{ms}$.

According to the Michaelis-Menten parameters, the average speed at 5 μM ATP is 0.13 $\mu\text{m/s}$. Therefore, one 8 nm step lasts 62 ms. The overlap is therefore calculated to be 51 ms, which means that for 51 ms two nucleotides are bound to kinesin. This value is probably overestimated, because kinesin walks slower with fluorescent ATP (V_{max} : 0.21 $\mu\text{m/s}$, personal communication S. Verbrugge), but it is not clear if this reduced velocity is due to a slower on- or off-rate of the fluorescent ATP. Only a lower off-rate would affect the measured ATP-binding time. However, we show for the first time, that it is possible to measure single ATP-binding events on single kinesins with millisecond accuracy.

4.4 Discussion and future prospects

The combination of FRET and confocal microscopy made it possible to measure single ATP-binding events. Although several groups succeeded to perform single-molecule FRET, none of them measured with such high acceptor concentrations and such a fast sampling rate. They used FRET either as a marker for conformational changes within one molecule (Mori *et al.*, 2007; Slaughter *et al.*, 2005; Tomishige *et al.*, 2006) or the interaction of two molecules at equimolar concentrations (Kapanidis *et al.*, 2006; Lee *et al.*, 2005; Steigmler *et al.*, 2004). In our experiments, the concentration of the acceptor (0.3 - 1 μM) was three orders of magnitudes higher than the concentration of the donor (0.1 – 0.5 nM). The ratio could be increased even more, if only the donor channel would be imaged. Because with increasing amounts of acceptor, the detecting avalanche diode is saturated.

This is the first time that we have direct insight into the chemo-mechanical cycle of kinesin-1 with millisecond time resolution. All single molecule motility assays with kinesin up to now were performed with a TIRF microscope and had imaging rates of 1 -60 frames/s (Lakamper *et al.*, 2003; Mori *et al.*, 2007; Tomishige *et al.*, 2006; Yildiz *et al.*, 2003).

This project is not only experimentally novel, but will also answer questions of conventional kinesin's mechanism. First experiments already showed that ATP is bound longer than half of the kinetic cycle. As a consequence it can be calculated how long two nucleotides are bound to the motor protein. Most kinesin researches assume in their model, that all reactions after ATP binding are ATP concentration independent (Cross, 2004; Gilbert *et al.*, 1998; Schief *et al.*, 2004). This would mean that the time where two nucleotides are bound is ATP concentration independent and

that only the ATP waiting time is concentration dependent. However, neither the overlapping time nor dependence on ATP concentration has been measured directly.

In addition to the experiments reported above we also measured single-molecule kinetics in dependence of the ATP concentration. Traces at higher ATP concentrations up to 40 μM showed the expected faster velocities and shorter nucleotide binding times. However, due to the worse signal-noise ratio the manual analysis described in the Results section was not applicable any more. Attempts to detect binding times by autocorrelation are underway but turned out to be difficult to interpret. Although it was possible to generate autocorrelation curves with high quality with non-fluorescent ATP, it was not possible to extract the actual ATP binding times from curves with fluorescent ATP. The mathematical problem still remains to be solved and needs further investigation. A method like this could deliver the ATP binding times at high fluorescent ATP concentrations. Especially measurements with fluorescent ATP only, are of great interest. Due to different affinities and off-rates of the two ATP derivatives, cycle time and ATP binding times can not be compared directly in mixed experiments, but in experiments with only fluorescent ATP.

However, we showed that our FRET construct in combination with the novel confocal setup provides a tool to look directly into the chemo-mechanical cycle of conventional kinesin. These data will yield answers to the question whether the reactions followed by the ATP binding event are ATP concentration dependent or not and how long these reactions take.

4.5 Material and Methods

4.5.1 Cloning, protein expression and purification

The used constructs are derived from the human conventional kinesin gene encoding 560 aa and no surface exposed cysteins (pHK560). This construct was truncated after the dimerisation domain (391 aa) and selected wildtype residues were changed to cysteines using a PCR-based mutagenesis protocol (Stratagene QuickChange, La Jolla, USA). These cysteines are close to the ATP binding pocket (S43C and T217C). Cloned in an expression vector (pET17b; Novagene, Madison, USA), the plasmids were transformed to the BL21Ril *E.coli* strain for expression. The proteins were purified sequentially with a phosphocellulose column followed by a HiTrap Q-Sepharose (GE Healthcare, Uppsala, Sweden) column on a FPLC system (Amersham Pharmacia Biotech, Buckinghamshire, UK). The protein concentration

was determined with a Coomassie Brilliant Blue based test (BioRad, Hercules CA, USA) and the degree of purity was estimated from a SDS-PAGE.

4.5.2 Protein labelling and spectroscopic assay

The purified motor protein was labelled with Atto488-maleimide (Attotec, Jena, Germany) or AlexaFluor555-maleimide (Invitrogen, Carlsbad CA, USA) by adding the dye (dissolved in DMSO) in a 4-fold excess over kinesin monomers and incubating for 45 min on ice. Free dye and inactive motors were separated from the labelled and active kinesins with microtubule co-sedimentation. Therefore, microtubules were decorated with labelled kinesin via AMP-PNP (non-hydrolysable ATP analogue) and sedimented through a 50% sucrose cushion by ultracentrifugation (80 000rpm, Beckmann Optima TL, TLA 100 rotor). The pellet was resuspended with ATP-containing BRB80 buffer, with the effect of releasing kinesin from the microtubules. The microtubules were again sedimented, while kinesins remained in the supernatant. After a second release step, the supernatants were combined and shock frozen in liquid nitrogen after addition of 10% glycerol. The dye concentration was determined in a spectrometer and the protein concentration with a Coomassie Brilliant Blue based test (BioRad, Hercules CA, USA). The usual labelling ratio was 1 fluorophore per 2 kinesin monomers.

To confirm FRET, the release steps were done with 1 mM fluorescent ATP (Cy3 or Alexa647). By using an Amicon Ultra4 Centrifugal Filter device (Molecular weight cut-off: 10 kDa; Millipore, Billerica, USA), the protein was concentrated, but the unbound fluorescent ATP could pass the membrane. The remaining protein solution was diluted and concentrated for three times to get rid of the majority of unbound fluorescent ATP. The emission intensity was scanned (donor Atto488: 510-650 nm, excitation 488 nm; donor Alexa555: 555-750 nm, excitation 535 nm) in a fluorimeter to confirm FRET. As a control, unfluorescent ATP was added to replace the fluorescent ATP in the binding pocket and another emission scan was performed.

4.5.3 TIRF assay

Biotin-labelled microtubules were fixed on the surface of a flow chamber which was incubated with 2 mg/ml BSA-biotin (Sigma-Aldrich Co., St. Louis, USA) and subsequently with 1 mg/ml Streptavidin in BRB80+ buffer and 20 μ M taxol. After washing with 1 mg/ml BSA in BRB80+ motility mix (0.1-0.5 nM Atto488-labeled kinesin, 20 μ M-2 mM ATP, oxygen scavenger (see above), 0.2 mg/ml casein, 100

mM KCl in BRB80+) was flushed in. The gliding activity was observed in an Olympus IX71 TIRF microscope with an excitation wavelength of 488 nm and a Hamamatsu C-9100 front-illuminated CCD-camera. The optical resolution was 160 nm per 2x2-binned pixel; the integration time was 200 ms.

Velocities and runlengths were measured using the manufacturer's software (Olympus Biosystems GmbH, Planegg, Germany). For statistical analysis SigmaPlot 2000 Software (Systat, Point Richmond, CA, USA) was used.

4.5.4 Confocal assay

The confocal assay and setup is describes in detail in (Verbrugge *et al.*, 2007).

Briefly:

Flow chambers were made with doublesticky tape. Microtubule seeds were polymerised by mixing 7.5 mM unlabelled tubulin, 2.5 mM tetramethylrhodamine (TMR)-labelled tubulin and 1 mM GMP-CPP (Jena Bioscience, Jena, Germany)) for 20 min at 36 °C. Afterwards they were stabilised with Pem80-taxol buffer (80 mM Pipes, 1 mM EGTA, 2 mM MgCl₂, pH 6.8, and 10 µM taxol) and injected into the sample lanes. After washing and blocking with 0.4 mg/ml casein, a mix with kinesin motors was flushed into the sample lane, after which the sample was sealed with vacuum grease. In all experiments an oxygen scavenger system (20 mg/ml glucoseoxidase, 35 catalase mg/ml, and 25 mM glucose), 4 mM DTT or TROLOX, and 10 mM taxol were added. In experiments with ATP concentration lower than 100 mM ATP an ATP regeneration system (10 mM phosphocreatine and 50 mg/ml creatine kinase) was added.

The excitation-laser was coupled into an inverted microscope (TE-2000-U Nikon, Tokyo, Japan) with a 100x oil immersion objective (Nikon Plan Fluor, numerical aperture 1.3). Fluorescence was imaged on a CCD camera (CoolsnapHQ, RoperScientific, Tucson, AZ) or focused onto an avalanche photodiode (APD) (SPQM-AQR-14, PerkinElmer, Vaudreuil, Quebec, Canada). Photons detected by the APD are converted to digital pulses, which were time tagged with electronic counterboard (6602, National Instruments, Austin, TX) with 12.5-ns time resolution. Arrival times of detected photons were stored on a computer using custom-built Labview software (Labview 7.1, National Instruments). To accurately position the confocal spot and scan the sample, we used a feedback controlled piezo translation stage (P-561, Physikalisches Instrumente, Karlsruhe, Germany).

Wide-field illumination and CCD camera detection were used to locate the fluorescently labelled microtubules. The sample was translated to position the confocal spot on a microtubule. Fluorophores on the microtubules were bleached before measuring the fluorescence of kinesins moving through the confocal spot.

The width of the confocal spot was obtained by fitting a Gaussian to an image of microtubules (spot-like light source). The width (defined as σ of the Gaussian) was determined to be 100 ± 3 nm (mean \pm SE).

4.6 References

- Auerbach A, Sachs F. 1984. Single-Channel Currents From Acetylcholine-Receptors In Embryonic Chick Muscle - Kinetic And Conductance Properties Of Gaps Within Bursts. *Biophysical Journal* 45(1):187-198.
- Brasselet S, Peterman EJG, Miyawaki A, Moerner WE. 2000. Single-molecule fluorescence resonant energy transfer in calcium concentration dependent cameleon. *Journal Of Physical Chemistry B* 104(15):3676-3682.
- Cross RA. 2004. The kinetic mechanism of kinesin. *Trends Biochem Sci* 29(6):301-309.
- Gilbert SP, Moyer ML, Johnson KA. 1998. Alternating site mechanism of the kinesin ATPase. *Biochemistry* 37(3):792-799.
- Ha T. 2001. Single-molecule fluorescence resonance energy transfer. *Methods* 25(1):78-86.
- Ha T, Enderle T, Ogletree DF, Chemla DS, Selvin PR, Weiss S. 1996. Probing the interaction between two single molecules: fluorescence resonance energy transfer between a single donor and a single acceptor. *Proc Natl Acad Sci U S A* 93(13):6264-6268.
- Hackney DD. 1995. Highly processive microtubule-stimulated ATP hydrolysis by dimeric kinesin head domains. *Nature* 377(6548):448-450.
- Haustein E, Schwille P. 2004. Single-molecule spectroscopic methods. *Curr Opin Struct Biol* 14(5):531-540.
- Kapanidis AN, Margeat E, Ho SO, Kortkhonjia E, Weiss S, Ebright RH. 2006. Initial transcription by RNA polymerase proceeds through a DNA-scrunching mechanism. *Science* 314(5802):1144-1147.
- Lakammer S, Kallipolitou A, Woehlke G, Schliwa M, Meyhofer E. 2003. Single fungal kinesin motor molecules move processively along microtubules. *Biophys J* 84(3):1833-1843.
- Lee JY, Okumus B, Kim DS, Ha T. 2005. Extreme conformational diversity in human telomeric DNA. *Proc Natl Acad Sci U S A* 102(52):18938-18943.

- Ma YZ, Taylor EW. 1997. Interacting head mechanism of microtubule-kinesin ATPase. *J Biol Chem* 272(2):724-730.
- Mori T, Vale RD, Tomishige M. 2007. How kinesin waits between steps. *Nature*.
- Neher E, Sakmann B. 1976. Single-channel currents recorded from membrane of denervated frog muscle fibres. *Nature* 260(5554):799-802.
- Schief WR, Clark RH, Crevenna AH, Howard J. 2004. Inhibition of kinesin motility by ADP and phosphate supports a hand-over-hand mechanism. *Proc Natl Acad Sci U S A*.
- Slaughter BD, Bieber-Urbauer RJ, Johnson CK. 2005. Single-molecule tracking of sub-millisecond domain motion in calmodulin. *J Phys Chem B* 109(26):12658-12662.
- Steigmiller S, Zimmermann B, Diez M, Borsch M, Graber P. 2004. Binding of single nucleotides to H⁺-ATP synthases observed by fluorescence resonance energy transfer. *Bioelectrochemistry* 63(1-2):79-85.
- Tomishige M, Stuurman N, Vale RD. 2006. Single-molecule observations of neck linker conformational changes in the kinesin motor protein. *Nat Struct Mol Biol* 13(10):887-894.
- Verbrugge S, Kapitein LC, Peterman EJ. 2007. Kinesin moving through the spotlight: single-motor fluorescence microscopy with submillisecond time resolution. *Biophys J* 92(7):2536-2545.
- Yildiz A, Forkey JN, McKinney SA, Ha T, Goldman YE, Selvin PR. 2003. Myosin V walks hand-over-hand: single fluorophore imaging with 1.5-nm localization. *Science* 300(5628):2061-2065.
- Yildiz A, Tomishige M, Vale RD, Selvin PR. 2004. Kinesin walks hand-over-hand. *Science* 303(5658):676-678.

5 Effect of spastic paraplegia mutations in KIF5A kinesin on transport activity

5.1 Abstract

Hereditary spastic paraplegia (HSP) is a neurodegenerative disease caused by motoneuron degeneration. It is linked to at least 30 loci, among them SPG10, which causes dominant forms and originates in point mutations in the neuronal Kinesin-1 gene (*KIF5A*). Here, we investigate the motility of KIF5A and four HSP mutants. All mutations are single amino-acid exchanges and located in kinesin's motor or neck-domain. Three of these mutations either reduce microtubule affinity, or gliding velocity, or both. In laser-trapping assays, none of the mutants moves more than a few steps along microtubules. Motility assays with mixtures of homodimeric wildtype, homodimeric mutant, and heterodimeric wildtype/mutant motors reveal that only one mutant reduces the gliding velocity at ratios as present in heterozygous patients. Attached to quantum dots as artificial cargo, these mixtures show that mutant kinesins lead to populations of quantum dots that either do not bind to microtubules, or lag behind in transport. These observations suggest that in SPG10 patients, HSP develops due to less frequent and slower axonal transport events, leading to deficient supply of the synapse.

5.2 Introduction

Kinesin superfamily proteins are typically ATP- and microtubule-dependent motor proteins (Woehlke and Schliwa, 2000). Members of the Kinesin-1 family (formerly conventional kinesins) are involved in intracellular long-distance transport, and especially important in axons and dendrites (Hirokawa and Takemura, 2004; Hirokawa and Takemura, 2005). Vertebrate Kinesin-1 motors consist of two heavy chains (KHC, 120 kDa) that are responsible for motor activity, and two light chains (64kDa, KLC) involved in cargo association (Vale and Fletterick, 1997). The N-terminal motor domains of the heavy chains function as a microtubule-activated ATPase and generate force and motility. Each ATP hydrolysis is coupled to an 8 nm step towards the plus-end of the microtubule (Hua *et al.*, 1997; Schnitzer and Block, 1997). The characteristic, processive hand-over-hand type motility requires coordinated activity of two coupled motor heads (Hackney *et al.*, 2003; Hancock and Howard, 1998).

The slow and the fast anterograde components of axonal transport seem to arise at least in part from Kinesin-1 action (Barry *et al.*, 2007; Brown, 2003; Shah and Cleveland, 2002). In vertebrates, one ubiquitous (uKHC or KIF5B), and two neuron-specific forms of KIF5 (KIF5A or nKHC, and KIF5C) are known (Kanai *et al.*, 2000; Navone *et al.*, 1992; Niclas *et al.*, 1994). There is strong evidence that KIF5A is the major anterograde motor for slow axonal transport of neurofilaments (Barry *et al.*, 2007; Xia *et al.*, 2003).

Mutations in KIF5A's motor domain have recently been shown to cause hereditary spastic paraplegia (HSP), a disorder characterised by progressive spastic weakness of the lower extremities (Blair *et al.*, 2006; Fichera *et al.*, 2004; Lo Giudice *et al.*, 2006; Reid *et al.*, 2002). It is a so-called 'dying-back' neuropathy because synapses degrade first (Casari and Rugarli, 2001; Gould and Brady, 2004). At least 30 genetic loci are linked to HSP, among them SPG10, which turned out to contain the gene for KIF5A (Reid *et al.*, 2002). SPG10 patients have point mutations in one copy of KIF5A, and these mutations are responsible for the disease (Blair *et al.*, 2006; Fichera *et al.*, 2004; Lo Giudice *et al.*, 2006; Reid *et al.*, 2002). Although the genetic cause of SPG10 is thus known today, the mechanism of pathogenesis is unclear. The inheritance is autosomal dominant, and therefore defective KIF5A alleles may lead to dysfunctional kinesin motors that inhibit microtubule-dependent transport directly. Judging from the literature, this mechanism is likely for one of the known mutants as a

similar mutation at the same position in Ncd and Kar3 led to a catalytically inactive, rigor microtubule-binding protein (Song and Endow, 1998). Alternatively, the patients may suffer from haplo-insufficiency, as proposed for SPG4 (Beetz *et al.*, 2006). To find out which mechanism is more likely, we investigate here the properties of KIF5A and four of the known HSP mutants in enzymatic, motility and cargo transport assays.

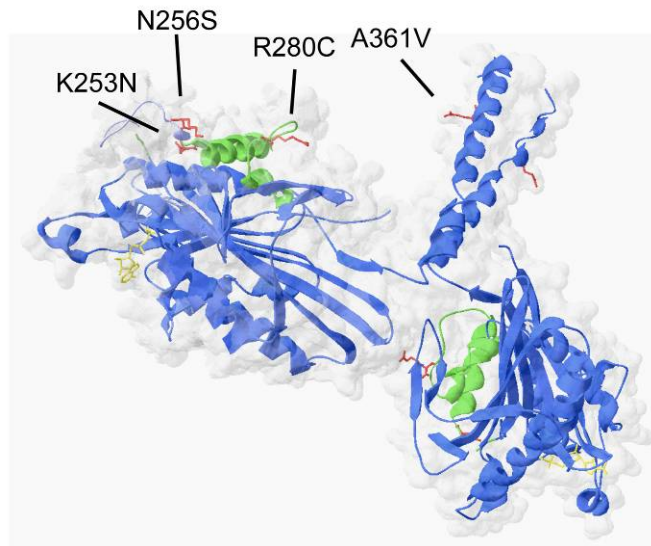


Figure 5.1 Location of HSP mutations.

The figure shows a ribbon model of dimeric rat kinesin (3KIN) with stick representations of exchanged amino acids (red). ADP ligands are yellow, structures underlying the microtubule-binding site are green.

We focus here on the three mutants found first (N256S, R280C and A361V; (Fichera *et al.*, 2004; Lo Giudice *et al.*, 2006; Reid *et al.*, 2002)), and one unpublished mutant found by one of the co-authors (K253N; R.S.). Two of the mutations (K253N and N256S) are located in loop 11, which connects microtubule and ATP-binding sites (Figure 5.1). The third mutation (R280C) is located directly in the microtubule-binding site (Alonso *et al.*, 1998; Woehlke *et al.*, 1997). To avoid oxidation artifacts *in vitro*, we introduced a serine residue instead of a cysteine. The A361V mutation is located in the neck. For the characterisation of these mutants, we used his-tagged, bacterially expressed proteins comprising the first 391 amino acids of KIF5A (or KIF5A mutant), followed by part of KIF5B's tail. The first coiled-coil of KIF5B's tail is known to bind unspecific to glass and carboxylated surfaces, allowing easy surface attachment for gliding assays (Coppin *et al.*, 1996; Jaud *et al.*, 2006; Kallipolitou *et al.*, 2001).

5.3 Results

5.3.1 Motility and processivity

To elucidate the basic properties of KIF5A and its HSP mutant forms, we performed multiple motor gliding assays. At high motor coating densities on glass coverslips the wildtype motor displaced microtubules at $0.73 \pm 0.02 \mu\text{m/s}$ (\pm standard error of the mean, s.e.m.). Except for the A361V mutant that was indistinguishable from wildtype, all other KIF5A mutants were significantly slower (Table I and Figure 5.2).

Noteworthy, only few microtubules bound to the R280S mutant, and if so the velocities varied widely (6 % standard deviation (s.d.) instead of 1 % for wildtype), suggesting a low microtubule affinity.

To find out whether gliding activity of KIF5A mutants was based on a cooperative effect, we measured velocities in dependence of coating densities on the coverslip. We estimated a critical concentration below which no microtubule binding occurred, and measured gliding velocities at this concentration. Here, the wildtype motor showed an elevated velocity compared to high coating densities ($0.88 \pm 0.01 \mu\text{m/s}$ vs $0.73 \mu\text{m/s}$) but except for the A361V mutant all mutants were slightly slower (Table I; Figure 5.2).

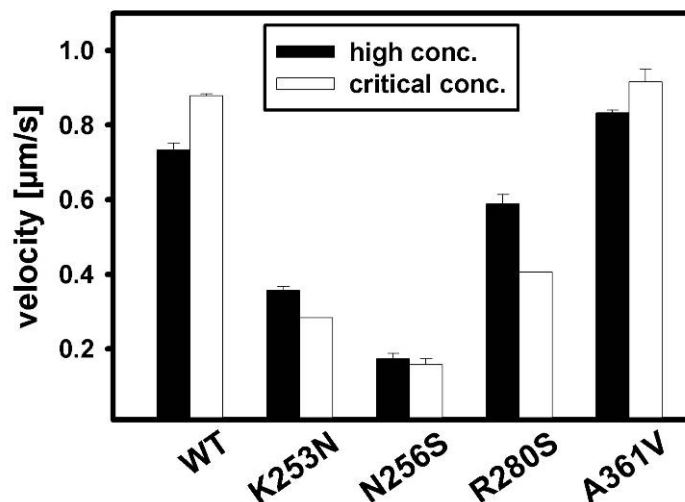


Figure 5.2 Multiple motor gliding.

Velocities at different motor densities. The bar graph shows the mean microtubule velocities and s.e.m. in standard gliding assays at high ($\sim 1 \mu\text{M}$) and low (critical concentrations, the lowest density where microtubule attachment occurred) motor surface densities. In contrast to wildtype and the A361V mutant, most mutant velocities slightly dropped at low density.

The critical concentrations of the mutants were quite different from wildtype, indicating largely altered microtubule affinities. The wildtype protein could be diluted to 19 nM. At this concentration microtubule single point attachments were observed, indicating that microtubules were tethered by only one kinesin motor (Hunt and Howard, 1993). None of the homodimeric mutants showed microtubules pivoting around a single point of attachment, suggesting that multiple motors are necessary to bind microtubules. Mutants also required up to one order of magnitude higher coating densities to promote microtubule motion, supporting that multiple motors are necessary for microtubule binding (Table I). The strongest effect was found in the R280S mutant (approximately 15-fold), in agreement with observations in high-density motility assays.

As these observations suggested that none of the mutants was able to promote processive single-molecule motility, we investigated their motility in optical laser trap assays (Jaud *et al.*, 2006; Svoboda *et al.*, 1993). To this end, microtubules were immobilised on the coverslip, motors attached to carboxylated polystyrene beads, and finally trapped in a laser beam. Single wildtype KIF5A motors showed long processive runs ($\geq 1 \mu\text{m}$) and single 8 nm steps could be distinguished (Figure 5.3).

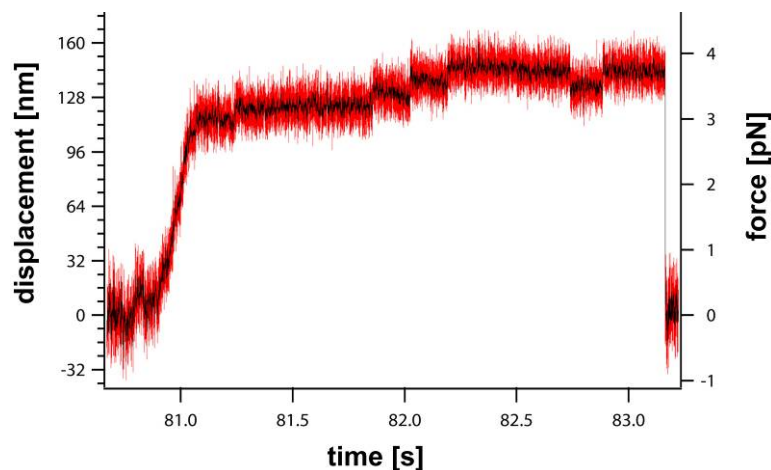


Figure 5.3 Example trace of laser trapping experiments with wildtype KIF5A.

The left y-axis shows displacements (nm), the right y-axis forces (pN). The example trace shows that wildtype KIF5A moves processively in steps of 8 nm. None of the mutants N253K, K256S or R280S produced similar traces. They only showed short, infrequent microtubule binding events at high densities and never moved in consecutive 8 nm steps.

In stark contrast, none of the mutants showed displacements of more than a few nm. This type of bead motility was only observed at high kinesin densities at which steps

could not be discerned. These data suggest that the SPG10 mutants are no longer processive.

5.3.2 Enzymatic activity

To measure altered microtubule affinities quantitatively, and to determine enzymatic velocities, we measured the microtubule-dependent ATP turnover in steady state assays (Huang and Hackney, 1994; Schafer *et al.*, 2003). As in motility assays, the N256S mutant was slowest but its microtubule affinity was only slightly decreased (Figure 5.4 and Table I). The K253N mutant reached two thirds of the wildtype k_{cat} , and showed significantly increased microtubule half-maximal activation constants ($K_{0.5,MT}$). The R280S mutant had such a low microtubule affinity that the assay did not allow adding saturating microtubule concentrations. Therefore, the extrapolated k_{cat} and, as a consequence, $K_{0.5,MT}$, are inaccurate. Still, they indicate that k_{cat} is not significantly affected but that $K_{0.5,MT}$ is at least one order of magnitude higher than wildtype.

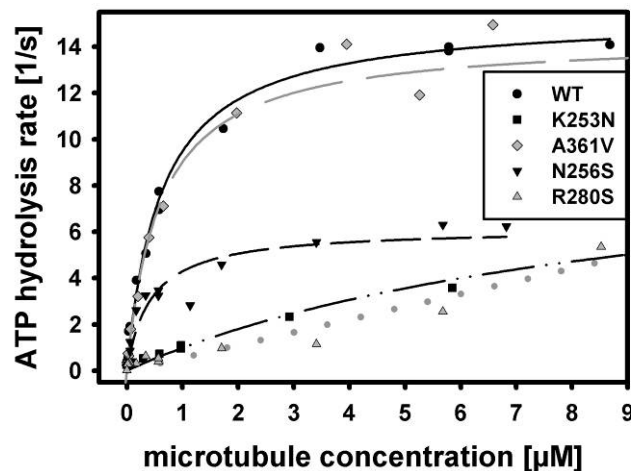


Figure 5.4 Steady-state ATPase activity.

The ATP turnover is plotted against the microtubule concentration and fitted using Michaelis-Menten kinetics. Maximal turnover rates (k_{cat}) and half-maximal activation constants ($K_{0.5,MT}$) were deduced from measurements of at least two independent protein preparations (Table I).

As in gliding assays, the A361V mutant did not show any significant difference to wildtype. We suspected that it might be a thermosensitive mutant, but prolonged incubation at 37 °C did not lead to any defects in gliding. Why this mutation causes HSP is therefore unclear from our *in vitro* studies. Possibly, the mRNA stability is affected, or the mutation represents an accidental polymorphism (it was found in only

one patient (Lo Giudice *et al.*, 2006)). For these reasons we did not investigate this mutant further.

5.3.3 Heterozygous patients

The above gliding and enzymatic assays suggested that KIF5A mutant motors involved in HSP either are slower (N256S), or have a reduced microtubule affinity (R280S), or both (K253N). However, these conclusions were based on observations of homodimeric mutant motors. In reality patients are heterozygous and possess one mutated and one intact KIF5A allele. If both alleles were expressed equally – and we did not find any reason why this should not be the case (Ding *et al.*, 2004) – one expects three populations of kinesin dimers: homodimeric wildtype motors, homodimeric mutant motors, and heterodimeric motors with one wildtype and one mutant subunit at a stoichiometry of 1:1:2 (Figure 5.5). The question therefore is why the inheritance of SPG10 is dominant and patients develop the disorder despite one intact copy of the KIF5A gene.

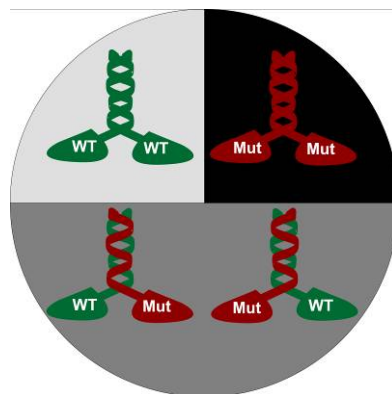


Figure 5.5 Expression levels in heterozygous patients.

Expression model. Patients have one wild type allele and one mutated allele for Kif5A. Assuming equal expression of the two protein chains, kinesins possibly dimerise as a homo- or heterodimer in a 1:2:1 ratio (wildtype:heterodimer:homodimeric mutant).

To address this question, we started using simple gliding assays with mixtures of wildtype and homodimeric mutant motors. We therefore mixed wildtype protein with homodimeric mutants at ratios from 50 % wildtype to 0.2 % wildtype, and observed the microtubule gliding velocity (Figure 5.6). One explanation for the dominant inheritance could be that the mutant motor slows down the microtubule gliding velocity in gliding assays of mixed motors. Only the N256S mutant behaved this way, and reduced the microtubule gliding velocity more than 2-fold at a 50:50 mixture of

wildtype and mutant motor (mixture: $0.39 \pm 0.01 \mu\text{m/s}$; wildtype: $0.88 \pm 0.01 \mu\text{m/s}$). The K253N mutant did not affect the velocity significantly below 99-fold excess, the R280S mutant interfered only slightly with the assay at a 500-fold excess (0.2% wildtype; Figure 5.6).

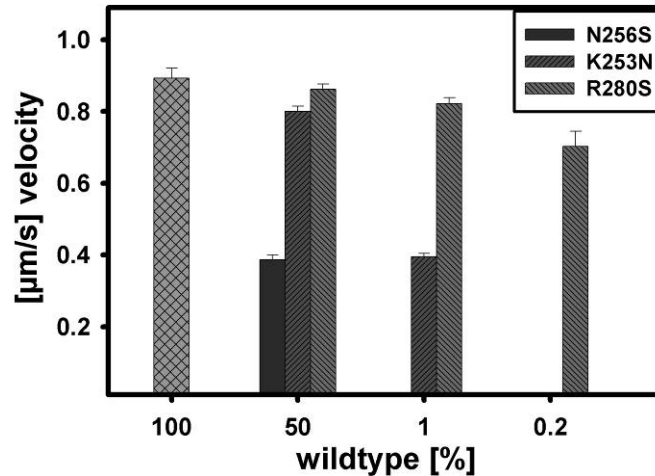


Figure 5.6 Dominance in vitro.

The bars and error bars represent average velocities and s.e.m. of mixtures of homodimeric wildtype and mutant motors at different ratios. Only the N256S mutant slowed down the microtubule velocity at equimolar stoichiometry to wildtype, the K253N and R280S mutants interfered only at large excess.

These mixed gliding assays showed that only the N256S mutant has a dominating effect, and that the mutations K253N and R280S do not interfere with wildtype motility *in vitro*.

5.3.4 Cargo transport assays

To answer the question whether heterodimeric mutants (one wildtype, one mutant subunit) are dominant over wildtype motors, we did not use the simplistic multi-motor gliding assay but a modified bead assay to mimic the cellular situation more realistically. We coated quantum dots (serving as an artificial, fluorescent cargo) with a 1:2:1 mixture of mutant homodimer : heterodimer : wildtype homodimer (Figure 5.7). We added motor in a stoichiometric excess of five (total motor dimers over quantum dots), based on previous reports on vesicle transport *in vivo* (Ashkin *et al.*, 1990; Hill *et al.*, 2004; Miller and Lasek, 1985). Assuming a Poisson distribution, the majority of quantum dots are expected to be coated with 3-6 motors, 3-4 % with only one motor (Figure 5.7).

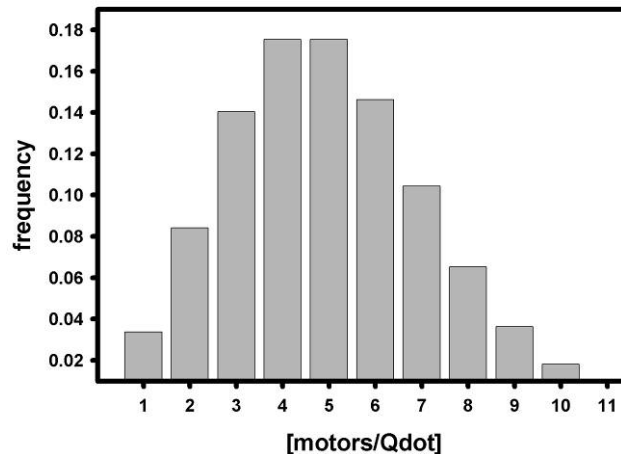


Figure 5.7 Poisson distribution.

The histogram shows calculated frequencies of KIF5A motors on quantum dots, assuming a Poisson distribution with 5-fold molar excess of motors over quantum dots. The majority of quantum dots is expected to be coated with three to six motors, approximately 3.5% of the quantum dots are coated with one motor, less than 24% are coated with more than six motors.

To understand the effect of defective motors on quantum dot transport we first measured the velocities of quantum dots. We added motor-coated quantum dots to a flow cell that had been prepared to contain surface-attached microtubules. We then recorded the quantum dot motility and analysed it using kymograms (Figure 5.8). The velocities were determined from the slopes of phases of uninterrupted movement and plotted into a histogram.



Figure 5.8 Kymograms of quantum dot motility.

Video sequences were reduced to one dimension along the length of a microtubule (y-axis; scale bar 5 μm), and resolved in time along the x-axis (1 min in total). Bright lines are moving quantum dots, their angles reflect the velocity. As an example, quantum dots coated with the N256S mutant move visibly slower than wildtype-coated dots.

In these assays, wildtype KIF5A transported quantum dots at a velocity of $0.79 \pm 0.02 \mu\text{m/s}$, comparable to velocities in conventional gliding assays. The K253S mutant displaced the cargo at a similar mean velocity ($0.78 \pm 0.01 \mu\text{m/s}$) but showed a

second peak in the histogram at lower velocities (Figure 3B). The N256S mutant slowed down the mean velocity modestly to $0.74 \pm 0.07 \mu\text{m/s}$. Here, the fraction of slowly moving quantum dots was much more pronounced and led to a clear increase of the standard deviation ($0.26 \mu\text{m/s}$ instead of $0.21 \mu\text{m/s}$). From a theoretical point of view, we expect three overlapping Gaussian distributions originating from three dimer populations. As indicated by curve fitting (data not shown), the variances of the velocities are too wide to distinguish the populations clearly.

In contrast to the other two mutants, the R280S mutants showed a slightly faster mean velocity in the cargo transport assay ($0.83 \pm 0.03 \mu\text{m/s}$). Possibly, the extremely low microtubule affinity of the mutant reduces the effective density of motor heads on the surface of the cargo. As in multiple motor gliding assays, this may have led to a higher velocity. These considerations suggest that cargo velocities in patients with the R280C mutation are not significantly altered.

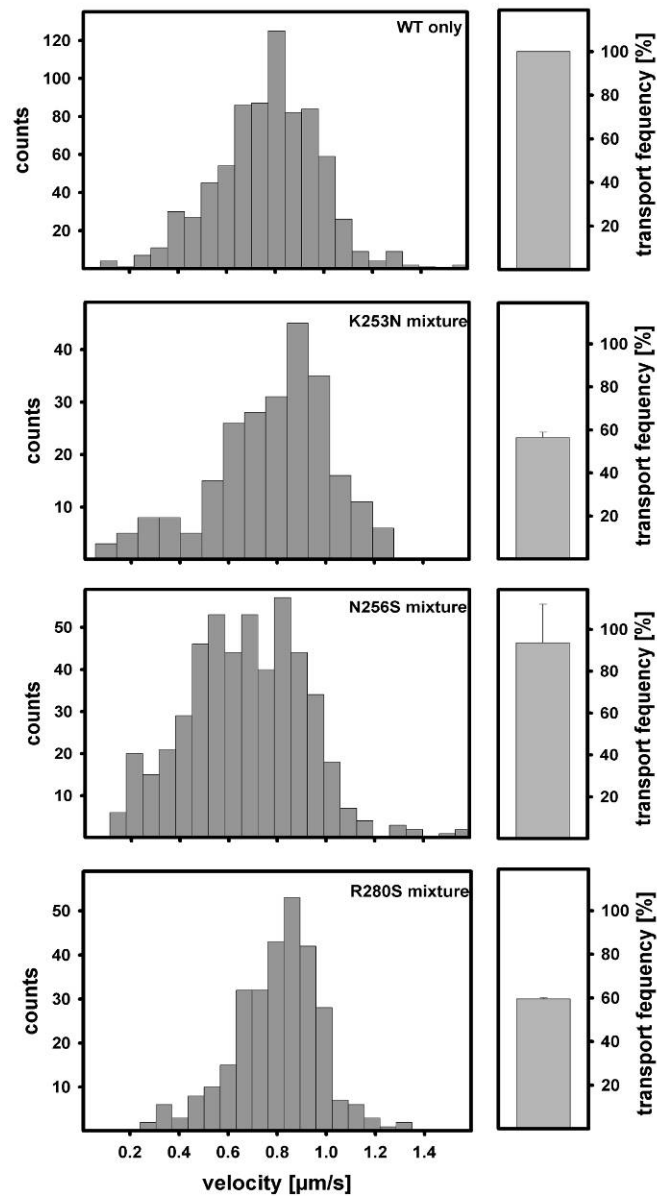


Figure 5.9 Cargo transport assay.

Histograms of velocities and transport frequencies. The histograms show velocity distributions of quantum dots coated with mixtures of wildtype and mutant KIF5A. The quantum dots were incubated with a 5-fold stoichiometric excess of motors. The mutants were tested as mixtures of 25 % wildtype, 50 % heterodimeric and 25 % homodimeric mutant motors, the ratio expected in patients. The velocities of wildtype KIF5A were distributed nearly Gaussian with a mean velocity of $0.79 \mu\text{m/s}$ and a standard deviation of $0.21 \mu\text{m/s}$. Mutant mixtures led to similar maximal velocities, but the K253N and N256S mutants caused more frequent slow events. The distribution of K253N velocities is clearly bimodal, that of N256S blurrier but clearly extended to slow velocities (standard deviation $0.26 \mu\text{m/s}$). The R280S mutant did not show an altered distribution because mutant-coated quantum dots rarely bound to microtubules. Next to the histograms bars indicate the fraction of motile quantum dots of all binding-competent quantum dots. This number was determined by comparison of microtubule-bound quantum dots in the presence of ATP and AMP-PNP, and standardised with regard to wildtype (see Material and methods). The error bars are standard errors from assays on two independent protein preparations.

Therefore, other defects have to cause the disease, possibly the amount or rate of cargo particles arriving at the synapse.

A reduced arrival rate of cargo particles could also result from a larger fraction of cargo particles unable to bind to microtubules. For this reason we added AMP-PNP to the quantum dot motility assay after three movies, and then counted the number of immobilised quantum dots per microtubule length. We then compared this number to the number of previously moving quantum dots per microtubule length and time of the same sample, and finally calculated a relative binding ratio. We set the ratio to 100% for wildtype, and compared the mutants with wildtype. The relative binding ratio of K253N- and R280S-coated quantum dots dropped to less than 60 % (Figure 5.9; mean of two independent protein preparations). The N256S mutant did not differ significantly from wildtype, suggesting that the N256S mutant does not reduce the cargo-microtubule binding frequency, but the K253N and R280S mutants do so.

Is this conclusion also valid for motor/cargo stoichiometries other than 1:5, as chosen in our assays? Most likely, the effect is even more pronounced at lower coating densities, and decreases if more than five motors bind to one cargo particle. This follows from Poisson statistics, which applies if wildtype/mutant dimers form randomly, and attach to quantum dots randomly (Figure 5.7). Our motility assays show that the slower moving quantum dot population causes approximately 10-30 % of the motility events, in agreement with a Poisson distribution. As the cargo-binding site is unaffected in HSP mutants, a Poisson distribution is also likely for the cargo-attachment of microtubule affinity mutants.

Table I Properties of HSP kinesin mutants

Every value is the averages of two independent protein preparations \pm s.e.m.. Velocities of gliding assays were determined by averaging the velocity of 20 microtubules. Here the s.e.m. was always below 0.06 $\mu\text{m/s}$. Velocities in Cargo Assay were determined by measuring more than 150 data points. SEM was in every case below 0.02 $\mu\text{m/s}$.

	Gliding Assay			ATPase Assay		Cargo Assay	
	Velocity [$\mu\text{m/s}$] (High density)	Velocity [$\mu\text{m/s}$] (Critical conc.)	Critical conc. [nM]	K_{cat} [ATP/s]	$K_{0.5, \text{MT}}$ [μM]	Velocity [$\mu\text{m/s}$]	Relative Activity [%]
WT	0.73 ± 0.02	0.88 ± 0.01	19-22 ^a	17.58 ± 2.50	0.95 ± 0.25	0.79 ± 0.02 $\sigma = 0.21$	100
K253N	0.36 ± 0.01	0.28^{b}	110 ^b	10.55 ± 0.06	7.68 ± 3.63	0.78 ± 0.01 $\sigma = 0.23$	56.5 ± 2.5
N256S	0.17 ± 0.01	0.16 ± 0.02	100-220 ^a	4.75 ± 1.31	0.43 ± 0.16	0.74 ± 0.07 $\sigma = 0.26$	93.5 ± 18.5
R280S	0.59 ± 0.03	0.41^{b}	340 ^b	n/a	n/a	0.83 ± 0.03 $\sigma = 0.20$	59.5 ± 0.5
A361V	0.83 ± 0.01	0.92 ± 0.03	50-180 ^a	9.75 ± 4.54	0.62 ± 0.00	n/d	n/d

(n/a: not applicable; extrapolation unreliable; n/d: not determined)

^a data only of one protein preparation available

^b first protein preparation – second protein preparation

5.4 Discussion

Spastic paraplegia patients belonging to the SPG10 group develop the disorder due to mutations in the KIF5A gene (Blair *et al.*, 2006; Fichera *et al.*, 2004; Lo Giudice *et al.*, 2006; Reid *et al.*, 2002). As the degeneration starts from synapses of long motoneurons, and KIF5A is one of the major anterograde motors of neuronal transport, the lack of kinesin cargo delivery at the axon tip is the likely reason for degeneration. There are two possible explanations why mutated KIF5A decreases the arrival rate of cargo at axon tips. Either, mutated kinesins act as brakes for cargo particles or even block microtubule tracks, or they are microtubule-binding incompetent and compete for binding sites at the cargo that then are inaccessible for intact motors. Both models could explain the dominant inheritance of SPG10. Our data suggest that the second model is likely for two of the mutants (N253K and R280C) because they do not interfere significantly with wildtype KIF5A in several types of motility assays. They have low microtubule affinities, indicating that they do not act as roadblocks (Figure 5.10). The first model may apply to a third mutant (N256S), which shows similar microtubule affinities as wildtype and slows down microtubule gliding velocities at equimolar amounts to wildtype (Figure 5.10). Noteworthy, this mutant does not bind microtubules in rigor, as expected from similar mutations in Kar3 and Ncd (Song and Endow, 1998). Here, the N to K exchange at this position decoupled microtubule binding and catalytic activity, leading to a constitutively tight microtubule-binding mutant.

	velocity	MT affinity	dominant	transport
K253N	↓	↓	-	↓
N256S	↓ ↓	-	+	-
R280S	-	↓ ↓	-	↓
A361V	-	-	n/d	n/d

Figure 5.10 Motility defects in HSP mutant kinesins.

The four investigated HSP mutant KIF5A motors show different defects *in vitro*. The velocity defect was deduced from conventional *in vitro* gliding assays on homodimeric mutants, the affinity defect from landing rates of microtubules to coated glass surfaces and ATPase assays, the dominance from the ability of the mutant to reduce the gross gliding velocity in mixed motor gliding assays, the transport frequencies from the ratio of quantum dots that bind to microtubules in the presence of AMP-PNP but not attach with ATP. n/d – not determined.

How is axonal transport affected by these molecular defects? In our experiments we addressed this question in transport assays with artificial cargo. We mimicked the situation in patients - all known patients are heterozygous - by mixing wildtype motors with homo- and heterodimeric mutants. These assays revealed that the presence of mutant motors leads either to slow moving cargo populations, or populations that almost never bind to microtubules, or both. As a result, the anterograde transport frequency will be lower, and the arrival of the cargo transported by mutant motors at the synapse largely delayed. This effect might be enhanced by the presence of retrograde motors at the cargo that could dominate the gross transport.

As discussed above, this explanation holds true even if cargo particles were transported by more or less than five motors, the number used in our assays. With fewer motors per cargo particle, the fraction of poorly transported cargo would even be larger because kinesins seem to attach to quantum dots randomly, leading to a Poisson distribution of the numbers of motors per cargo (Figure 5.7). Accordingly, a lower coating density makes it more likely to find cargo particles attached to mutant motors only, leading to a more pronounced phenotype.

It is not exactly known how many motors are involved in the transport of cellular cargo *in vivo*. Electron microscopy indicates that several motor proteins are present at one cargo vesicle, and the excess of five chosen in our assays is realistic (Ashkin *et al.*, 1990; Hill *et al.*, 2004; Miller and Lasek, 1985). Such vesicles have been suspected to be the cargo in fast axonal transport (Barry *et al.*, 2007). Molecular evidence suggests that Kinesin-1 is a major player in fast anterograde axonal transport, and therefore our experiments might be directly applicable to neurons (Barry *et al.*, 2007; Shah and Cleveland, 2002). The K253N and R280S mutants would diminish the fraction of transported cargo, the N256S heterodimer mutant would slow down each cargo vesicle it is attached to.

Alternatively, axonal degeneration in HSP patients might be induced by altered slow axonal transport. The most likely cargo of slow transport are neurofilaments, and there is strong evidence that KIF5A is the major anterograde motor for transport of neurofilament precursors (Barry *et al.*, 2007; Xia *et al.*, 2003). It is unknown, however, how many motors are attached to one neurofilament precursor complex. Still, the lack of neurofilament supply to the synapse is a plausible reason for neurodegeneration, as the mouse knockout mutants of several neurofilament components and the conditional mouse KIF5A knockout lead to neurodegeneration (Yuan *et al.*, 2006).

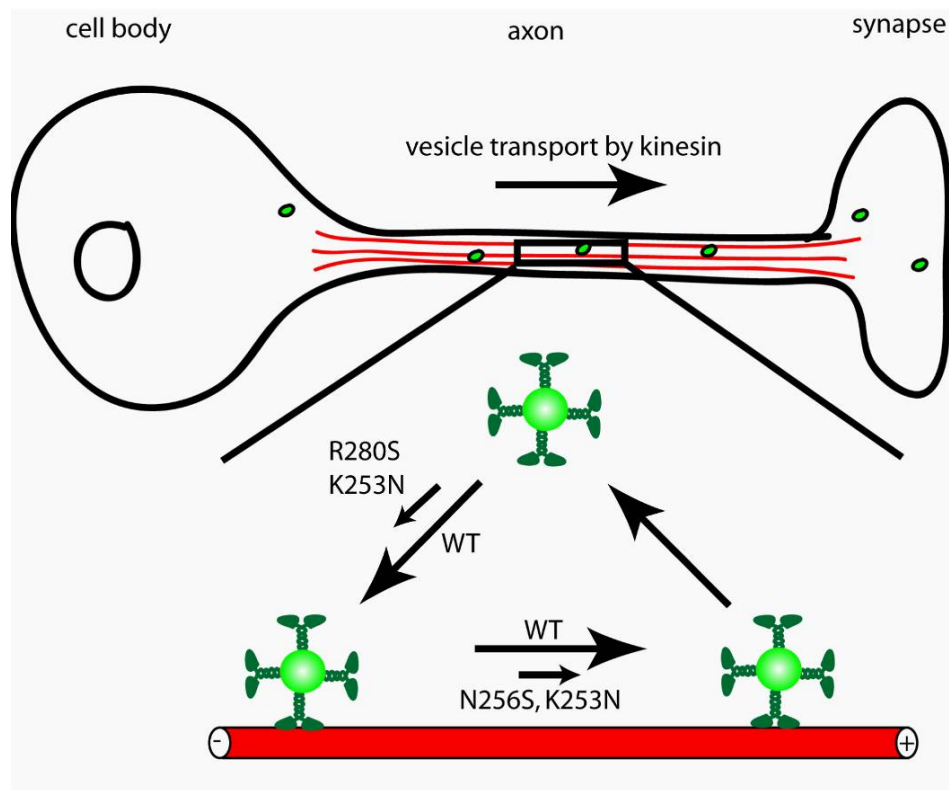


Figure 5.11 Model for emergence of transport defects.

According to theoretical models the anterograde axonal transport rate is determined by cargo binding and detachment frequencies, and the velocity and runlength of microtubule-attached cargo (Brown *et al.*, 2005; Craciun *et al.*, 2005). The mutants K253N and R280S diminish cargo attachment rates (shorter arrow), the mutants K253N and N256S the velocity of cargo.

The velocity of the slow axonal transport component is much slower than the velocity of KIF5A, and seems to emerge due to frequent, long pauses of the cargo. They make up 97 % of the time and are likely to involve a number of regulatory steps (Brown *et al.*, 2005; Craciun *et al.*, 2005). We imagine that the HSP KIF5A mutants N253K and R280C still possess the regulatory mechanisms of wildtype but rarely bind to microtubules in the activated state (Figure 5.11). The K256S mutant will bind as frequently as wildtype but move slower. This, again, would lead to infrequent arrival of cargo at the synapse and would be enhanced by the presence of normal retrograde motors.

Regardless of which component is affected the gross effect of the investigated HSP mutations on cargo transport is amazingly mild. SPG10 patients still have 25 % wildtype KIF5A dimers, and mixed motor assays indicate that the majority of cargo particles still move at wildtype rates, even in the presence of mutant motors. This may explain the late onset of the disease in patients with the K253N (R.S., unpublished)

and the R280S mutation at ages between the second and the fourth life decade (Blair *et al.*, 2006; Fichera *et al.*, 2004; Lo Giudice *et al.*, 2006; Reid *et al.*, 2002). The N256S mutation leads to more severe effects and has a dominant effect *in vitro*, correlating with an early onset of clinical symptoms before the age of 20. It will be interesting to investigate the mutants in a cellular environment that includes regulatory mechanisms for kinesin activity and retrograde motors at the cargo. Retrograde motors are likely to enhance the lag between slow and normal cargo populations. Still, the basic effects of the K253N, R280S and N256S mutations on transport are clear from our experiments and may open ways to suppress the progress of neurodegeneration, possibly by introducing excess KIF5A wildtype motor.

5.5 Materials and methods

5.5.1 Cloning, protein expression and purification

All constructs are based on a synthetic gene encoding the N-terminal 391 amino acids of KIF5A and its mutants (Sloning GmbH, Puchheim, Germany), cloned into a pET 24a vector (Merck, Darmstadt, Germany). 160-amino acids of the human kinesin (uKHC or KIF5B) tail were added by cloning and followed by a Strep- or His-tag sequence (Qiagen, Hilden, Germany). For the expression of heterodimers the inserts of Strep-tag mutant vectors were cloned into the His-tag wildtype vector.

Homodimeric protein was expressed in *E. coli*; lysed and purified in a phosphate buffer (50 mM Na₂HPO₄, 250 mM NaCl, 2 mM MgCl₂) over Ni-NTA-columns, followed by a Q-Sepharose anion exchange column in pipes buffer (25 mM Na-Pipes, 2 mM MgCl₂, 1 mM EGTA, pH=6.9). Heterodimers were tandem purified by a Ni-NTA-column, followed by a Strep-Tactin column. Protein concentrations were determined by a Bradford test (BioRad, Hercules, USA) or from a SDS-Gel with a BSA concentration series (analysis with ImageJ). Microtubules were prepared from pig brain tubulin and polymerised as described (Mandelkow *et al.*, 1985), the Atto488 (AttoTec, Siegen, Germany), tetramethylrhodamine and biotin labelled tubulin was obtained as published (Hyman *et al.*, 1991).

5.5.2 ATPase assay

Microtubule activated steady-state ATPase rates were determined in a coupled enzymatic Assay (Huang and Hackney, 1994; Kallipolitou *et al.*, 2001). The assay

was performed in 12A25+ buffer (12.5 mM AcesKOH, 25 mM potassium acetate, 5 mM MgCl₂, 0.5 M EGTA, pH 6.8) at 22 °C. The measurements were done at increasing microtubule concentrations; the k_{cat} was obtained from the extrapolated turnover at infinite microtubule concentration. $K_{0.5,MT}$ was determined at an ATP concentration of 1 mM. All values were determined on two independent protein preparations.

5.5.3 Gliding assays

A flow cell was incubated for 5 min with hTail-tagged motors in dilution buffer (10 mM ATP, 1 mg/ml BSA, 150 mM NaCl in BRB80+ (80 mM PIPES·KOH, pH 6.8, 5 mM MgCl₂, 1 mM EGTA)). After washing with blocking buffer (1 mg/ml BSA in BRB80+), the flow chamber was filled with Atto488-labelled microtubules in motility buffer (2 mM ATP, 20 µM taxol, 1 mM DTT, 0.1 mg/ml glucose oxides, 0.37 mg/ml casein, 0.02 mg/ml catalase, 2.25 mg/ml glucose). All Assays were performed at 22°C. Gliding microtubules was observed by total internal reflection microscope (see below) and the velocity 20 microtubules was measured using the manufacturers' software (Olympus Biosystems GmbH, Planegg, Germany). All measurements were based on two independent protein preparations.

5.5.4 Laser Trapping assay

Optical trapping experiments were performed in a custom built optical trap described (Finer *et al.*, 1994) . Beads were captured in the beam of a 8 W Nd:YAG laser (Coherent Deutschland GmbH, Germany) focused through a high numerical aperture objective (NA=1.45, Olympus Deutschland GmbH, Germany). The position of trapped beads was detected by bright field imaging onto a quadrant diode (SPOT4D, UDT Sensors Inc., CA, USA). Data were acquired by an A/D converter board (NI-PCI-6259, National Instruments, Germany) with a sampling frequency of 40 kHz per channel and stored without prior filtering. Fluorescently labelled microtubules were fixed to the glass surface of a flow chamber by the use of the biotin-streptavidin system (see above) and imaged with TIRF. Kinesin molecules were allowed to adsorb to carboxylated polystyrene beads (532 nm, Polysciences Inc., USA) as described (Jaud *et al.*, 2006). Data from optical trapping experiments were analysed using IGOR Pro 4.01 (WaveMetrics, Portland, OR, USA).

5.5.5 Quantum dot assays

Biotin- and tetramethylrhodamine-labelled microtubules were attached to the surface of a flow chamber that had been incubated with 2 mg/ml BSA-biotin (Sigma-Aldrich Co., St. Louis, MO, USA) and 1 mg/ml streptavidin in BRB80+ buffer with 20 μ M paclitaxel. 160 nM carboxylated Qdots525 (Invitrogen, Carlsbad, USA) were mixed with 800 nM with kinesin in BRB80+, 1 mM ATP and 1 mg/ml casein. The solution was stored on ice for at least 5 minutes. After washing the flow chamber with 1 mg/ml BSA in BRB80+ motility mix (1 μ l quantum dots coated with kinesins, 2 mM ATP, oxygen scavenger (see above), 0.2 mg/ml casein, 1 mM DTT in BRB80+) was flushed in. The gliding activity was observed in an Olympus IX71 TIRF microscope with an excitation wavelength of 488 nm and a Hamamatsu C-9100 front-illuminated CCD camera. The optical resolution was 160 nm per 2x2-binned pixel, the integration time 200 ms.

To determine the number of binding-competent quantum dots in the flow chamber, 5 μ l of 100 mM AMP-PNP was added to the edge of the flow chamber after recording of three movie sequences in the presence of 2 mM ATP. When all quantum dots were static (approximately 3 min) images were recorded. The number of quantum dots per microtubule length was counted, and compared to the number of moving quantum dots per time and microtubule length in the presence of ATP. Relative values were calculated by setting wildtype to 100 %. All measurements were confirmed by a second independent protein preparation.

5.5.6 Data analysis

Movies taken from the quantum dot assay were analysed with ImageJ. The 'Brightest Point Projection' command showed moving quantum dots as a line, which were then converted to time-space plots (kymograms). From these kymograms velocities were calculated in areas of constant velocity. In parallel, the number of events was counted. The length of microtubules and number of attached quantum dots after AMP-PNP addition was also analysed in ImageJ. For statistical analysis SigmaPlot 2000 and Sigma Stat 3.1 Software (Systat, Point Richmond, CA, USA) was used.

5.6 References

- Alonso MC, van Damme J, Vandekerckhove J, Cross RA. 1998. Proteolytic mapping of kinesin/ncd-microtubule interface: nucleotide-dependent conformational changes in the loops L8 and L12. *Embo J* 17(4):945-951.
- Ashkin A, Schutze K, Dziedzic JM, Euteneuer U, Schliwa M. 1990. Force generation of organelle transport measured in vivo by an infrared laser trap [see comments]. *Nature* 348(6299):346-348 issn: 0028-0836.
- Barry DM, Millecamps S, Julien JP, Garcia ML. 2007. New movements in neurofilament transport, turnover and disease. *Exp Cell Res* 313(10):2110-2120.
- Beetz C, Nygren AO, Schickel J, Auer-Grumbach M, Burk K, Heide G, Kassubek J, Klimpe S, Klopstock T, Kreuz F, Otto S, Schule R, Schols L, Sperfeld AD, Witte OW, Deufel T. 2006. High frequency of partial SPAST deletions in autosomal dominant hereditary spastic paraplegia. *Neurology* 67(11):1926-1930.
- Blair MA, Ma S, Hedera P. 2006. Mutation in KIF5A can also cause adult-onset hereditary spastic paraplegia. *Neurogenetics* 7(1):47-50.
- Brown A. 2003. Axonal transport of membranous and nonmembranous cargoes: a unified perspective. *J Cell Biol* %R 101083/jcb200212017 160(6):817-821.
- Brown A, Wang L, Jung P. 2005. Stochastic Simulation of Neurofilament Transport in Axons: The "Stop-and-Go" Hypothesis. *Mol Biol Cell* 16(9):4243-4255.
- Casari G, Rugarli E. 2001. Molecular basis of inherited spastic paraplegias. *Curr Opin Genet Dev* 11(3):336-342.
- Coppin CM, Finer JT, Spudich JA, Vale RD. 1996. Detection of sub-8-nm movements of kinesin by high-resolution optical-trap microscopy. *Proc Natl Acad Sci U S A* 93(5):1913-1917.
- Craciun G, Brown A, Friedman A. 2005. A dynamical system model of neurofilament transport in axons. *Journal of Theoretical Biology* 237(3):316.
- Ding C, Maier E, Roscher AA, Braun A, Cantor CR. 2004. Simultaneous quantitative and allele-specific expression analysis with real competitive PCR. *BMC Genet* 5:8.
- Fichera M, Lo Giudice M, Falco M, Sturnio M, Amata S, Calabrese O, Bigoni S, Calzolari E, Neri M. 2004. Evidence of kinesin heavy chain (KIF5A) involvement in pure hereditary spastic paraplegia. *Neurology* 63(6):1108-1110.
- Finer JT, Simmons RM, Spudich JA. 1994. Single myosin molecule mechanics: piconewton forces and nanometre steps. *Nature* 368(6467):113-119.
- Gould RM, Brady ST. 2004. Neuropathology: many paths lead to hereditary spastic paraplegia. *Curr Biol* 14(20):R903-904.

- Hackney DD, Stock MF, Moore J, Patterson RA. 2003. Modulation of kinesin half-site ADP release and kinetic processivity by a spacer between the head groups. *Biochemistry* 42(41):12011-12018.
- Hancock WO, Howard J. 1998. Processivity of the motor protein kinesin requires two heads. *J Cell Biol* 140(6):1395-1405.
- Hill DB, Plaza MJ, Bonin K, Holzwarth G. 2004. Fast vesicle transport in PC12 neurites: velocities and forces. *Eur Biophys J*.
- Hirokawa N, Takemura R. 2004. Molecular motors in neuronal development, intracellular transport and diseases. *Curr Opin Neurobiol* 14(5):564-573.
- Hirokawa N, Takemura R. 2005. Molecular motors and mechanisms of directional transport in neurons. *Nat Rev Neurosci* 6(3):201-214.
- Hua W, Young EC, Fleming ML, Gelles J. 1997. Coupling of kinesin steps to ATP hydrolysis. *Nature* 388(6640):390-393.
- Huang TG, Hackney DD. 1994. Drosophila kinesin minimal motor domain expressed in Escherichia coli. Purification and kinetic characterization. *J Biol Chem* 269(23):16493-16501.
- Hunt AJ, Howard J. 1993. Kinesin swivels to permit microtubule movement in any direction. *Proc Natl Acad Sci U S A* 90(24):11653-11657.
- Hyman A, Dreschel D, Kellogg D, Salser S, Sawin K, Steffen P, Wordeman L, Mitchison T. 1991. Preparation of Modified Tubulins. *Meth Enzymol* 196:478.
- Jaud J, Bathe F, Schliwa M, Rief M, Woehlke G. 2006. Flexibility of the neck domain enhances Kinesin-1 motility under load. *Biophys J* 91(4):1407-1412.
- Kallipolitou A, Deluca D, Majdic U, Lakamper S, Cross R, Meyhofer E, Moroder L, Schliwa M, Woehlke G. 2001. Unusual properties of the fungal conventional kinesin neck domain from *Neurospora crassa*. *Embo J* 20(22):6226-6235.
- Kanai Y, Okada Y, Tanaka Y, Harada A, Terada S, Hirokawa N. 2000. KIF5C, a novel neuronal kinesin enriched in motor neurons. *J Neurosci* 20(17):6374-6384.
- Lo Giudice M, Neri M, Falco M, Sturnio M, Calzolari E, Di Benedetto D, Fichera M. 2006. A missense mutation in the coiled-coil domain of the KIF5A gene and late-onset hereditary spastic paraplegia. *Arch Neurol* 63(2):284-287.
- Mandelkow E-M, Herrmann M, Rühl U. 1985. Tubulin Domains Probed by Limited Proteolysis and Subunit-specific Antibodies. *J Mol Biol* 185:311-327.
- Miller RH, Lasek RJ. 1985. Cross-bridges mediate anterograde and retrograde vesicle transport along microtubules in squid axoplasm. *J Cell Biol* 101(6):2181-2193.
- Navone F, Niclas J, Hom-Booher N, Sparks L, Bernstein HD, McCaffrey G, Vale RD. 1992. Cloning and expression of a human kinesin heavy chain gene: interaction of the COOH-terminal domain with cytoplasmic microtubules in transfected CV-1 cells. *J Cell Biol* 117(6):1263-1275.

- Niclas J, Navone F, Hom-Booher N, Vale RD. 1994. Cloning and localization of a conventional kinesin motor expressed exclusively in neurons. *Neuron* 12(5):1059-1072.
- Reid E, Kloos M, Ashley-Koch A, Hughes L, Bevan S, Svenson IK, Graham FL, Gaskell PC, Dearlove A, Pericak-Vance MA, Rubinsztein DC, Marchuk DA. 2002. A kinesin heavy chain (KIF5A) mutation in hereditary spastic paraplegia (SPG10). *Am J Hum Genet* 71(5):1189-1194.
- Schafer F, Deluca D, Majdic U, Kirchner J, Schliwa M, Moroder L, Woehlke G. 2003. A conserved tyrosine in the neck of a fungal kinesin regulates the catalytic motor core. *Embo J* 22(3):450-458.
- Schnitzer MJ, Block SM. 1997. Kinesin hydrolyses one ATP per 8-nm step. *Nature* 388(6640):386-390.
- Shah JV, Cleveland DW. 2002. Slow axonal transport: fast motors in the slow lane. *Curr Opin Cell Biol* 14(1):58-62.
- Song H, Endow SA. 1998. Decoupling of nucleotide- and microtubule-binding sites in a kinesin mutant. *Nature* 396(6711):587-590 issn: 0028-0836.
- Svoboda K, Schmidt CF, Schnapp BJ, Block SM. 1993. Direct observation of kinesin stepping by optical trapping interferometry [see comments]. *Nature* 365(6448):721-727.
- Vale RD, Fletterick RJ. 1997. The design plan of kinesin motors. *Ann Rev Cell Dev Biol* 13:745-777.
- Woehlke G, Ruby AK, Hart CL, Ly B, Hom-Booher N, Vale RD. 1997. Microtubule interaction site of the kinesin motor. *Cell* 90(2):207-216.
- Woehlke G, Schliwa M. 2000. Walking on two heads: the many talents of kinesin. *Nat Rev Mol Cell Biol* 1(1):50-58.
- Xia CH, Roberts EA, Her LS, Liu X, Williams DS, Cleveland DW, Goldstein LS. 2003. Abnormal neurofilament transport caused by targeted disruption of neuronal kinesin heavy chain KIF5A. *J Cell Biol* 161(1):55-66.
- Yuan A, Rao MV, Sasaki T, Chen Y, Kumar A, Veeranna, Liem RK, Eyer J, Peterson AC, Julien JP, Nixon RA. 2006. Alpha-internexin is structurally and functionally associated with the neurofilament triplet proteins in the mature CNS. *J Neurosci* 26(39):10006-10019.

Summary

This thesis deals with the mechanism of various kinesin motor proteins. Kinesin converts chemical energy into mechanical energy. Precisely, the molecular motor hydrolyses ATP and uses the energy to step along microtubules. One amazing property of some kinesins, called processive motors, is that they can step on microtubules for several encounters without detaching. This property can only be maintained if the two heads are highly coordinated. Chapter 2 addresses the question where the structural determinants are to enable processive movement. Chapter 3 further investigates the structural basis of stepping and analyses which elements of the motor ensure precise coordination of both motor domains in processive kinesins. Chapter 4 aims to resolve ATP-binding times at single kinesin heads using fluorescent ATP analogues in a microscopic assay. This data will yield new insight into the coordination of the two motor domains of processive Kinesin-1 motors. Chapter 5 applies molecular techniques to understand degeneration of neurons caused by defective kinesins in patients suffering from a hereditary form of spastic paraplegia. Here, the coordination of the two heads is disturbed in most cases.

The results of each chapter can be summarised as follows:

Chapter 2: To find out which parts of kinesin are required for coupling of kinesin's two motor heads, chimaeras with swapped domains of the processive *Neurospora crassa* kinesin (NcKin) and its non-processive counterpart NcKin3 were tested for their motile properties. The chimaera with the NcKin motor domain and the NcKin3 neck/stalk portion moved processively along microtubules although with a significantly decreased average runlength, suggesting a perturbing effect of the non-processive neck. The reverse chimaera containing motor domains of the non-processive kinesin NcKin3 was unable to perform processive movement, despite presence of the

Kinesin-1 neck coiled-coil. These observations suggest that determinants of processivity are in the motor core and that this processive movement is enhanced by the neck.

Chapter 3: It is thought that stepping of kinesin is initiated by a conformational change of a part termed neck-linker, which docks onto the core motor domain upon ATP binding. The exact effect of this neck-linker docking on the subsequent microtubule binding is unknown. To address this question we introduced reversible disulfides bridges (crosslinkable cysteines) to simulate the docked neck-linker conformation. The motility of Kinesin-1 motors with a docked neck-linker was severely affected. Furthermore, crosslinking led to a much lower microtubule affinity. Based on our experiments we suggest that neck-linker docking alters microtubule affinity of the individual heads during the chemo-mechanical cycle, which may help the rear head detaching when the front head has taken a step.

Chapter 4: Although it is now generally accepted that kinesin moves along microtubules in a stepwise hand-over-hand fashion, the coupling of stepping and ADP-release from the rear head is still controversial. To clarify this issue, we established a novel single-molecule method to observe FRET between fluorescently labelled human ubiquitous kinesin and ATP. This setup allowed observing single ATP binding events directly while human kinesin was stepping along the microtubule. In motility assays these labelled kinesins moved at wild type velocity and reached normal run lengths, indicating normal kinetic behaviour. Single ATP turnovers were measured in a confocal microscope setup with a sub-millisecond time-resolution. Here, the confocal spot was focussed on a microtubule along which moving donor-labelled kinesins were visible as bell-shaped fluorescence time traces. FRET could be observed in acceptor and donor channel with low fluorescent ATP concentrations. To achieve a higher ATP concentration, we added non-fluorescent ATP and measured ATP binding times, and compared it with the duration of a single step. We found that one ATP is bound longer than the step of one head endures, indicating an overlap of the nucleotide binding times of the two heads.

Chapter 5: Hereditary spastic paraplegia (HSP) is a neurodegenerative disease caused by motoneuron degeneration. We investigated the motility of KIF5A and four HSP mutants. All mutations were single amino-acid exchanges and located in kinesin's motor or neck-domain. Three of these mutations either reduced microtubule affinity, or gliding velocity, or both. In laser-trapping assays, none of the mutants moved more than a few steps along microtubules. Motility assays with mixtures of

Summary

homodimeric wildtype, homodimeric mutant, and heterodimeric wildtype/mutant motors revealed that only one mutant reduced gliding velocity at ratios as present in heterozygous patients. Attached to quantum dots as artificial cargo, mixtures simulating the situation in patients showed that mutant kinesins led to populations of quantum dots that either do not bind to microtubules, or lag behind in transport. These observations suggest that HSP develops in SPG10 patients due to less frequent and slower axonal transport events, leading to deficient supply of the synapse.

Publications

Chapter 2:

Adio S, Jaud J, Ebbing B, Rief M, Woehlke G

The determinants of kinesin's processive motility are located in the motor domain.

EMBO J., submitted

Chapter 3:

Hahlen K, Ebbing B, Reinders J, Mergler J, Sickmann A, Woehlke G

Feedback of the kinesin-1 neck-linker position on the catalytic site.

J Biol Chem. 2006 Jul 7;281(27):18868-77. PMID: 16682419

Chapter 4:

Ebbing B, Verbrugge S, Woehlke G, Peterman E

Time-resolved FRET between Kinesin-1 and its substrate ATP

project in progress

Chapter 5:

Ebbing B, Mann K, Starosta A, Jaud J, Schöls L, Schüle R, Woehlke G

Effect of spastic paraplegia mutations on KIF5A transport activity.

Hum Mol Genet. 2008 Jan 18; [Epub ahead of print] PMID: 18203753

Meeting Abstracts

Ebbing B, Mann K, Schüle R, Woehlke G

Hereditary Spastic Paraplegia Caused by Kinesin-1 Mutants.

32nd FEBS Congress Molecular Machines 2007 July 7.-12. Vienna, Austria

Ebbing B, Mann K, Schüle R, Woehlke G

A neurodegenerative disease is caused by defects in velocity, microtubule affinity and runlength of Kinesin-1 mutants.

51st Annual Meeting of the Biophysical Society 2007 March 3.-7., Baltimore, USA

Ebbing B, Schliwa M, Woehlke G

Single molecule studies of the molecular motor kinesin.

3rd Munich Symposium on Cell Dynamics: from Molecular Structure to Cellular Motility
2005 October 5.-7., Munich, Germany

Ebbing B, Müller S, Solovei I, Cremer T, David CN, Alexandrova O

Spatial Organization of Centromeres in the Interphase Nucleus of Hydra.

International Workshop on Hydra and the Evolution of Signalling Pathways 2003
September 15.-18., Tutzing, Germany

Curriculum Vitae

Personal Information

Bettina Ebbing (Dipl.-Biol.)

Physik Department (E22 Biophysics), TU München

James-Franck-Str., 85748 Garching, GERMANY

Tel.: +49/89/289-12495

E-mail: bettina.ebbing@lrz.uni-muenchen.de

Academic Career

Since Apr 07	continuation of PhD thesis at the Department of Physics, E22 Biophysics, group of PD Dr. G. Woehlke, Technical University Munich, Germany
Sept 04- Mar 07	PhD Thesis at the Institute for Cell Biology, group of PD Dr. G. Woehlke, LMU Munich, Germany
Jan 03- Oct 03	Diploma Thesis at the Department Biology II, Prof. C.N. David, LMU Munich, Germany “Nuclear Architecture in Hydra: Confocal imaging and 3D-reconstruction of centromeric organisation”
Oct 98- Dec 02	Studies for a graduation in Biology (LMU Munich)
Major:	Zoology (Cell biology)
Minors:	Anthropology and Human Genetics Zoology (Neurobiology) Physiological Botany
Jul 98	Abitur at Gymnasium Geretsried, Germany

Grants and Fellowships

Laserlab Europe has granted a collaborative visit to the Laser Center Vrije Universiteit Amsterdam, 2006 Mai 29. - June 9., Amsterdam, Netherlands

FEBS Youth Travel Fund has granted the assistance to "Optical Techniques for Cell Physiology and Developmental Biology, 3rd Workshop, 2005 March 30.-April 9., Plymouth, UK"

Honors and Awards

Selected for an oral presentation at the **6th FEBS Young Scientist Forum: Molecular Networks 2007** July 5.-7., Vienna, Austria

Elected student of the International Graduate Program "Protein Dynamics in Health and Disease" of the **EliteNetwork Bavaria**, since 2006 September

Work experience and teaching

- | | |
|------------------|--|
| Oct 06 – Feb07 | Supervision of master thesis of Klaudiusz Mann "Kinetic properties of KIF5A mutant proteins linked to Hereditary Spastic Paraplegia" |
| Feb 05 / 06 / 07 | Support of the practical course „Molekulare Zellbiologie des Zytoskeletts“, LMU Munich, Germany |
| Mar 04 – Apr 04 | Internship at Qit Madagascar Minerals (QMM), Fort Dauphin, Madagascar |
| Nov 03 – Feb 04 | Student trainee at Labor für medizinische Genetik Dr.med. Hans-Georg Klein, Martinsried, Germany |
| Aug 01 – Oct 01 | Internship at Scil Biomedicals, Martinsried, Germany |
| Nov 98 – Nov02 | Working student at Kanzler Fachbuchhandlung für Naturwissenschaft und Technik, Munich, Germany |
| Jul 98 – Aug 98 | Internship at Siemens Ireland Ltd., Dublin, Ireland |

I thank...

... PD Dr. Günther Woehlke for his supervision, support and assistance in the lab and all the other skills needed to be a good scientist.

... Prof. Dr. Manfred Schliwa for his guidance and support during my time in his laboratory. I am grateful for his election into the EliteNetwork of Bavaria, which helped me a lot.

... Dr. Zeynep Ökten, Dr. Sarah Adio, Dr. Johann Jaud and Dr. Katrin Koch for many lively discussions and active support in the lab and life in general.

... all the people from the Schliwa lab, especially Sven Leier, Renate Dombi, Hieu Ho, Maria Beer for their great assistance and help.

... Klaudiusz Mann and Agata Starosta, who taught me the pleasure of supervising.

... Sander Verbrugge and Dr. Erwin Petermann for the great collaboration and the good time in Amsterdam.

... all the people from E22, who gave me a warm welcome and were great fellows in the last year of my thesis.

...my parents Heide and Richard Ebbing. Without their support I would have never reached my goals. I also thank my brother Axel Ebbing for being an advisor and friend in all situations of life.

Last but definitively not least:

...Florian Lechner for his patience and understanding, for his motivation and cheering me up during hard times.